2017

Experimental study on corroded steel beams rehabilitated using BFRP wrap

Sahan Yashoda Jayasuriya
University of Windsor

Experimental study on corroded steel beams rehabilitated using BFRP wrap

By

Sahan Jayasuriya

A Thesis
Submitted to the Faculty of Graduate Studies
through the Department of Civil and Environmental Engineering
in Partial Fulfillment of the Requirements for
the Degree of Master of Applied Science
at the University of Windsor

Windsor, Ontario, Canada

2017

Experimental study on corroded steel beams rehabilitated using BFRP wrap

By

Sahan Jayasuriya

APPROVED BY:

V. Stoilov
Department of Electrical and Computer Engineering

R. Balachandar
Department of Civil and Environmental Engineering

S. Kenno, Special Member
MEDA Limited

S. Das, Advisor
Department of Civil and Environmental Engineering

T. Bolisetti, Co-advisor
Department of Civil and Environmental Engineering

April 24, 2017

DECLARATION OF CO-AUTHORSHIP AND PREVIOUS PUBLICATION

I. Co-Authorship Declaration

I hereby declare that this thesis incorporates material that is result of joint research, as follows:

This thesis incorporates the outcome of a joint research undertaken in collaboration with MEDA Limited under the supervision of Dr. Das and Dr. Bolisetti. The collaboration is covered in Chapters 1-6 of the thesis. In all cases, the key ideas, primary contributions, experimental designs, data analysis and interpretation, were performed by the author, and the contribution of co-authors, Dr. Kenno and A. Bastani was primarily through advice and technical knowledge.

I am aware of the University of Windsor Senate Policy on Authorship and I certify that I have properly acknowledged the contribution of other researchers to my thesis, and have obtained written permission from each of the co-author(s) to include the above material(s) in my thesis.

I certify that, with the above qualification, this thesis, and the research to which it refers, is the product of my own work.

II. Declaration of Previous Publication

This thesis includes one original paper that has been previously submitted for publication in peer reviewed journals, as follows:

Thesis Chapter	Publication title/full citation	Publication status
Chapters 1-6	Jayasuriya S., Bastani A., Kenno S., Bolisetti T., Das S., "Rehabilitation of corroded steel beam using BFRP fabric," *Steel and Composite Structures*	Submitted

I certify that I have obtained a written permission from the copyright owner(s) to include the above published material(s) in my thesis. I certify that the above material describes work completed during my registration as graduate student at the University of Windsor.

I declare that, to the best of my knowledge, my thesis does not infringe upon anyone's copyright nor violate any proprietary rights and that any ideas, techniques, quotations, or any other material from the work of other people included in my thesis, published or otherwise, are fully acknowledged in accordance with the standard

referencing practices. Furthermore, to the extent that I have included copyrighted material that surpasses the bounds of fair dealing within the meaning of the Canada Copyright Act, I certify that I have obtained a written permission from the copyright owner(s) to include such material(s) in my thesis.

I declare that this is a true copy of my thesis, including any final revisions, as approved by my thesis committee and the Graduate Studies office, and that this thesis has not been submitted for a higher degree to any other University or Institution.

ABSTRACT

There are many structurally deficient bridges in service all around North America. These bridges can cause a potential danger to public safety, and thus, are in desperate need of replacement or rehabilitation. Flexural rehabilitation of corroded steel beams using Carbon Fibre Reinforced Polymer (CFRP) and Glass Fibre Reinforced Polymer (GFRP) have been studied in the past. However, studies have not been conducted on the rehabilitation of corroded steel beams using Basalt Fibre Reinforced Polymer (BFRP). This research examined the feasibility and effectiveness of using BFRP fabric for the rehabilitation of corroded steel beams by performing full-scale tests and developing finite element models. The study found that both yield and ultimate load capacities of a corroded steel beam can be fully restored provided sufficient thickness of BFRP fabric is used. It may be difficult to fully restore the ductility of a corroded steel beam; however, the ductility can be improved and the improvement depends on the thickness of BFRP fabric.

To my parents who guided me

To my supervisor who supported me

To my friends who helped me

Thank You

ACKNOWLEDGEMENTS

I wish to express my appreciation for MEDA Limited for providing technical assistance necessary for this investigation. The financial assistance for this project was provided by MEDA Limited located in Windsor, ON and Ontario Centres of Excellence (OCE) located in Toronto, ON, Canada.

I would like to thank Dr. Das and Dr. Bolisetti for providing me the guidance I needed to complete this project. I would also like to express my appreciation to the committee members: Dr. Kenno, Dr. Balachandar, and Dr. Stoilov for their constructive suggestions to improve this thesis.

I am also grateful towards Matt St. Louis, Lucian Pop, my brother and all my friends who helped me greatly in the lab. A special thanks goes to Amirreza, who helped me immensely throughout the entire project.

Finally, I'd like to thank my family (especially mom and dad) for their continuous support and guidance.

TABLE OF CONTENTS

LIST OF TABLES

LIST OF FIGURES

LIST OF APPENDICES

CHAPTER 1

Introduction[1]

1.1 General

Fibre Reinforced Polymers (FRPs) are composite materials containing an epoxy matrix reinforced with fibres. Common types of FRPs are Carbon (CFRP), Glass (GFRP), Aramid (AFRP) and Basalt (BFRP). Due to its high strength-to-weight ratio, the use of FRPs has been beneficial for the rehabilitation of structures in recent years.

Basalt rocks are melted, and then drawn through bushings to create filaments. These filaments are easily manufactured to create fabrics. Due to its composition of rock, Basalt fabrics are corrosion resistant and environmentally friendly. In this study, the effectiveness of Basalt fabrics for rehabilitating corroded steel beams is explored.

1.2 Statement of Problem

Many bridges in the US and Canada are in need of rehabilitation or replacement. There are about 56,000 structurally deficient bridges in the US (FHA, 2017) and the average age of US bridges is about 42 years (ASCE, 2013). In Canada, more than 40% of bridges were built over 50 years ago (Adhikari et al. 2013). It is also estimated that, one-third of Canada's highway bridges have structural deficiencies and a short remaining service life (NRC, 2013). The average age of bridges in North America has been increasing steadily (Hammad et al. 2007).

For reinforced concrete and steel bridges, corrosion is one of the main causes of deterioration, and the rate of corrosion is accelerated due to the widespread use of de-icing salts in North America. As the amount of corrosion increases, these corroded bridges eventually become structurally deficient, and becomes a potential danger to public safety.

[1] This chapter is the outcome of joint research

Replacement of these deficient structures would cost taxpayers millions and would cause numerous traffic delays. However, rehabilitation of these damaged bridges offers a cost-friendly and time-efficient solution. Due to its high strength-to-weight ratio, FRPs have recently been explored as a solution for bridge rehabilitation.

BFRP is a new product and has only come to the forefront for repair purposes in the last few years. Some studies have been conducted on the rehabilitation/strengthening of concrete structures with BFRP fabric. However, no studies on the rehabilitation of corroded steel structures using BFRP fabric were found during the literature review.

1.3 Objectives and Scope

This research was conducted in order to determine the effectiveness of rehabilitating corroded steel beams using BFRP fabric. The objectives of this research study are the following:

a) To determine the change in load-carrying capacity of corroded steel beams after rehabilitation using BFRP.
b) To determine any changes in ductility due to the rehabilitation.
c) To model the behaviour of rehabilitated beams using finite element analysis.
d) To determine the optimum thickness of BFRP needed for different percentages of corrosion using finite element models.

This study used steel beams with the section W150x24, and nine full-scale tests were conducted.

The finite element models were created using ABAQUS (Simulia 2016), which is a commercially available finite element software. The purposes of developing the finite element models were to be able to predict the failure of rehabilitated beams as well as to be able to vary the number of BFRP layers and corrosion percentages, in order to determine the optimum BFRP thickness for the rehabilitation scheme.

1.4 Organization of Thesis

This thesis contains four major chapters (Chapters 2-5), which contains the bulk of the research study. Chapter 2 describes previous research studies that were undertaken on the topic. Chapter 3 describes the experimental methodology followed during this research study. Chapter 4 discusses the experimental results. Chapter 5 discusses the finite element analysis and parametric study.

CHAPTER 2
Literature Review[2]

2.1 General

Corrosion is one of the main causes of deterioration for steel bridges. The five most common types of corrosion are; uniform corrosion, galvanic corrosion, crevice corrosion, pitting corrosion, and stress-induced corrosion. Uniform corrosion causes a uniform loss of area throughout the member. Galvanic corrosion is caused by the contact of two dissimilar materials in a conductive medium. Crevice corrosion is caused by a stagnant microenvironment which leads to the depletion of oxygen within the crevice, such as underneath a bolt. Pitting corrosion causes small pits to form on the metal and these small pits penetrate deep into the metal, while showing little signs of corrosion on the outside. Stress-induced corrosion forms in areas where the stress concentration of the metal is higher. Localized corrosion types (pitting, crevice, and stress-induced corrosion) are more dangerous due to the accelerated rate of corrosion in a localized environment. However, all of these types of corrosion cause a loss of mass and thus, decreases the load carrying capacity of the member. In order for a member to be structurally sufficient, the corrosion of the member needs to be repaired (rehabilitated) or entire corroded member must be replaced with a new member. However, replacement of these structurally deficient structures is expensive and would cause traffic delays and interruptions. However, rehabilitation offers a cost-friendly solution to a problem, which is becoming an issue in North America.

2.2 Corrosion Repair

Corroded steel beams can be rehabilitated using many different methods. Some of the methods available are rehabilitation using steel, CFRP (carbon fibre reinforced polymer),

[2] This chapter is the outcome of joint research

GFRP (glass fibre reinforced polymer), and BFRP (basalt fibre reinforced polymer) fabrics. This section examines different methods of rehabilitation.

2.2.1 Corrosion Repair with Steel

Corrosion rehabilitation with steel includes either welding or bolting steel plates to the tension flange of a corroded beam after the beam has been cleaned of the corrosive products. However, this procedure is labour intensive and time consuming. Further, this procedure introduces the potential for weld cracking failure at steel plate ends when the welding method is used in the rehabilitation. Regions of high stress concentrations could develop near bolts when the bolting method is used (Galal et al. 2012). Welding and bolting also create the potential for future crevice corrosion and galvanic corrosion, which could cause a rapid decline in the service life of a steel structure.

2.2.2 Corrosion Rehabilitation with CFRP Fabrics

Many studies have been conducted on the rehabilitation of concrete beams and girders with CFRP fabric. Concrete girders reinforced with CFRP fabric were tested in shear failure, flexural failure (Garden et al. 1997, Photiou et al. 2006) and bond behaviour (Soudki and Sherwood 2003). Concrete slab-column connections reinforced with CFRP fabrics have been tested in shear (Haralji and Soudki 2003). Many more studies have been conducted on the use of CFRP fabrics to reinforce concrete structures. However, only a few studies have been conducted on the reinforcement of steel structures using CFRP.

A concerning issue with the use of CFRP fabrics for steel rehabilitation is the increased possibility of galvanic corrosion. The cause for galvanic corrosion is the electrochemical coupling of two dissimilar metals, which creates an electric current. CFRP and steel are dissimilar metals, hence, direct contact between steel and CFRP needs to be avoided. Therefore, the use of an E-glass layer was recommended to electrically insulate CFRP and steel (Gillepsie and Mertz 1996).

In a study conducted by Tavakkolizadeh and Saadtamanesh (2003), three large-scale steel-concrete composite girders were tested using CFRP sheets. The effectiveness of the sheets was observed by applying one, three, and five layers of CFRP fabrics to 25%, 50%, and 100% area loss of the tension flange. The beams had a span length of 4.78 m. Unidirectional pultruded CFRP sheets with a width of 76 mm and thickness of 1.27 mm were bonded to the beams. Figure 2.1 shows the cross-sectional view and the corrosion details. Figures 2.2 – 2.4 display the load-deformation curves for girders with 25% area loss with one layer of CFRP, 50% area loss with three layers of CFRP, and 100% area loss with five layers of CFRP, respectively. All rehabilitated girders achieved larger ultimate load capacities as compared to the virgin girder. The ultimate load capacity increased by 19.1%, 80.2%, and 9.6% for the rehabilitated girders with 25% area loss (with one layer of CFRP), 50% area loss (with three layers of CFRP) and 100% area loss (with five layers of CFRP), respectively, as compared to the virgin girder. However, for most of the rehabilitated girders, the elastic stiffness was not fully recovered. When compared to the virgin girder, the elastic stiffness of the girder with 25% area loss (with one layer of CFRP), 50% area loss (with three layers of CFRP) and 100% area loss (with five layers of CFRP) were -8.9%, +2.4% and -13.5%.

Galal et al. (2012) tested thirteen W150x30 steel (reference) beams to evaluate the behaviour of deteriorated and CFRP-retrofitted steel girders. These beams had a span length of 1.6 m and were tested in four-point bending. The different amounts of simulated corrosion were 33% and 50%. These corrosion percentages were achieved by simulating an area loss in the tension flange. Local corrosion and spread corrosion were simulated by creating holes or notches in the tension flange. One of the objectives was to evaluate the effectiveness of transverse wrapping for delaying the debonding of CFRP fabrics, thus allowing the beam to carry a larger load. This objective was accomplished by varying the layers of transverse CFRP fabric. Figure 2.5 shows load-deflection curves for the control corroded beam as well as the two beams tested with and without transverse layers of CFRP. These results indicated that the transverse layers of CFRP fabric did not have a significant effect on delaying the debonding of longitudinal CFRP plates. The yield and ultimate load capacities were slightly increased from 250 kN to 260 kN and 344 kN to 347 kN,

respectively. The mode of failure for these beams was the debonding of CFRP plates. Another objective of this study was to determine the effectiveness of different epoxies on the load carrying capacity of retrofitted steel beams. Beams with spread and local corrosion were tested with five layers of CFRP fabrics while the type of epoxy was varied (viscous and saturating epoxies). Figure 2.6 shows the load-deflection curves of the beams with two different epoxies. It was found that the type of adhesive had a slight influence on the yield load capacity, while displaying a significant influence on the ultimate load capacity and mode of failure. Beams bonded with viscous epoxy showed a higher ultimate load than beams bonded with saturating epoxy. For beams with 33% area loss, the P_u/P_y ratio for saturating and viscous epoxies were 1.25 and 1.48, respectively. For 50% area loss, the P_u/P_y ratio for saturating and viscous epoxies were 1.45 and 1.57, respectively. The modes of failure of these beams were either rupture of CFRP fabrics or debonding.

A total of six steel-concrete composite beams were tested by Sen et al. (2001). Each specimen was a W200x36 (W8x24) (reference) beam acting compositely with a 114 mm thick, 0.71 m wide reinforced concrete slab. Each of these specimens were 6.1 m long and were tested in four-point bending until the yield load capacity of the tension flange was reached. The beams were then repaired using 2 mm and 5 mm thick CFRP fabrics. In order to prevent end peeling, the ends of the CFRP fabrics were clamped. In an attempt to prevent adhesive failure, bolts were used in addition to epoxy in some beams. The most common mode of failure for these beams was CFRP rupture near bolts. This is likely due to high stress concentrations which could develop near the bolts. It was observed that the elastic stiffness increased as the thickness of CFRP increased as shown in Figures 2.7 and 2.8. The increase of ultimate load capacity ranged from 9% to 52%, with the larger ultimate load capacity increases resulting from thicker CFRP.

Manalo et al. (2016) tested the use of CFRP fabric for repairing corroded and cracked steel beams by testing three 3 m long beams in four-point bending. Two beams were simulated with defects. One beam had a simulated crack, while the other had 80% simulated corrosion. These two beams were repaired using 15 mm, and 11 mm thick CFRP laminates and the results were compared to the control beam. The simulated corrosion was filled with

epoxy grout, while a 1200 mm length patch repair was used for both repaired beams. The laminates were wrapped around the flange and covered half of the web. The ultimate load capacities of the rehabilitated cracked and corroded beams increased by 3% and 8%, respectively, as compared to the control beam. The stiffness of the rehabilitated beams also increased by about 16%. All the beams failed due to lateral instability after yielding, and no plastic hinge was observed.

2.2.3 Strengthening Steel Beams with GFRP Fabrics

The flexural performance of GFRP fabrics was tested by conducting full-scale tests on three beams in four-point bending (El Damatty et al. 2003). Three W150x37 steel beams with a span length of 2.8 m were used in this experiment (One control beam and two strengthened beams). GFRP fabrics with a thickness of 19 mm was used, and this fabric had a tensile strength of 206.85 MPa and an elastic modulus of 17.2 GPa. The GFRP fabrics were cut to size and externally bonded to the top and bottom flanges of the strengthened beams. The strengthened beams showed increases of 15%, 23%, and 78% in the elastic stiffness, yield moment, and ultimate moment, respectively. The load-deflection curves of these beams are shown in Figure 2.10 and the failure of a strengthened beam is shown in Figure 2.11.

2.2.4 Flexural Repair Using BFRP Fabrics

BFRP materials are relatively new to the construction industry and hence, a limited number of research papers on use of BFRP products in rehabilitation of damaged structures are available. Research articles on the use of BFRP fabrics for the rehabilitation of steel structures were not found. However, some studies were conducted using BFRP fabrics for flexural rehabilitation/strengthening of concrete beams. This section briefly discusses the results of these studies, as relative to the objectives of this research.

Sim et al. (2005) conducted tests to compare the durability of BFRP, GFRP, and CFRP. Alkali resistance, weathering resistance, and thermal stability tests were conducted to assess the durability of the above FRPs. For alkali resistance and weathering resistance

tests, the CFRP fibres did not lose a significant amount of strength, while a similar rate of deterioration was observed for GFRP and BFRP fibres, as shown in Figures 2.12 and 2.13. The thermal stability test showed that the BFRP fibres did not lose any strength, while the strength of CFRP and GFRP fibres deteriorated significantly, as shown in Figure 2.14.

Sim et al. (2005) also conducted ten full-scale four-point bending tests on 2.4 m long concrete beams. An equivalent amount of flexural steel reinforcement was provided to each beam and stirrups were provided to ensure flexural failure. The parameters for the beams were: length of BFRP, and the amount of layers used. The lengths of the applied BFRP varied between the full span length (L) and 0.8L. The amount of BFRP layers was varied to one, two, and three. Most of these beams exhibited flexural failure, while only one beam failed due to debonding of the BFRP fabrics. The increase in yield load capacity for one, two and three layers of BFRP applied over 0.8L were 15%, 26%, 27%, respectively. The increase in ultimate load capacity for one, two, and three layers of BFRP applied over 0.8L were 0%, 16%, and 29%, respectively. The study concluded that the length of BFRP is not a significant factor in the strengthening, and the increase of yield and ultimate load capacities was larger as the layers of BFRP were increased.

The performance of BFRP fabrics was compared with CFRP and GFRP fabrics by externally bonding the aforementioned FRPs to reinforced concrete beams for strengthening and testing the beams in four-point bending (Huang et al. 2013). A total of nine beams each 2 m long (span length of 1.8 m) were constructed and these beams were externally bonded with one and two layers of CFRP, GFRP, and BFRP fabrics. The yield load capacity, ultimate load capacity, and ductility of the beam strengthened with two layers of BFRP fabrics were improved by 18%, 17%, and 22%, respectively, as compared to the control beam (unstrengthened beam). The yield load of the beam reinforced with BFRP was 3% lower than the beam reinforced with CFRP and was 14% higher than the beam reinforced with GFRP. The ultimate load of the beams increased by 18%, 25%, and 20% for BFRP, CFRP and GFRP, respectively. Interfacial debonding was the most common type of failure which occurred in the rehabilitated/strengthened beams and it was determined that including U-wraps at the end points of the longitudinal fabric was more

efficient that multiple U-wraps across the length of the FRP fabrics. It was also determined that the performance of BFRP lies between CFRP and GFRP and the cracking of concrete can be effectively inhibited by externally bonding BFRP to reinforced concrete beams.

A concern raised in some of the studies (Sen et al. 2001, Liu et al. 2005) was the propagation of local stress concentrations in areas where corrosion was simulated using holes or notches. Since these types of defects cause abrupt discontinuations in the steel, local stress concentrations were present in the rehabilitated beams, which increased the possibility of debonding.

2.3 Debonding Issues

In order to avoid debonding issues, there are three steps, which should be followed when rehabilitating beams using FRPs (Gillepsie and Mertz 1996, El Damatty et al. 2003, Al-Saidy et al. 2004, Chen and Das 2008):

1. Surface preparation; beams are usually sandblasted if any corrosion or paint exists on the surface to which the epoxy is to be applied (Sim et al., 2005).
2. A layer of primer is applied to ensure a good bond between the steel and epoxy. McKnight et al. (1994) examined potential surface preparation techniques for steel-adhesive bonding, and it was observed that the use of Silane coupling agents improved the bond between steel and adhesives.
3. Apply epoxy and FRP layer(s) to the beam.

The strengthening of steel beams using FRP is based on the concept that the FRP will solely transfer the tensile loads once the tension flange of the beam has yielded. Since FRP layers are bonded to the beams using an epoxy, premature failure of the epoxy will limit the amount of load which can be applied to rehabilitated beams. Epoxy debonding has been a major issue for these types of rehabilitation since it doesn't allow researchers to realize the full potential load which can be applied to a rehabilitated beam.

Sen et al. (2001) used bolts on the tension flange to prevent debonding, and clamps were used at the ends of the FRP to prevent end peeling. However, failure usually occurred around bolts due to high stress concentrations. Using a larger quantity of smaller bolts was suggested to minimize the magnitude of localized concentrated stresses. Liu et al. (2001) suggested applying GFRP perpendicularly to the longitudinal reinforcement to prevent the peel off of FRP laminates.

2.4 Composite Materials

2.4.1 General

Composite materials are often the combination of two different constituents which when combined, gives the material unique properties. A composite can be defined as the combination of a matrix (epoxy, polyester, polyimide etc.) and reinforcement (glass, aramid, carbon etc.). The reinforcement is responsible for bearing the load and the matrix material is responsible for transferring the load evenly to the reinforcement.

Composite materials have been used for centuries, mainly to improve undesirable properties of individual materials. For example, using steel to reinforce concrete due to the weak nature of concrete under tensile loads. Another composite material is fibreglass, which has a plastic matrix and glass as reinforcement. The plastic matrix allows the composite material to be bent, which would normally fracture the glass fibres.

2.4.2 Fibre Reinforced Polymer (FRP)

Fibre Reinforced Polymers are composite materials which use different types of fibres as the reinforcement and different types of adhesives as the matrix. Some of the different types of fibres are carbon, aramid, glass, and basalt. The matrix usually consists of epoxy; however, polyester, polyimide etc. are used for different applications. For example, polyimide is a heat-resistant material and has found uses in electrical and aerospace

industries. Due to the high variety of available epoxies and fibres, different combinations of FRPs can be produced to satisfy the strengthening requirements of various projects.

2.4.3 Advantages of FRPs

FRPs have a very high strength-to-weight ratio, in addition to very good physical and chemical properties, such as weathering resistance (freeze-thaw resistance and ultra-violet light resistance), alkali resistance, and fire resistance. Different types of FRPs are more resistant to some of the categories above than others as shown by Sim et al. (2005). In general, FRPs deteriorate at a much lower rate than steel or concrete. Also, additives can be utilized if a specific type of weathering is to be resisted.

2.4.4 Basalt Fibre

Basalt rocks are magmatic rocks which are available abundantly around the world. The production of Basalt fibres starts by crushing basalt aggregate into fine grains sized 5 – 12 mm. Then this raw material is liquefied in a furnace at a temperature of 1500 ± 50ºC, and once homogenous, it enters a feeder where strands of continuous elementary fibres are formed by extension and reeled to a pulling mechanism. Then an oil agent is applied and all fibres are gathered to create one complex thread or fibre. These continuous complex fibres are rolled on a removable bobbin. Once the fibres have been dried, several full bobbins are taken for rewinding to receive a roving with the necessary number of compositions (Composites UK, 2014).

2.4.5 Epoxy

Epoxies are generally categorized into thermoset and thermoplastic epoxies. The bonds between molecules of thermoset epoxies are irreversible, while bonds between molecules of thermoplastic epoxies can be broken by applying heat.

Thermoset epoxies usually consist of two parts: resin and hardener (catalyzer), which are always mixed in different amounts and set to cure. Once the epoxy is cured, it behaves as

a solid and the molecular bonds created during curing are irreversible even under heat. Epoxy can be used on many materials, such as; wood, glass, concrete, and metals. The resin and hardener should be mixed with care to ensure air bubbles are not allowed into the mix, as the presence of air bubbles will reduce the strength of epoxy.

2.5 ASTM Standards

2.5.1 Standard Tensile Test for BFRP

ASTM D3039/D3039M–14 standard (ASTM 2014) specifies a test method for determining the tensile properties of polymer matrix composite materials reinforced by high-modulus fibres. The standard specifies that the coupons should have a length of 250 mm, width of 15 mm and a gauge length of 138 mm. The thickness of the specimen is not specified, as the specimen thickness depends on the thickness of the FRP. The thickness of BFRP used in this study was only about 0.45 mm which could not be gripped by the testing machine. Thus, four tabs were fabricated and epoxied onto the specimen in order to transfer the load to the specimen. The tabs were made from GFRP circuit boards from the companies Electro Sonic and Mouser Electronics (model number 64p44we). The ends of the tabs were bevelled at a 45^{o} angle to create a smooth transition from the tabs to the coupon specimens. The alignment of the fibres was a critical factor for this test because misaligned fibres can break earlier than the other fibres, causing the cross-sectional area to be reduced and thus reduce the amount of load the specimen is able to carry.

2.5.2 Standard Tensile Test for Steel

ASTM E8/E8M-15a standard (ASTM 2015) was used to determine the tensile properties of the steel used in the experiments. Using this ASTM standard, modulus of elasticity, the yield strength, yield point of elongation, tensile strength, elongation and reduction of area can be determined. The test specimens are machined to the standard shape as shown in Figure 2.15. The speed of testing machine should be set for a strain rate of 0.05 and 0.5 mm/mm/min. Extensometers can be used to measure the strain of the specimen.

2.6 Summary

Corrosion is a very common problem for many types of infrastructure in North America. Steel bridges are the most vulnerable type of infrastructure to corrosion due to the high amounts of de-icing salts used on bridges. Many bridges in North America are past design life and hence, must be replaced or rehabilitated. Since replacement of these bridges would cost ample amounts of time and money, rehabilitation is a more viable option.

Rehabilitation of steel beams using FRPs is common and an abundant amount of research has been conducted on the rehabilitation of steel beams using different types of FRPs, such as CFRP and GFRP. However, no research has been conducted on the effectiveness of using BFRP fabrics for rehabilitating corroded steel beams.

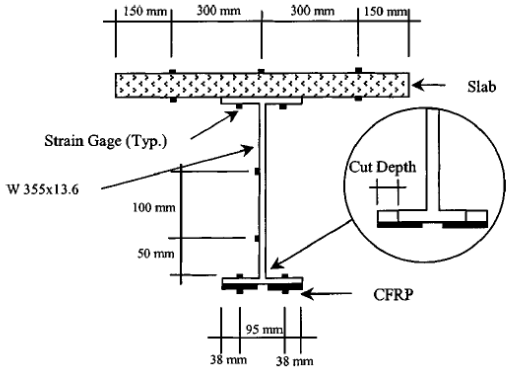

Figure 2.1: Cross-sectional view and corrosion details
(Tavakkolizadeh and Saadatmanesh 2003)

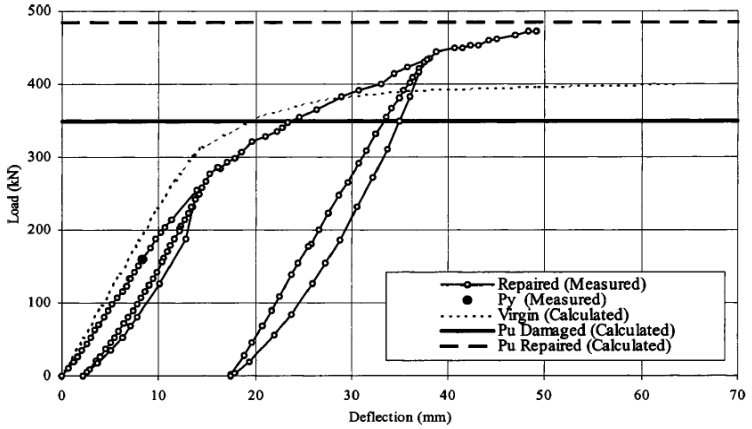

Figure 2.2: Load-deflection curve for rehabilitated 25% area loss beam
(Tavakkolizadeh and Saadatmanesh 2003)

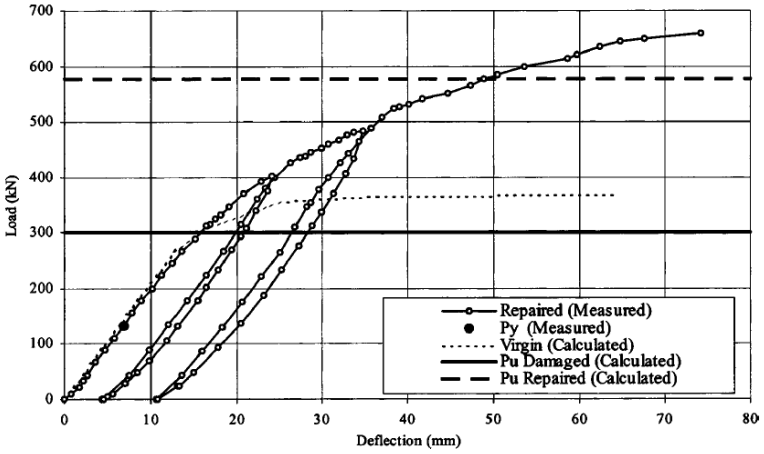

Figure 2.3: Load-deflection curve for rehabilitated 50% area loss beam
(Tavakkolizadeh and Saadatmanesh 2003)

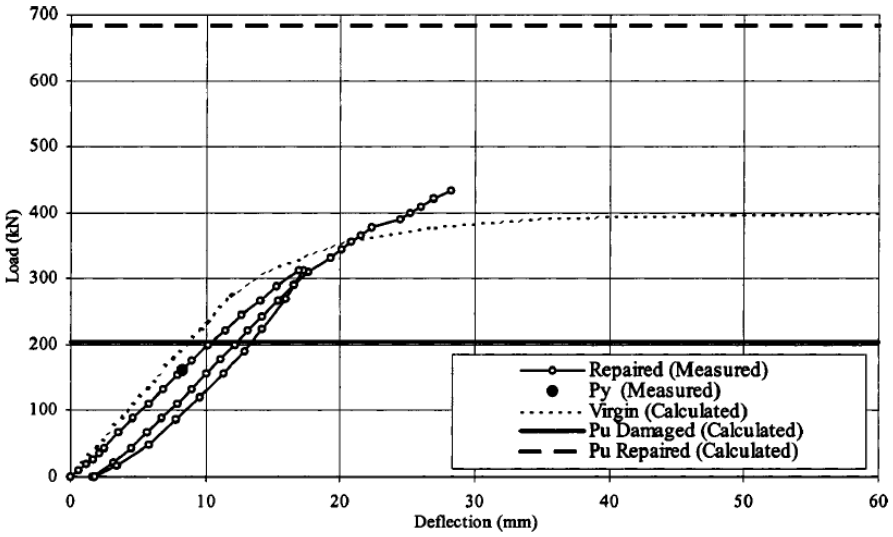

Figure 2.4: Load-deflection curve for rehabilitated 100% area loss beam (Tavakkolizadeh and Saadatmanesh 2003)

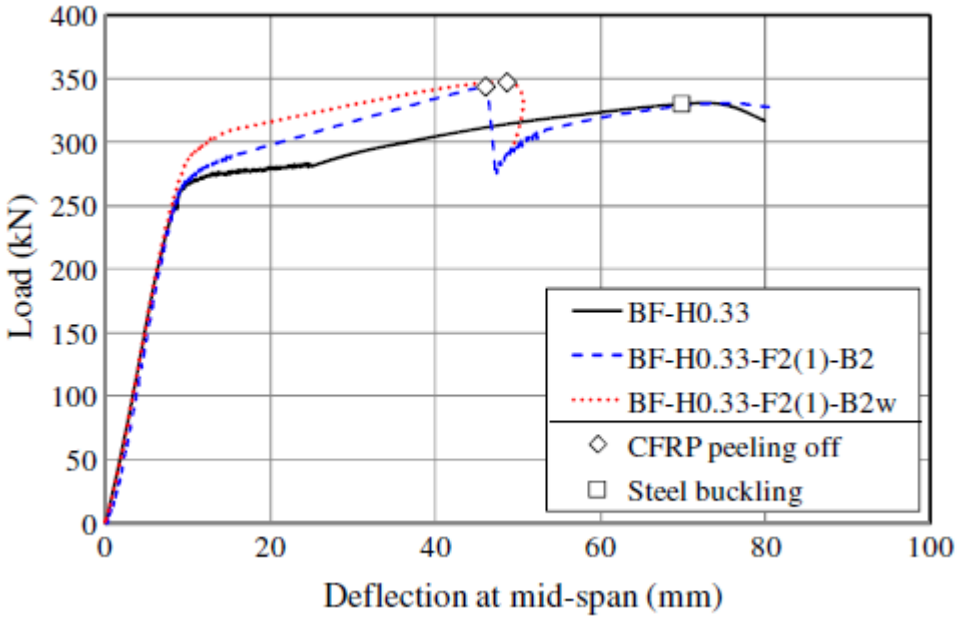

Figure 2.5: Load-deflection curve (Galal et al. 2012)

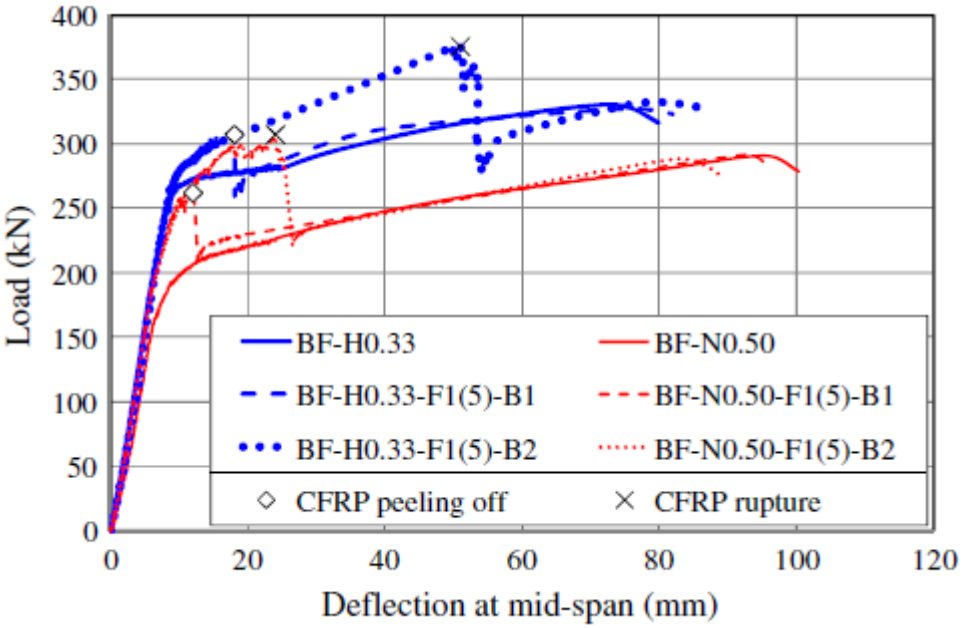

Figure 2.6: Load-deflection curve using two different epoxies (Galal et al. 2012)

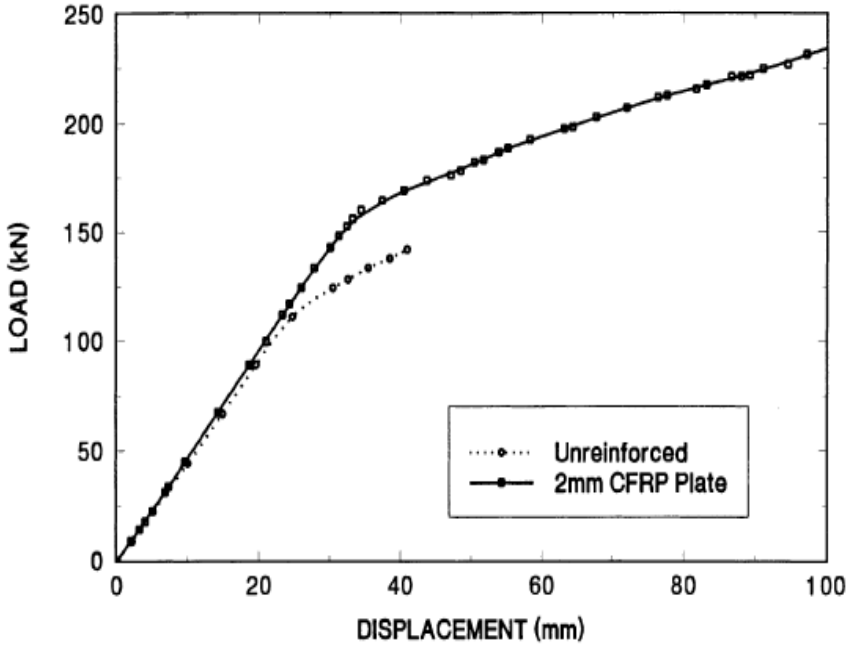

Figure 2.7: Load-displacement curve of beam repaired with 2 mm CFRP (Sen et al. 2001)

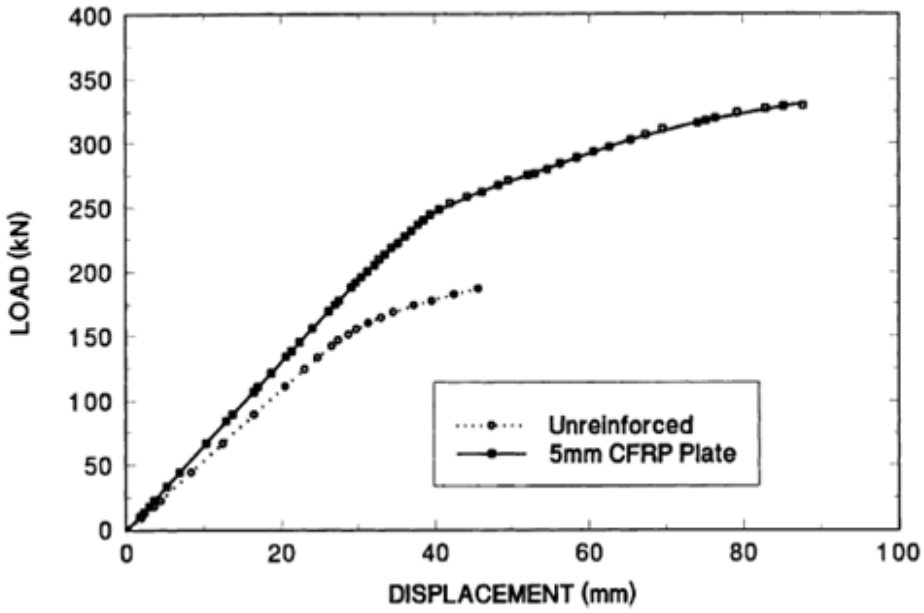

Figure 2.8: Load-displacement curve of beam repaired with 5 mm CFRP (Sen et al. 2001)

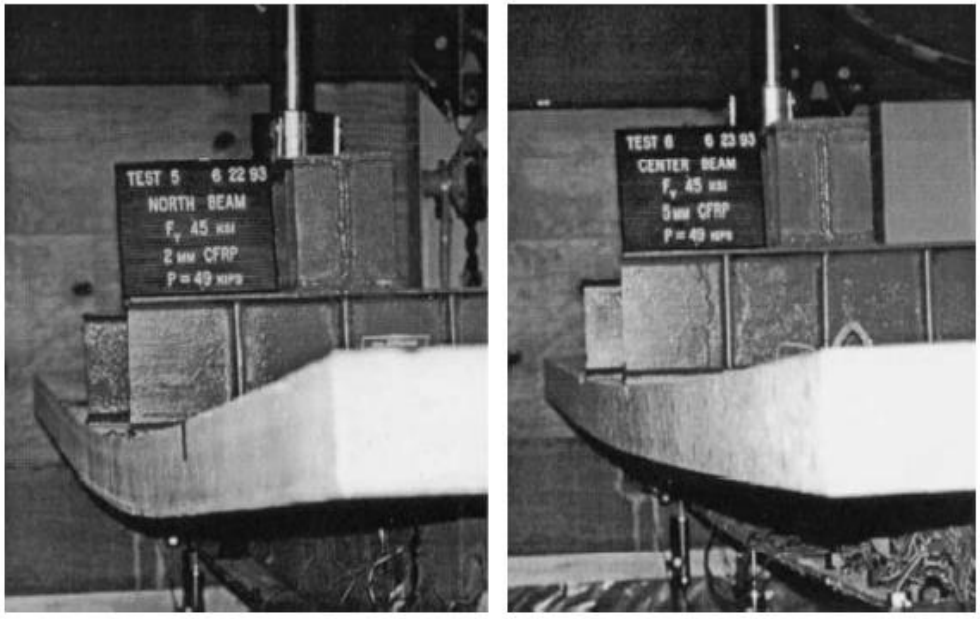

Figure 2.9: Deflected shape of repaired beams at 218 kN (Sen et al. 2001)

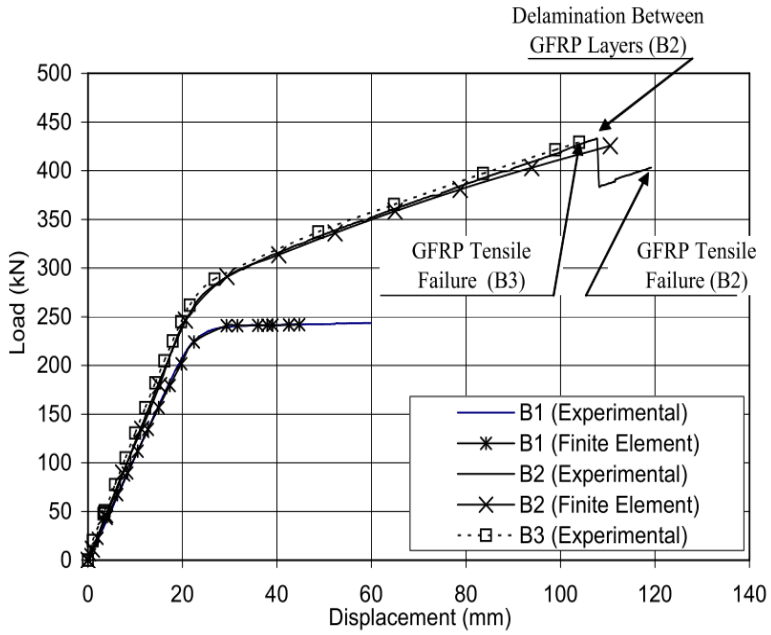

Figure 2.10: Load-deflection curves (El Damatty et al. 2003)

Figure 2.11: Failure of strengthened beam (El Damatty et al. 2003)

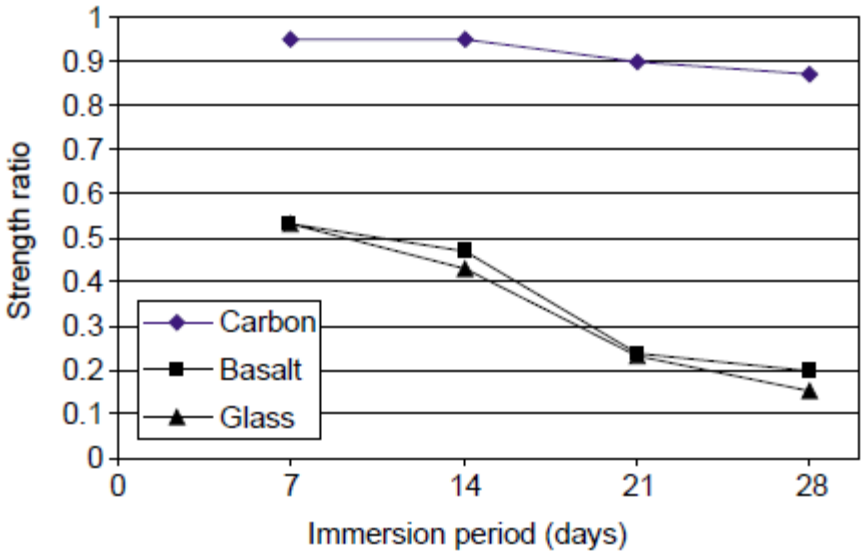

Figure 2.12: Alkali resistance (Sim et al. 2005)

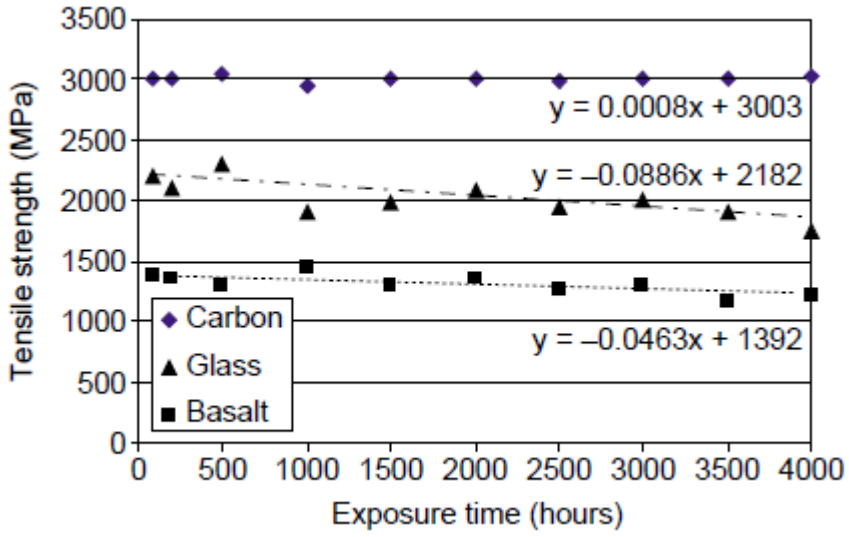

Figure 2.13: Weathering resistance (Sim et al. 2005)

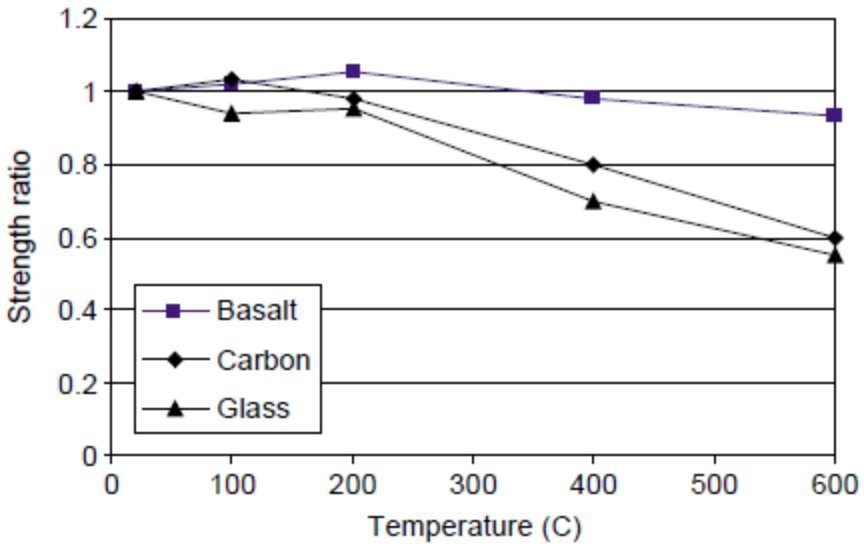

Figure 2.14: Thermal stability (Sim et al. 2005)

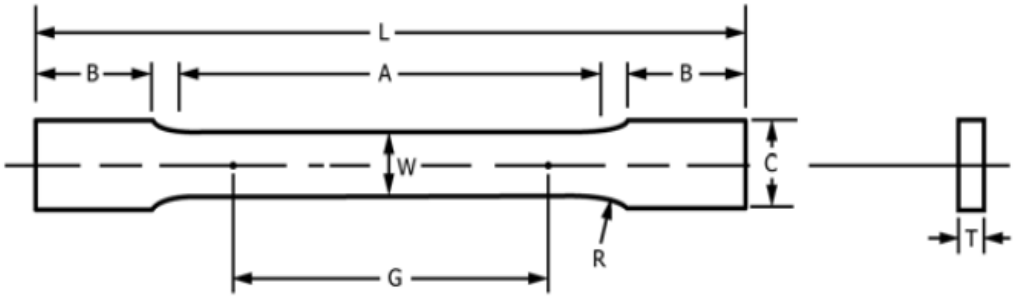

Figure 2.15: ASTM E8/E8M test specimen shape

CHAPTER 3

Experimental Program[3]

3.1 Introduction

The main objective of this experimental program was to determine the effectiveness of flexural rehabilitation of corroded steel beams using BFRP fabrics.

The experimental program consisted of nine steel W150x24 (W6x16 Imperial) sections. Three beams were designated as control and control corrosion specimen. Six beams were rehabilitated or strengthened by externally bonding BFRP or CFRP sheets to the bottom flange. This chapter describes the test specimens, materials used, instrumentation, experimental setup, and the rehabilitation scheme used in this study.

3.2 Experimental Program

Nine test specimens were supplied by Tilbury Steel. These specimens were fabricated and tested in the University of Windsor's Structural Engineering Lab. The test specimens are identified using different labels which describe the specimen. The labels CC and RB denote control corrosion and rehabilitated beam, respectively, and the percentage of corrosion is indicated (if there is any) in front of this label. For example, the specimen 20CC represents the control corrosion specimen with 20% corrosion. The naming for the rehabilitated specimens is based on the extent of corrosion and the number of layers of fabric used. For example, the specimen, 20RB4L-B indicates that this beam specimen had 20% loss in flange thickness (20) resulting from the corrosion and the beam was rehabilitated (RB) with four layers (4L) of BFRP fabric (-B). The test matrix is shown in Table 3.1.

[3] This chapter is the outcome of joint research

3.3 Description of Test Specimen

Each specimen was 2 meters long with a wide flange I-shaped cross-section (W150x24 - metric, W6x16 - Imperial), and the span length of each specimen was 1.5 meters.

The W150x24 section and 1.5 m span length were chosen in order to minimize the possibility of lateral-torsional buckling after trial testing several beam sections and several span lengths.

3.3.1 Detail of Corrosion

The corrosion of beams were created by machining the bottom flange of the beams at mid-span. A circular shape with a length of 100 mm was machined with a computer numerical control (CNC) machine, as shown in Figures 3.1 and 3.2. The middle of the corroded beams was made to be the apex of the circular shape, which in result, produced beams with the desired percentage of corrosion at the middle of beams. The width of the corrosion was equal to the width of the beam (102 mm). Details of the corrosion from the plan view and front view are shown in Figures 3.3 and 3.4, respectively.

3.4 Material Properties

The materials used in the tests included structural steel, BASF Primer, BASF epoxy, BFRP dry fabric, and CFRP dry fabric.

3.4.1 Steel

Grade W350 structural steel was used in this study and the steel beams were purchased from Tilbury Steel. Tensile properties of the structural steel were determined by testing coupons in accordance with ASTM E8/E8M-15a (ASTM 2015). Five coupons were tested and the stress-strain curve of one of the coupons is shown in Figure 3.5. The average yield

strength, elastic modulus, and ultimate strength of the samples were found to be 379 MPa, 205 GPa, and 484 MPa, respectively.

3.4.2 Composite Strengthening System

The composite strengthening system used in this study was the MasterBrace FIB System produced by BASF, The Chemical Company. The BFRP fabric was provided by Sudaglass, and the CFRP fabric (Sikawrap Hex dry fabric (230c)) was manufactured by Sika Canada Inc. The composite strengthening system included MasterBrace Primer (P3500), MasterBrace Putty (F2000), and MasterBrace Saturant (SAT 4500).

MasterBrace Primer is a two component solvent-less epoxy system, which when mixed, yields a medium viscosity primer that penetrates the pore structure of the steel substrate to provide a high bond base coat. MasterBrace Putty is a high viscosity epoxy paste used to level small surface defects, and provide a smooth surface to which the MasterBrace system will be applied. MasterBrace SAT 4500 is a low viscosity, high strength adhesive used for bonding FRP sheets to concrete, steel, or wooden surfaces. Each component is a two-part epoxy (resin and hardener). The mix ratios (resin: hardener) are 100:30, 100:30, and 100:60 by weight, for the saturant, putty, and primer, respectively.

The MasterBrace primer is first applied to the steel surface and allowed to become tack-free before the saturant and fabric are applied. The BFRP fabric is saturated in epoxy and is applied onto the beam with a roller. After the epoxy is allowed to cure for seven days, as per manufacturer's instructions, the BFRP fabrics act as an externally bonded reinforcement system which increases the load capacity of rehabilitated beams. These materials used in the experiments are shown in Appendix II.

3.4.3 Basalt Fibre Reinforced Polymer Tensile Test

Properties of the BFRP dry fabric (UD-200-13-60) were found by testing coupons in accordance with ASTM D3039/D3039M-14 (ASTM 2014). The standard encourages the use of tabs at the ends of coupon specimen to ensure load is distributed evenly to the coupon

and the specimen does not rupture due to stress concentrations at the grips. Tabs were first immersed in epoxy, then BFRP fabric was placed on top of the tabs, and finally the fabric was immersed in epoxy. During this process, it is essential that the fabric orientation remains straight, as any variation in the fabric orientation would cause inaccurate results. The tabs were made of Epoxy Glass Composite board produced by Vector Electronics. Any excess epoxy was grinded off to ensure a smooth, flat grip between the tabs and grips. An MTS machine with a 50 kN capacity was used to apply the tension load to the BFRP coupon specimens. Figures 3.6 and 3.7 show a coupon specimen before and after the tension test. Figure 3.8 shows the stress-strain curves for the BFRP coupon specimens.

Five BFRP coupons were tested and consistent results were obtained, as per ASTM standard specifications. The modulus of elasticity was calculated between 100 MPa and 300 MPa when the stress-strain curve is linear. The average modulus of elasticity of the five specimens was found to be 23.1 GPa (Table 3.2). The average ultimate stress of the specimens was 459 MPa (Table 3.3) and the average ultimate strain of the specimens was 0.022 mm/mm (Table 3.4).

3.4.4 Carbon Fibre Reinforced Polymer Tensile Test

Similar to the tensile test of BFRP fabric, CFRP coupons were also tested according to ASTM D3039/D3039M – 14. The average ultimate stress, ultimate strain, and modulus of elasticity were found to be 1469.7 MPa, 154.3 GPa, and 0.0092, respectively. In comparison to BFRP fabrics, the CFRP fabrics showed a much larger ultimate stress and modulus of elasticity, however, the ultimate strain of CFRP fabrics was much lower. The stress-strain and load per mm width curves are shown in Figures 3.10 and 3.11. The properties of the CFRP fabrics can be found in Tables 3.5 - 3.7.

3.5 Rehabilitation Method

This section discusses surface preparation, application of primer, preparation of fabrics, and the application of epoxy (as shown sequentially in Appendix III).

3.5.1 Surface Preparation

In order to create a proper bond between steel beams and FRP, the bonding surface of the steel must be cleaned of any oil, grease, or debris. The most common method of surface cleaning for adhesive bonding is by abrasion, followed by solvent cleaning (McKnight et al. 1994). The surface preparation of the rehabilitated beams is described in the following steps.

1. The steel beams were sandblasted to a “white metal finish”, which ensures the surface does not have any oil or grease.
2. The surface was then cleaned with compressed air to ensure all debris was removed.
3. A layer of MBrace P3500 Primer was applied to the bottom flange of the beam and the bottom half of the web to create a basecoat, which enhances the bond between the composite system and the steel. The epoxy must be applied once the primer is tack-free (approximately 5 hours from the application of primer) and within 24 hours of the application of primer.
4. Prior to application of the longitudinal FRP, the corroded area is filled with small FRP strips in order to fill the gap created by the corrosion and to avoid stress concentrations at the ends of the corrosion.

3.5.2 Resin and Primer Preparation

The epoxy and the primer used in this study both contained resin and hardener which were to be mixed together. The quantities of resin and hardener were both measured very accurately using a kitchen scale before mixing together. Inaccurate quantities of resin or hardener could result in debonding or soft mixes, both of which are undesirable.

The resin was pre-mixed for three minutes before adding hardener. Once the hardener was added, the combination was mixed for five minutes. In order to avoid entrapping air bubbles, the mixer was always kept below the air surface. The mixing ratios of primer and epoxy by weight were 100:60 (Resin:Hardener) and 100:30 (Resin:Hardener), respectively.

3.5.3 Application of FRP

1. The FRP was cut into the required size. The width of the FRP layers was equal to the width of the steel beams which was 102 mm. The lengths of the FRP layers were subtracted by 20 mm from one layer to the next in order to taper the termination length of the layers.
2. Primer was mixed and applied onto the beam. Once the primer was tack-free, epoxy was ready to be applied.
3. The epoxy was mixed, and the small pieces of FRP which fill the corroded area was attached using a wet layup method.
4. To create the base layer of epoxy, a large amount of epoxy was poured over the bottom flange, and the epoxy was evenly distributed using a small paint roller. Enough epoxy must be used to ensure a strong base layer was created and the first layer of FRP was saturated.
5. The first layer of longitudinal FRP was placed over the bottom flange and the first layer was rolled over using the small paint roller. Epoxy was poured over the first layer and the epoxy was distributed using the paint roller. Since the fabric absorbs epoxy, it can easily be seen when the fabric was fully saturated. The next layers of FRP followed the same procedure and were only added when the previous layer was fully saturated.
6. Once all the longitudinal layers were attached to the beam, two layers of 590 mm wide FRP “cross-wraps” were bonded transversely to reduce the risk of debonding as used in previous researches (Nanni et al. 2001). The rehabilitation scheme is shown in Figure 3.12.
7. Once the FRP was attached to the beam, a thin layer of plastic was placed over the beam. Air pockets between the plastic and epoxy were removed manually by pressing the plastic in different directions. A wooden board was placed over the bottom flange and two L-shaped wooden boards were placed on the webs. Weights were placed over the wooden board on the bottom flange, and clamps were used to secure the boards. This created a smooth surface on the FRP to which strain gages were added.

8. The beams were allowed to cure in room temperature for seven days before testing.

3.6 Instrumentation

This section describes the instruments used in these tests and their purpose. One loadcell was attached to the hydraulic actuator, and two loadcells were placed on the supports to ensure equal distribution of the load. Linear potentiometers were used to measure the deflection of the beams. 5 mm strain gages were used to measure the strain on the steel and FRP. Two inclinometers were used to measure the angle of curvature of the beams.

3.6.1 Strain Gages

Kyowa strain gages type KFRP-5-120-C1-1 were used for all the tests. These strain gages had a length of 5 mm, a gage resistance of 120 ohms and a gage factor of two.

Eight strain gages were placed at the mid-span of the rehabilitated beams and four were placed at the mid-span of the control and control corrosion beams as shown in Figure 3.13. Prior to attaching strain gages to the steel substrate, the steel surface was grinded to a "white metal finish", and the surface was wiped with acetone to remove any grease or oil. Then the strain gages were attached using Loctite 401 strain gage glue, which provided a very strong bond between the strain gage and steel. The leads of the strain gages were soldered, and electrical tape was placed under the leads in order to prevent any electrical conduction.

3.6.2 Linear Variable Differential Transformers

Linear Variable Differential Transformers (LVDTs) were used to measure the deflection of beams at different locations. Three LVDTs with a maximum stroke of 150 mm were placed on the bottom of the beam at ¼, ½, and ¾ span lengths to obtain the deflection profile of the tested beams. Two LVDTs were attached on the loading actuator to measure the displacement of the actuator. One LVDT was placed at the mid-span perpendicular to the web to measure the lateral deflection.

3.6.3 Loading System

A universal loading actuator and a very stiff loading beam were used for the application of four-point bending load. Load was transferred from the actuator to the loading beam, and the load was further transferred from the loading beam to the specimen at a spacing of 500 mm. A loadcell of 1500 kN capacity was attached to the actuator and two loadcells of 444 kN capacity were placed below the pin and roller supports of the specimen.

3.6.4 Data Acquisition System

National Instruments Labview was used to record all measurements. Seven modules and 15 channels were used to collect measurements for the control and control corrosion specimen, while seven modules and 21 channels were used to collect data for the rehabilitated specimen. The rate of data collection was one reading per second.

3.6.5 Test Setup

The beams were set up to have a span length of 1500 mm and a point spacing of 500 mm. Very large rigid steel blocks were used to support the beams at its' ends. The pin and roller setup was used at the ends of the beams as well as the loading points.

The test setup was complete once strain gages, LVDTs, loadcells and inclinometers were all connected to the data acquisition system. The complete test setup is shown in Figure 3.14.

3.7 Summary

This chapter described the corrosion details, material properties, test setup, rehabilitation method and instrumentation.

Table 3.1: Test matrix

Beam ID	Percentage of Corrosion	Number of FRP Layers Used	Type of FRP Used	Thickness of FRP (mm)
Control	0	-	-	-
20CC	20	-	-	-
40CC	40	-	-	-
0RB7L-B	0	7	Basalt	3.15
20RB4L-B	20	4	Basalt	1.80
20RB7L-B	20	7	Basalt	3.15
40RB7L-B	40	7	Basalt	3.15
40RB10L-B	40	10	Basalt	4.50
40RB3L-C	40	3	Carbon	0.78

Table 3.2: Modulus of elasticity of BFRP coupon specimens

Specimen	Modulus of Elasticity (GPa)	Average (GPa)	Standard Deviation	Coefficient of Variance
1	22.5	23.1	0.96	4.2%
2	22.1			
3	22.8			
4	23.4			
5	24.6			

Table 3.3: Ultimate stress of BFRP coupon specimens

Specimen	Ultimate Stress (MPa)	Average (MPa)	Standard Deviation	Coefficient of Variance
1	471.6	459.0	29.8	6.5%
2	437.1			
3	437.5			
4	442.9			
5	505.8			

Table 3.4: Ultimate strain of BFRP coupon specimens

Specimen	Ultimate Strain (%) (mm/mm)	Average (%) (mm/mm)	Standard Deviation (%)	Coefficient of Variance
1	2.11	2.16	0.15	7.2%
2	2.30			
3	2.07			
4	1.98			
5	2.35			

Table 3.5: Modulus of elasticity of CFRP coupon specimens

Specimen	Modulus of Elasticity (GPa)	Average (GPa)	Standard Deviation	Coefficient of Variance
1	146.1	154.3	15.0	9.7%
2	142.5			
3	179.3			
4	157.1			
5	146.4			

Table 3.6: Ultimate stress of CFRP coupon specimens

Specimen	Ultimate Stress (MPa)	Average (MPa)	Standard Deviation	Coefficient of Variance
1	1611.9	1469.7	154.7	10.53%
2	1599.5			
3	1329.7			
4	1280.5			
5	1526.8			

Table 3.7: Ultimate strain of CFRP coupon specimens

Specimen	Ultimate Strain (%) (mm/mm)	Average (%) (mm/mm)	Standard Deviation (%)	Coefficient of Variance
1	1.06	0.92	0.13	14.6%
2	1.04			
3	0.77			
4	0.80			
5	0.93			

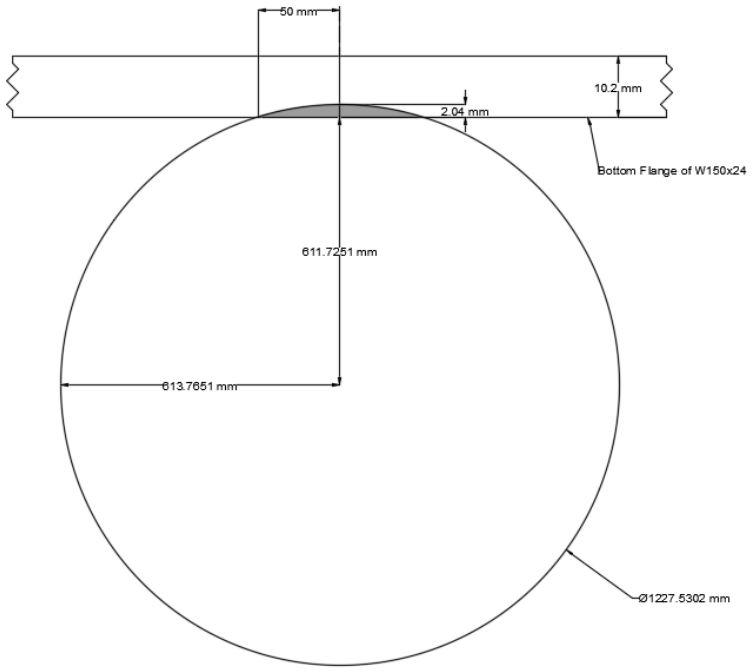

Figure 3.1: Circular shape used to simulate 20% corrosion

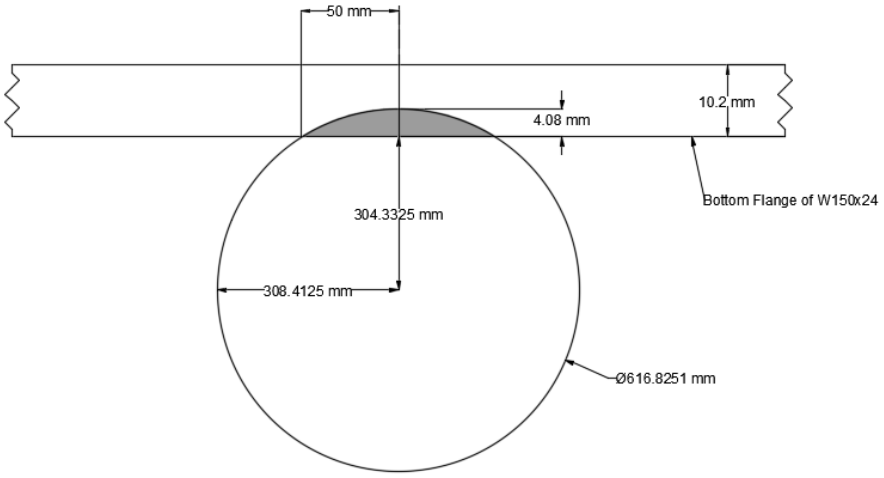

Figure 3.2: Circular shape used to simulate 40% corrosion

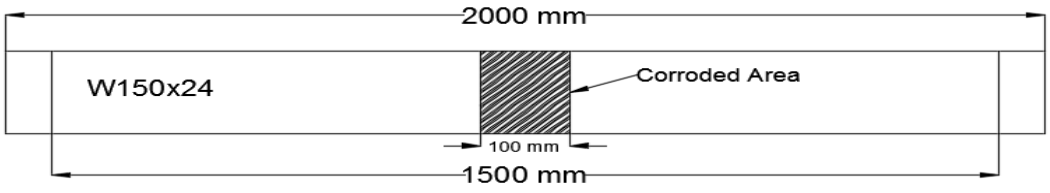

Figure 3.3: Plan view of corrosion

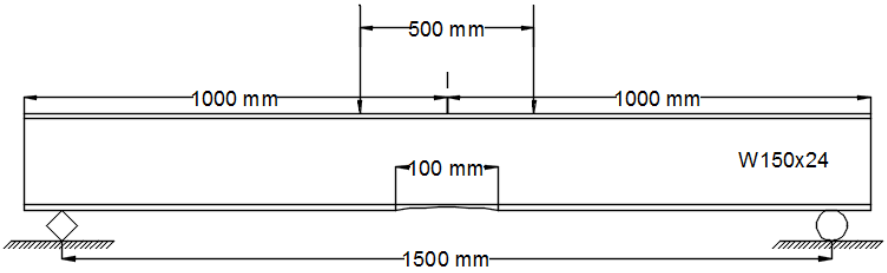

Figure 3.4: Front view of corrosion

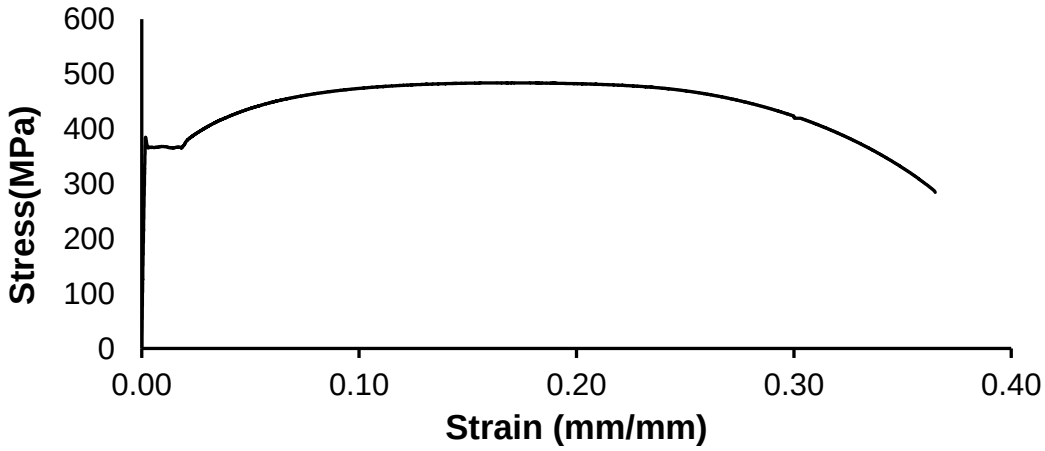

Figure 3.5: Stress-strain curve of a sample steel coupon

Figure 3.6: Basalt coupon before test

Figure 3.7: Basalt coupon after test

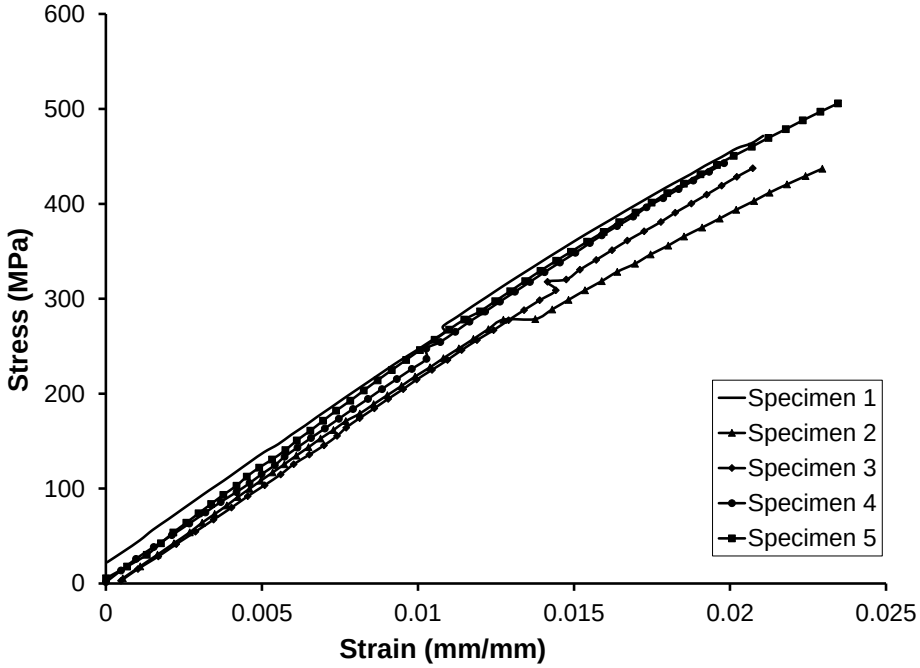

Figure 3.8: Stress-strain curves for basalt coupons

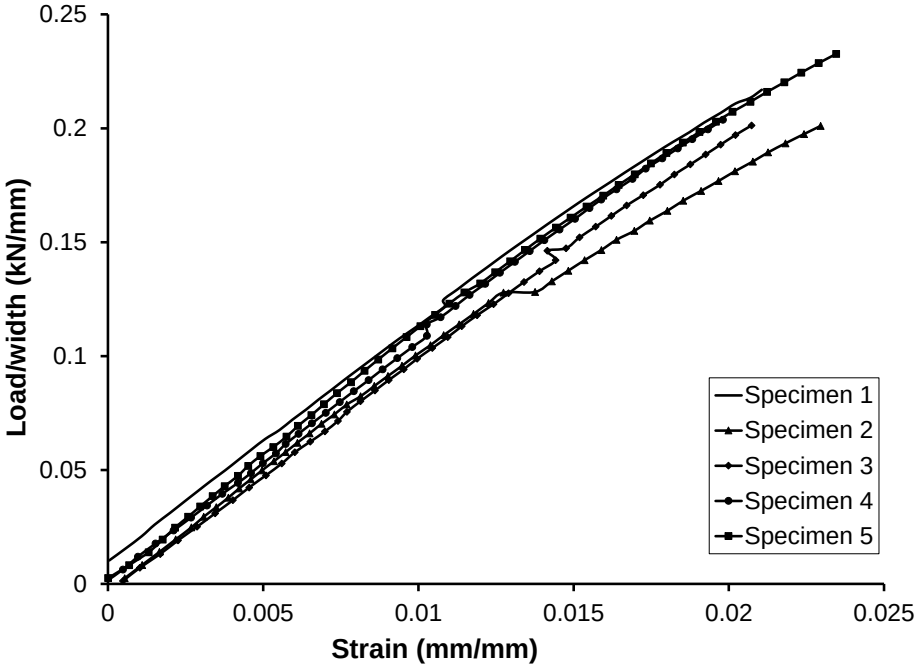

Figure 3.9: Load/mm width vs. strain curve for basalt coupons

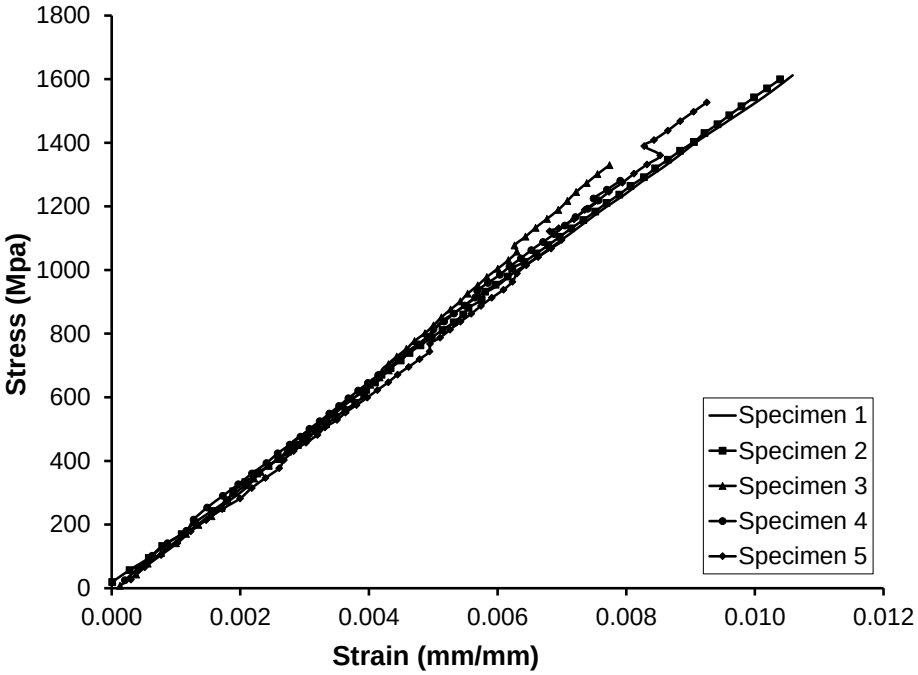

Figure 3.10: Stress-strain curve of CFRP coupon specimens

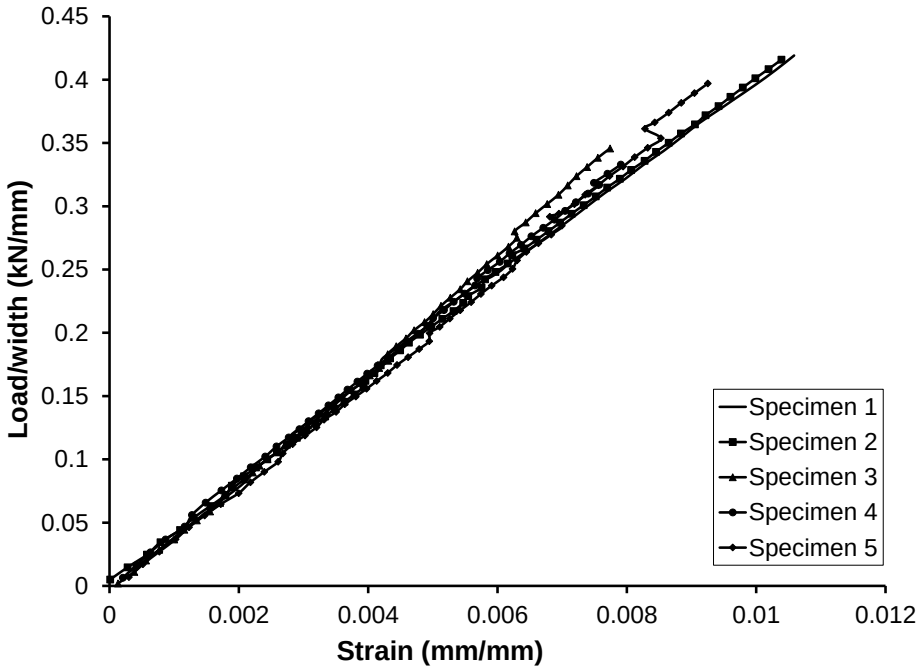

Figure 3.11: Load/mm width vs. strain curve of CFRP coupon specimens

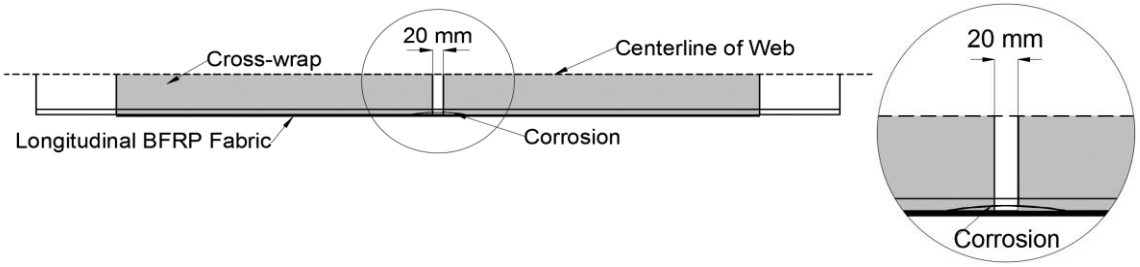

Figure 3.12: Layout of FRP rehabilitation scheme

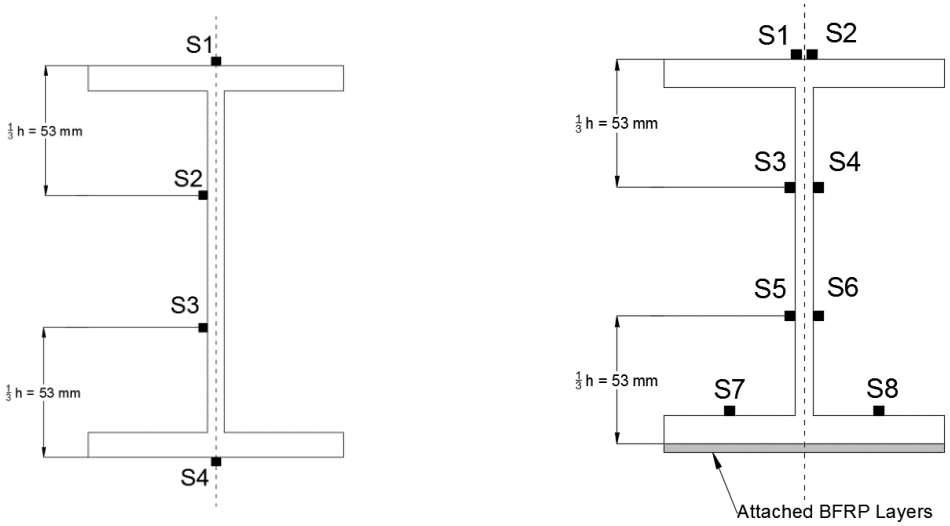

Figure 3.13: Strain gage locations

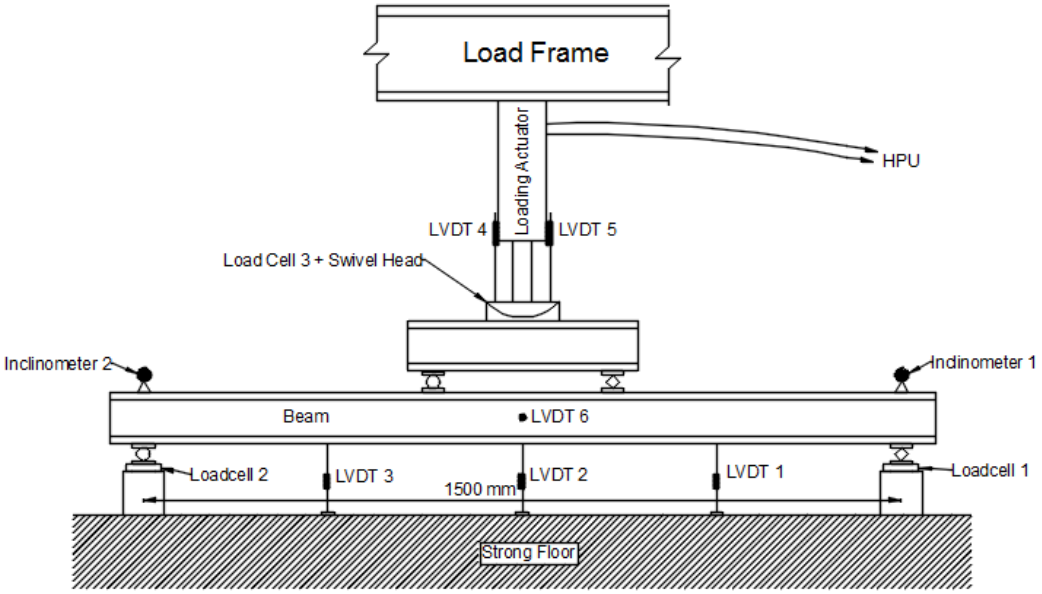

Figure 3.14: Test setup

CHAPTER 4

Experimental Results and Analysis[4]

4.1 General

This chapter describes the effectiveness of flexural rehabilitation of corroded steel beams using BFRP and CFRP fabrics. The effects of the rehabilitation scheme were observed by the changes in load-deflection curves, neutral axis depth, and ductility.

4.2 Estimation of BFRP Layers

An estimation of the optimum amount of BFRP layers was needed for the rehabilitation of corroded beams. In order to estimate the optimum number of layers, the thickness of BFRP added was converted to an equivalent thickness of steel using the modular ratio. Then the depth of the neutral axis and bending stiffness (EI) of the rehabilitated beams were calculated. However, the estimation assumes uniform corrosion of a certain percentage throughout the beam, while only the mid-span is corroded. Due to this difference of area in the estimation and reality, the load capacity of rehabilitated beams was better than initial estimations. The sample calculations for the initial estimation of 20RB7L-B is included in Appendix I.

4.3 Behaviour of 20% Corrosion Rehabilitated Beams with BFRP

4.3.1 Load-Deflection Behaviour

The load-deflection behaviour of the 20% corrosion rehabilitated beams is shown in Figure 4.1. The comparison of the yield and ultimate loads of the 20% corrosion rehabilitated beams is shown in Table 4.1.

[4] This chapter is the outcome of joint research

As can be found in Figure 4.1, the control (virgin) specimen exhibited yield and ultimate load capacities of 277 kN and 318 kN, respectively. The test of the control beam specimen was terminated at about 70 mm mid-span deflection and at that point, the load capacity of the beam began to drop. The yield load was obtained when the strain value of the bottom flange reached yield strain of 0.2%. The ultimate load in this study was considered as the maximum load that the beam specimen was able to carry.

The yield loads of the control (virgin) beam and 20% control corrosion beam (20CC) were 277 kN and 257 kN, respectively. The ultimate loads of the control beam and 20CC beam were 318 kN and 309 kN, respectively, as shown in Table 2. Hence, the drop in yield and ultimate load capacities of beam specimen 20CC, with respect to the control specimen were 7.2% and 2.8%, respectively.

The beam 20RB4L-B which had the same level of corrosion (20%) as beam 20CC was rehabilitated using four layers of BFRP fabric. As can be found from Figure 4.1, the beam 20RB4L-B attained a yield load of 272 kN and an ultimate load of 324 kN. Hence, the beam specimen 20RB4L-B exhibited increases of 5.8% and 4.9% in the yield and ultimate load carrying capacities, respectively, as compared to 20CC. However, the specimen 20RB4L-B exhibited a slightly less yield load capacity (272 kN) than the control (virgin) beam specimen (277 kN). Even though this specimen, 20RB4L-B could not fully reach the yield load of the control specimen, it was able to restore and slightly exceed the ultimate load capacity of the control specimen. The beam failed at its ultimate capacity due to rupture in the BFRP fabric when mid-span deflection was 42 mm. However, the loading was continued until a mid-span deflection of about 70 mm was achieved. Since the BFRP fabric ruptured at a 42 mm deflection, this beam beyond this deflection behaved like the control corrosion beam (20CC).

The specimen 20RB7L-B also had the same level of corrosion (20%) and this specimen was rehabilitated using seven layers of BFRP fabric. The objective was to study if the yield load capacity of the rehabilitated beam could be restored to the level of the control (virgin) beam using more BFRP fabric. As can be found in Figure 4.1, the yield and ultimate loads

of the 20RB7L-B specimen were 277 kN and 341 kN, respectively. Hence, the yield and ultimate load capacities of this rehabilitated specimen were 7.8% and 10.4% higher than the 20CC specimen. However, the yield load capacity of the specimen 20RB7L-B was same as the yield load of the control (virgin) beam specimen, and the ultimate load capacity was 7.2% higher than the control (virgin) beam. Like rehabilitated specimen, 20RB4L-B, this rehabilitated beam also failed due to rupture in the fabric, but at a higher deflection of 52.7 mm. These results demonstrate that the yield and ultimate load capacities of a steel beam with thickness loss of 20% in the bottom flange can be restored to the level of an uncorroded virgin beam if a sufficient number of BFRP fabric layers is used in the rehabilitation, and if debonding of BFRP fabric can be avoided.

4.3.2 Elastic Stiffness

The comparison of elastic stiffness for the 20% corrosion rehabilitated beams is shown in Table 4.2. The elastic stiffness of the control (virgin) and 20CC specimens were found to be 30.8 kN/mm and 28.6 kN/mm, respectively. Hence, the reduction in stiffness in specimen 20CC was 7.1% as shown in Table 2. The rehabilitated specimens 20RB4L and 20RB7L exhibited elastic stiffness values of 30.2 kN/mm and 32.6 kN/mm, respectively. Hence, this study found that the elastic stiffness of a 20% corroded beam can be almost restored using four layers of BFRP and the elastic stiffness can exceed the control beam when seven layers of BFRP fabric are used.

4.4 Behaviour of 40% Corrosion Rehabilitated Beams

4.4.1 Load-Deflection Behaviour of BFRP Rehabilitated Beams

The load-deflection behaviours of the BFRP rehabilitated beams with 40% corrosion and the control beam are shown in Figure 4.6. The yield loads of the control (virgin) and 40CC specimens were 277 kN and 242 kN, respectively. The ultimate loads of the control and 40CC specimen were found to be 318 kN and 286 kN, respectively. The decrease in yield

and ultimate load capacities for 40CC as compared to the control specimen were 12.6% and 10.1%, respectively, as shown in Table 4.3.

The 40RB7L-B specimen had the same amount of corrosion (40%) as 40CC, and was rehabilitated with seven layers of BFRP fabric. The yield and ultimate loads of this specimen were 250 kN and 313 kN, respectively. Hence, the yield and ultimate load capacities increased by 3.3% and 9.4%, respectively, as compared to the 40CC specimen. This specimen failed to reach the yield load capacity of the control beam specimen (277 kN). However, it exceeded the load capacity of the control beam in the deflection range of 18 mm to 40 mm, and reached an ultimate load capacity (313 kN) very close to the control (virgin) specimen (318 kN). This specimen failed at a deflection of 40 mm, due to the rupture of BFRP.

Similar to 40RB7L-B, the specimen 40RB10L-B also had 40% area loss in the bottom flange. This specimen was rehabilitated with ten layers of BFRP fabric. The objective was to achieve a higher yield load capacity than 40RB7L-B. The yield and ultimate load capacities of specimen 40RB10L-B were 260 kN and 340 kN, respectively, as shown in Table 4.3. The yield and ultimate load capacities of this specimen increased by 7.4% and 18.9%, respectively, as compared to the 40CC specimen. The yield load capacity of 40RB10L-B (260 kN) did not reach the yield load capacity of the control beam (277 kN). However, the ultimate load capacity of 40RB10L-B exceeded the ultimate load capacity of the control beam at a deflection of 14 mm and above until it failed. The specimen 40RB10L-B exhibited a much higher ultimate load capacity (340 kN) than the control (virgin) specimen (318 kN). The cause of failure for this specimen was BFRP fabric rupture, which occurred at a deflection of 53.3 mm. Hence, the study found that the ultimate load capacity of a steel beam with 40% corrosion can be restored to the level of a control (virgin) beam specimen. With ten layers of BFRP fabric, the ultimate load capacity increased by 6.9% as compared to the control (virgin) specimen. However, the study shows that the increase in the thickness of BFRP fabric from seven to ten layers resulted in a small improvement (about 10 kN) in the yield load. Hence, the number of BFRP fabric layers

needs to be increased even further to be able to restore the yield load capacity to the level of an uncorroded virgin beam.

4.4.2 Load-Deflection Behaviour of CFRP Rehabilitated Beam

The load-deflection behaviour of specimen 40RB3L-C and the load-deflection behaviour of the 40% corrosion rehabilitated beams with BFRP fabrics is shown in Figure 4.11. The comparison of yield and ultimate loads is shown in Table 4.3. The yield and ultimate loads of specimen 40RB3L-C were 257 kN and 295 kN, respectively. This indicates increases of 6.2% and 3.1% in the yield and ultimate load capacities, respectively, compared to the 40CC specimen.

This specimen was not able to reach the yield or ultimate capacity of the control specimen. This specimen showed decreases of 7.2% for the yield and ultimate loads, compared to the control beam. As shown in Figure 4.11, the specimen exceeded the load capacity of the control beam from a deflection of 20 mm to 22 mm, at which point, the CFRP fabrics ruptured and the load reduced significantly.

4.4.3 Elastic Stiffness

The comparison of the elastic stiffness of the 40% corrosion rehabilitated beams is shown in Table 4.4. The elastic stiffness of the control and 40CC specimens were found to be 30.8 kN/mm and 27.2 kN/mm, respectively. The reduction in elastic stiffness of specimen 40CC was 11.7%, as compared to the control specimen. The elastic stiffness of rehabilitated specimens 40RB7L-B and 40RB10L-B were found to be 31.3 kN/mm and 31.7 kN/mm, respectively, which indicates the loss of elastic stiffness due to 40% corrosion in the flexural region, can be fully restored using seven or more layers of BFRP fabrics.

The specimen 40RB3L-C had a slight decrease of 0.6% in elastic stiffness compared to the control specimen and had an increase of 12.5%, compared to 40CC. Compared to the BFRP rehabilitated beams, the elastic stiffness of specimen 40RB3L-C was lower than both BFRP rehabilitated beams. Since only one test was conducted for beams rehabilitated with CFRP

fabrics, a direct comparison of BFRP and CFRP regarding improvement of elastic stiffness cannot be made.

4.5 Behaviour of Strengthened (Uncorroded) Beam with BFRP Fabrics

4.5.1 Load-Deflection Behaviour

The strengthened specimen 0RB7L-B was externally bonded with seven layers of BFRP fabrics and its' results are compared with the control specimen. The load-deflection behaviour of the control and strengthened specimens are shown in Figure 4.12. The comparison of the yield and ultimate load capacities are shown in Table 4.5.

The yield and ultimate loads of 0RB7L-B were 287 kN and 351 kN, respectively, and had increases of 3.6% and 10.4% in yield and ultimate load capacities, respectively, as compared to the control specimen. The mode of failure for this specimen was BFRP fabric rupture which occurred partially at a deflection of 50 mm and then completely at a deflection of 54 mm. The results of this specimen showed that strengthening with BFRP fabrics will result in a slight increase of the yield load capacity and a significant increase of the ultimate load capacity.

4.5.2 Elastic Stiffness

The elastic stiffness values of the control and strengthened specimen are shown in Table 4.6. The elastic stiffness of the control and 0RB10L-B specimen were 30.8 kN/mm and 34.8 kN/mm, respectively. Hence, the elastic stiffness of the strengthened specimen was increased by 13.0%, as compared to the control specimen.

4.6 Strain Compatibility and Neutral Axis

W150x24 beams have a depth of 160 mm and the neutral axis depth of an uncorroded beam is 80 mm. However, as corrosion is simulated in the mid-span of the bottom flange, the

neutral axis depth decreases. Using strain gage data of the tested specimen, the location of the neutral axis for the corroded and rehabilitated specimen were compared.

The depth of the neutral axis was measured from the top of the beam for all beams tested in this study. The neutral axes depths were calculated at a mid-span deflection of 30 mm. This deflection was chosen to discuss the change in neutral axis depth in the plastic region before rupture has occurred.

4.6.1 20% Corrosion Rehabilitated Beams

The strain-deflection plots for the control, 20CC and 20% corrosion rehabilitated specimen with BFRP fabrics are shown in Figures 4.14 – 4.17. Strain gages with negative values are located in the compression zone and the strain gages with positive values are located in the tension zone. Using this strain data, the neutral axes for the beams were found.

The locations of the neutral axes for the 20% corrosion rehabilitated beams are shown in Figure 4.18. The neutral axis depth for the control, 20CC, 20RB4L-B and 20RB7L-B were 80 mm, 75 mm, 78 mm, and 83.6 mm, respectively. This data is very close to the theoretical neutral axis depth values of the control and 20CC which were 80 mm, and 74.1 mm respectively. The neutral axis depth of 20RB4L-B was slightly increased, as compared to 20CC, however, the neutral axis depth of this specimen was not rehabilitated to the level of the virgin control specimen.

The rehabilitated specimen 20RB7L-B was able to reach and exceed (83.6 mm) the neutral axis depth of the control specimen (80 mm). Hence, the positive effect of BFRP fabrics on the neutral axes of 20% corroded beams can be seen. The optimum amount of layers for the neutral axis depth to be rehabilitated to the depth of a control (virgin) beam, lies between four and seven BFRP fabric layers.

4.6.2 40% Corrosion Rehabilitated Beams

The strain-deflection plots for the control, 40CC and 40% rehabilitated specimen are shown in Figures 4.14, 4.19 – 4.21.

Figure 4.22 shows the neutral axis depth for the 40% corrosion rehabilitated specimen. The depth of neutral axes of the control and 40CC specimens were 80 mm and 64.5 mm, respectively. The depth of neutral axes of rehabilitated specimens 40RB7L-B and 40RB10L-B were 75.5 mm and 76 mm, respectively. The neutral axis depths of these rehabilitated specimens were not fully restored to the level of the control (virgin) beam, however, the effectiveness of the rehabilitation scheme can be found by the significant increase of neutral axes depths, as compared to the 40CC specimen.

The strain-displacement plot for the 40RB3L-C specimen is shown in Figure 4.23, and the strain compatibility is shown in Figure 4.24. The neutral axis depth for this specimen was 72.7 mm. This is a significant increase compared to the 40CC specimen, as the neutral axis of 40RB3L-C was moved midway between the control and 40CC specimen. The neutral axis value for this specimen was obtained at a deflection of 20 mm, due to early fabric rupture which occurred at a deflection of 21 mm.

4.6.3 Strengthened (Uncorroded) Beam with BFRP

The strain-displacement graphs for the control and strengthened beams are shown in Figures 4.14 and 4.25, respectively, and the strain compatibility is shown in Figure 4.26. The neutral axis depth of the strengthened beam was 82.4 mm, which was slightly larger than the neutral axis of the control beam (80 mm). However, the requirement of seven layers of BFRP fabric for this slight improvement is undesirable.

4.7 Ductility of Rehabilitated/Strengthened Beams

In this section, the ductility of the strengthened and rehabilitated beams is discussed and compared to the control (virgin) and control corrosion (CC) specimens. Two different ductility measures were computed using Equations 4.1 and 4.2, and the values are reported in Tables 4.7 and 4.8. These are displacement ductility (μ_Δ) and energy dissipation (μ_E) ratios as previously used by other researchers (Yuan et al. 2013, Tomlinson and Fam 2014).

$$\mu_\Delta = \frac{\Delta_U}{\Delta_Y} \qquad \text{Equation 4.1}$$

$$\mu_E = \frac{E_U}{E_Y} = \frac{\int_0^{\Delta_U} P(\Delta)d\Delta}{\int_0^{\Delta_Y} P(\Delta)d\Delta} \qquad \text{Equation 4.2}$$

In the above equations, Δ_U is the deflection at ultimate load, Δ_Y is the deflection at the yield load, E_U is the total energy dissipated at ultimate load, E_Y is the total energy dissipated at yield load, P is the load applied to the beam, and Δ is the mid-span deflection of the beam.

As shown in Tables 4.7 and 4.8, control (virgin) and 20CC specimens exhibited larger displacement ductility and energy dissipation ratios than the 20% corrosion rehabilitated beams (20RB4L-B and 20RB7L-B). Hence, the ductility of the 20% rehabilitated beams was not fully restored to the level of a control (virgin) or 20CC specimen. This reduction of ductility is attributable to the brittle nature of BFRP. This finding agrees with previous studies where concrete beam specimens were used (Sim et al. 2005, Huang et al. 2013).

The ultimate load capacity of 40CC occurred at a mid-span deflection of 48.5 mm, and the load capacity dropped as the test continued, as shown in Figure 4.6. Hence, displacement ductility and energy dissipation ratios for 40CC are lower, as compared to the control and 20CC specimens. The rehabilitated beams with 40% corrosion defect could not restore the ductility to the level of a control (virgin) specimen. However, the ductility of specimen 40RB10L-B exceeded the ductility of the 40CC specimen, which indicates that a small increase in ductility can possibly be achieved through rehabilitation using BFRP.

The beams rehabilitated/strengthened with BFRP had ultimate deflections which ranged between 40 and 55 mm, and similar values of displacement-ductility were found for all the beams bonded with BFRP. The ultimate deflection of 40RB3L-C was significantly lower than any beam bonded with BFRP, as it failed around a deflection of 21.6 mm. This resulted in a significantly lower displacement-ductility ratio for the specimen, which can be attributed to the extremely brittle nature of CFRP. These results showed that even though the ductility of BFRP rehabilitated beams will not reach the ductility of a virgin beam, the ductility of beams bonded with BFRP is much greater than beams bonded with CFRP.

The total amount of energy expended, and the total amount of elastic energy which was recoverable was determined by calculating the area under load-deflection curves as shown in Figure 4.27. These energy values are shown in Table 4.8. A general increase in the total energy can be seen for the rehabilitated beams when compared to the control corrosion beams. The amount of elastic energy and the percentage of inelastic energy dissipation is generally the same for all the tested beams, since only the bare steel is active after FRP rupture.

The ultimate strain of BFRP fabrics is only 2.2% which is much lower than steel. BFRP fabrics are a very brittle material compared to steel, and the rupture of this fabric occurs suddenly, without any warning. Therefore, rehabilitation with BFRP fabrics does not offer much ductility to the steel near its ultimate strain. However, the ductility performance is significantly improved with BFRP fabrics as compared to CFRP fabrics, and the ductility performance can be improved further with increased layers of BFRP fabrics.

4.8 Summary

This chapter discussed the load-deflection behaviour, strain behaviour and ductility behaviour of all the tested beams.

Table 4.1: Yield and ultimate loads of 20% corrosion rehabilitated specimens

	Control	20CC	20RB4L-B	20RB7L-B
Py (kN)	277	257	272	277
Pu (kN)	318	309	324	341
Change in Py (%) Compared to Control	-	-7.2	-1.8	0.0
Change in Pu (%) Compared to Control	-	-2.8	+1.9	+7.2
Change in Py (%) Compared to 20CC	+7.8	-	+5.8	+7.8
Change in Pu (%) Compared to 20CC	+2.9	-	+4.9	+10.4

*Py indicates yield load, Pu indicates ultimate load

Table 4.2: Elastic stiffness of 20% corrosion rehabilitated specimens

	Control	20CC	20RB4L-B	20RB7L-B
Stiffness (kN/mm)	30.8	28.6	30.2	32.6
Deflection at Yield (mm)	9.0	9.0	9.0	8.5
Change in Stiffness Compared to Control (%)	-	-7.1	-1.9	+5.8
Change in Stiffness Compared to 20CC (%)	+7.7	-	+5.6	+14.0

Table 4.3: Yield and ultimate loads of 40% corrosion rehabilitated specimens

	Control	40CC	40RB7L-B	40RB10L-B	40RB3L-C
Py (kN)	277	242	250	260	257
Pu (kN)	318	286	313	340	295
Change in Py Compared to Control (%)	-	-12.6	-9.7	-6.1	-7.2
Change in Pu Compared to Control (%)	-	-10.1	-1.6	+6.9	-7.2
Change in Py (%) Compared to 40CC	+14.5	-	+3.3	+7.4	+6.2
Change in Pu (%) Compared to 40CC	+11.2	-	+9.4	+18.9	+3.1

*Py indicates yield load, Pu indicates ultimate load

Table 4.4: Elastic stiffness of 40% corrosion rehabilitated specimens

	Control	40CC	40RB7L-B	40RB10L-B	40RB3L-C
Stiffness (kN/mm)	30.8	27.2	31.3	31.7	30.6
Deflection at Yield (mm)	9.0	8.9	8.0	8.2	8.4
Change in Stiffness Compared to Control (%)	-	-11.7	+1.6	+2.9	-0.6
Change in Stiffness Compared to 40CC (%)	+13.2	-	+15.1	+16.5	+12.5

Table 4.5: Yield and ultimate loads of strengthened and control specimen

	Control	0RB7L-B
Py (kN)	277	287
Pu (kN)	318	351
Change in Py (%)	-	+3.6
Change in Pu (%)	-	+10.4

*Py indicates yield load, Pu indicates ultimate load

**Changes in Py and Pu are measured with respect to the Control

Table 4.6: Elastic stiffness of strengthened and control specimen

	Control	0RB7L-B
Stiffness (kN/mm)	30.8	34.8
Change in Stiffness (%)	-	+13.0
Deflection at Yield (mm)	9.0	8.3

*Changes in stiffness are measured with respect to the Control

Table 4.7: Displacement-ductility of tested specimens

Specimen Name	Deflection at Yield Load (mm)	Deflection at Ultimate Load (mm)	Displacement-Ductility Ratio (μ_Δ)	$\mu_\Delta/\mu_{\Delta(Control)}$	$\mu_\Delta/\mu_{\Delta(CC)}$
Control	9.0	70.0	7.8	-	-
20CC	9.0	67.0	7.4	0.95	-
40CC	8.9	48.5	5.4	0.77	-
20RB4L-B	9.0	42.0	4.7	0.60	0.64
20RB7L-B	8.5	47.6	5.6	0.74	0.74
40RB7L-B	8.0	40.0	5.0	0.64	0.83
40RB10L-B	8.2	53.3	6.5	0.81	1.05
40RB3L-C	8.4	21.6	2.6	0.33	0.43
0RB7L-B	8.3	50.2	6.0	0.77	-

Table 4.8: Energy dissipation ratios of tested specimens

Specimen Name	Energy Dissipation Ratio (μ_E)	$\mu_E/\mu_{E(control)}$	$\mu_E/\mu_{E(CC)}$	Total Energy (J)	Elastic Energy (J)	Inelastic Energy Dissipation (%)
Control	14.82	-	-	19975.8	1339.3	93.3
20CC	14.11	0.95	-	19064.6	1105.0	94.2
40CC	11.30	0.76	-	18823.4	1073.1	94.1
20RB4L-B	8.34	0.56	0.59	20053.6	1285.3	93.6
20RB7L-B	11.33	0.77	0.80	20565.2	1266.1	93.8
40RB7L-B	9.70	0.66	0.86	19482.5	1132.8	94.2
40RB10L-B	12.70	0.86	1.12	20443.0	1182.8	94.2
40RB3L-C	4.20	0.28	0.37	18412.5	1212.0	93.4
0RB7L-B	11.61	0.78	-	21241.7	1351.5	93.6

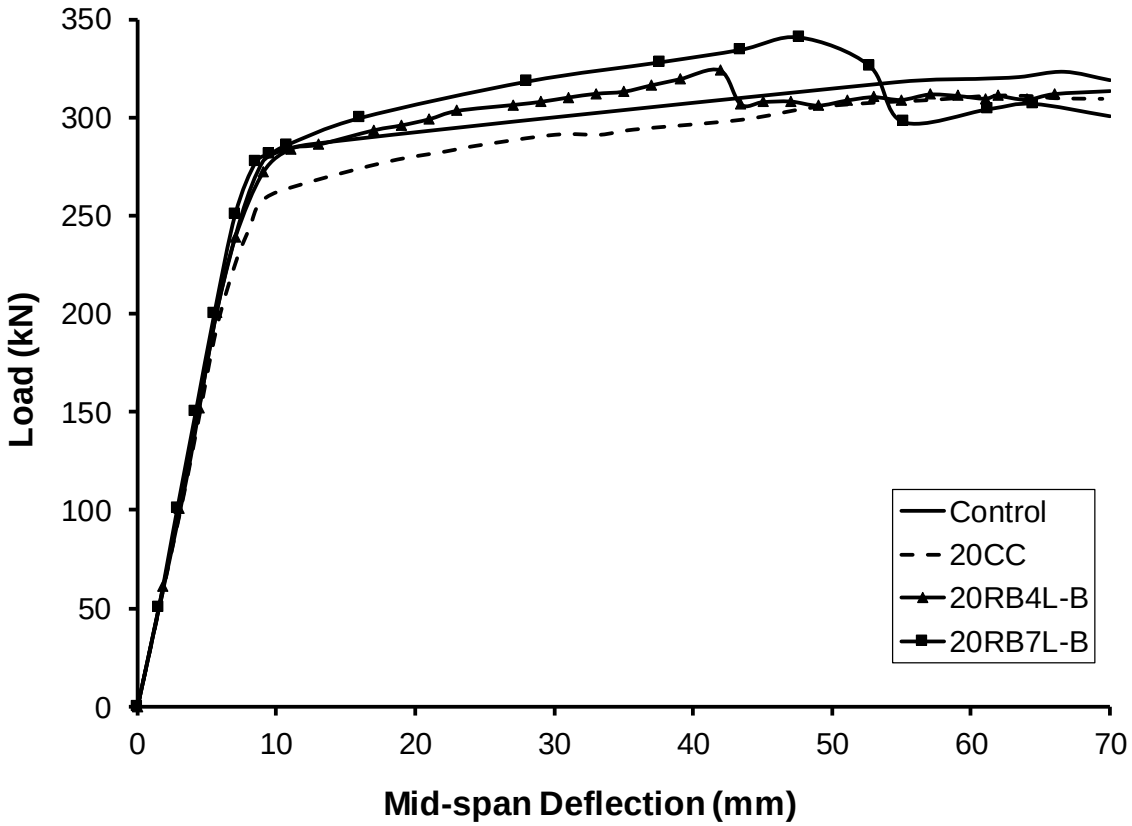

Figure 4.1: Load-deflection curves of 20% corrosion rehabilitated specimens

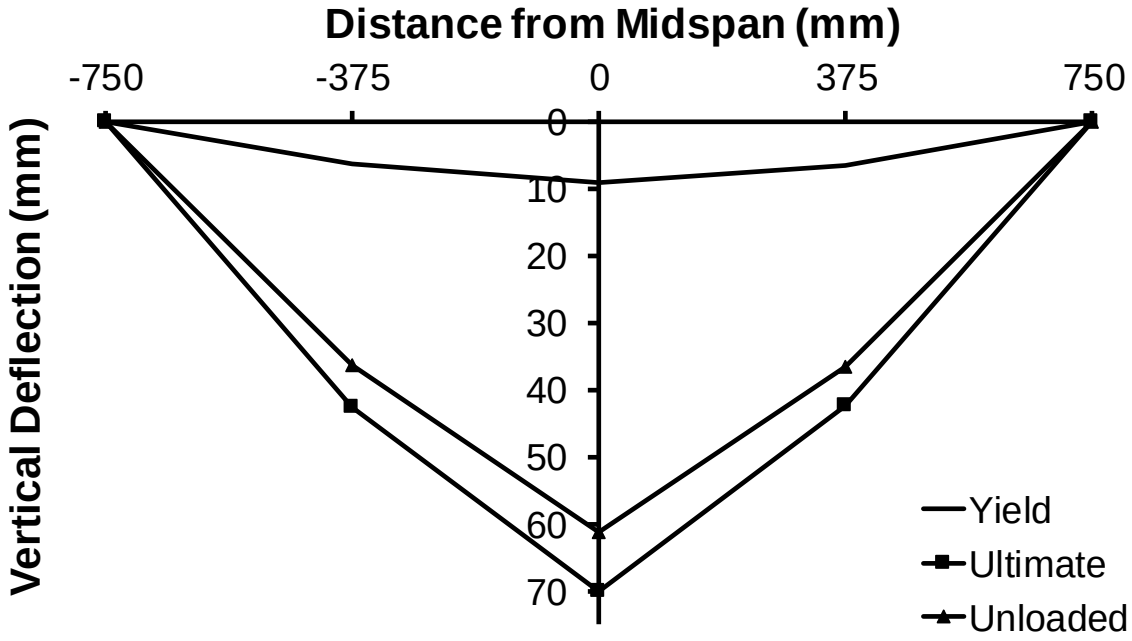

Figure 4.2: Deflection profile of control specimen

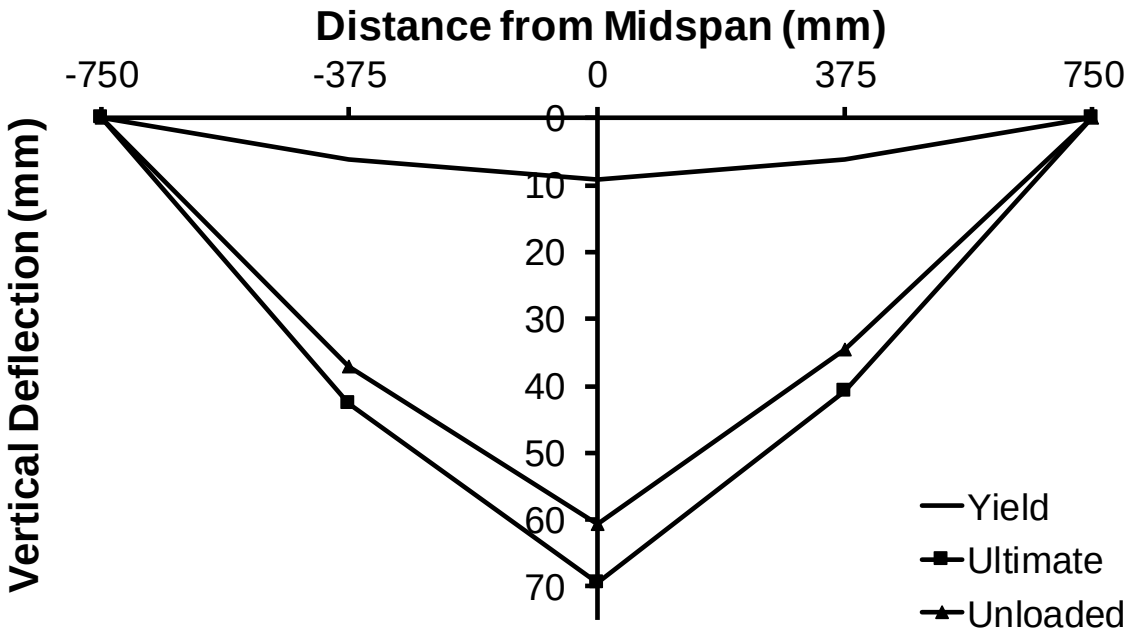

Figure 4.3: Deflection profile of 20CC specimen

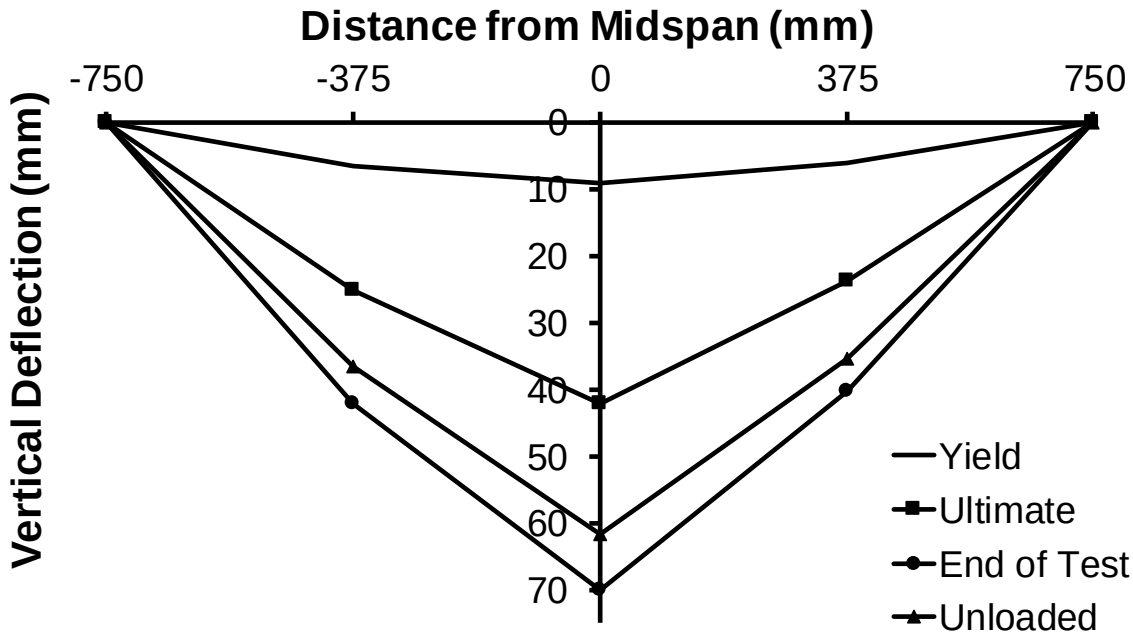

Figure 4.4: Deflection profile of 20RB4L-B specimen

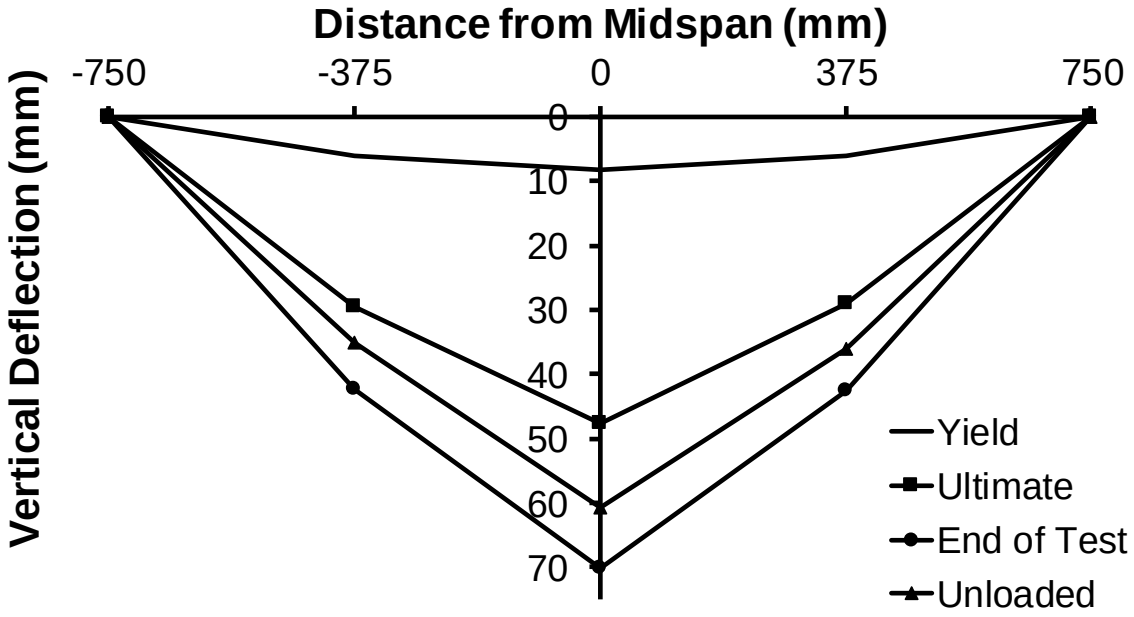

Figure 4.5: Deflection profile of 20RB7L-B specimen

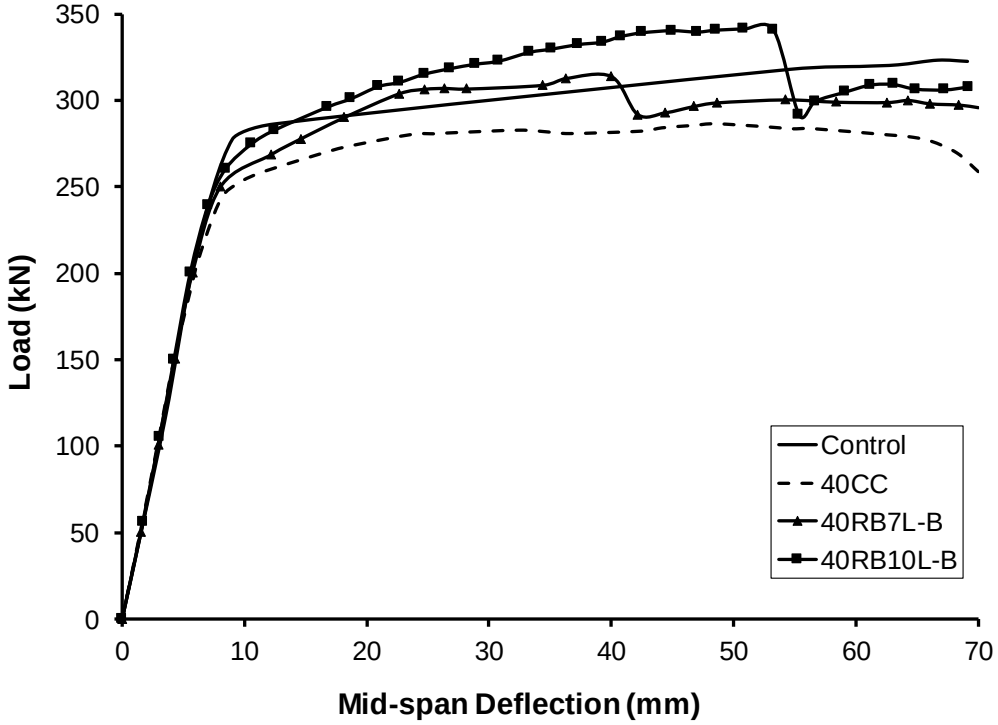

Figure 4.6: Load-deflection curves of 40% corrosion rehabilitated specimens (BFRP)

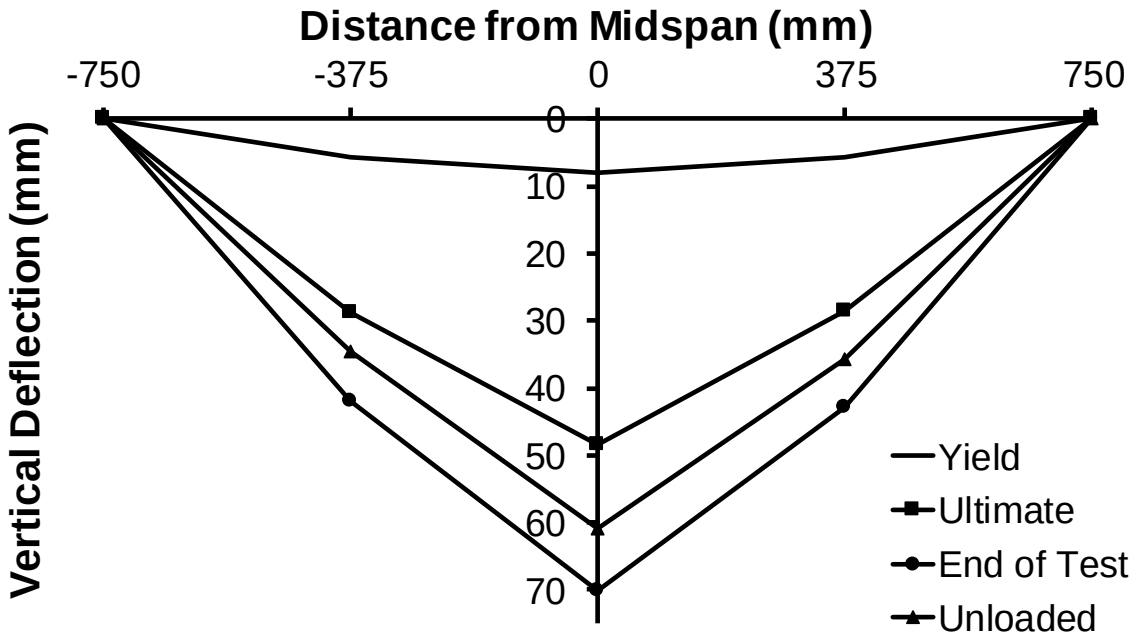

Figure 4.7: Deflection profile of 40CC specimen

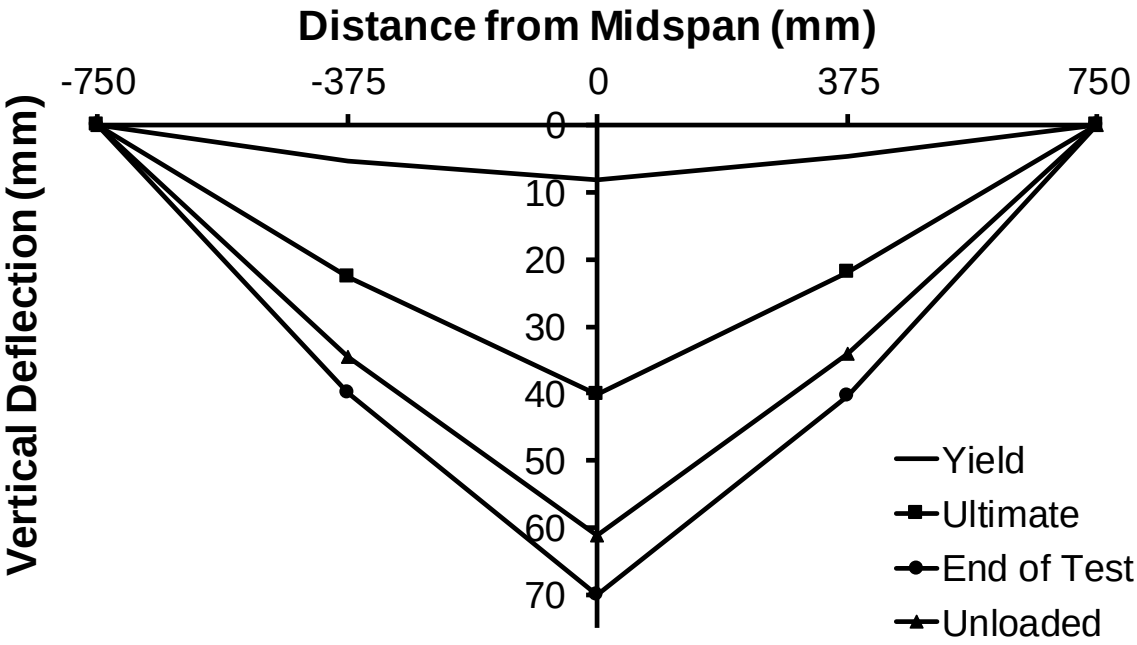

Figure 4.8: Deflection profile of 40RB7L-B specimen

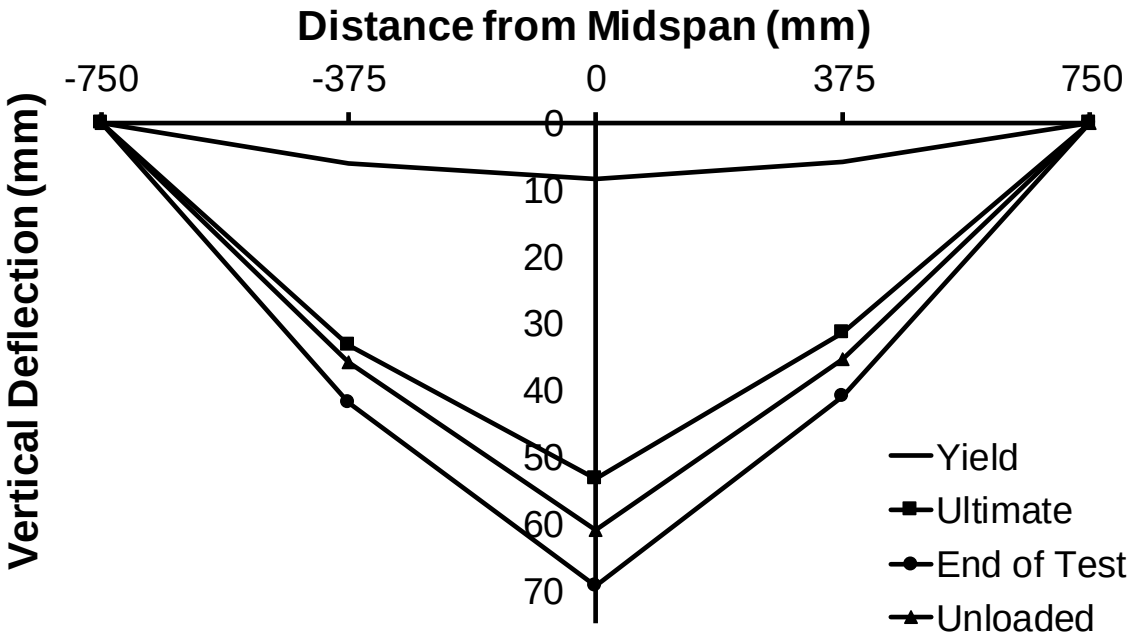

Figure 4.9: Deflection profile of 40RB10L-B specimen

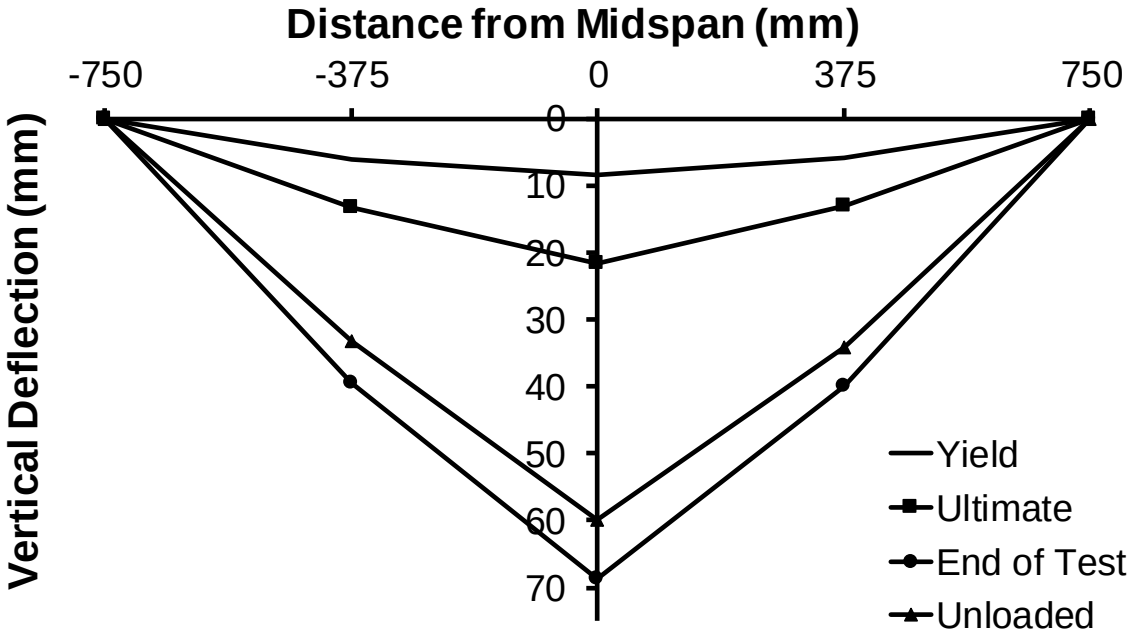

Figure 4.10: Deflection profile of 40RB3L-C specimen

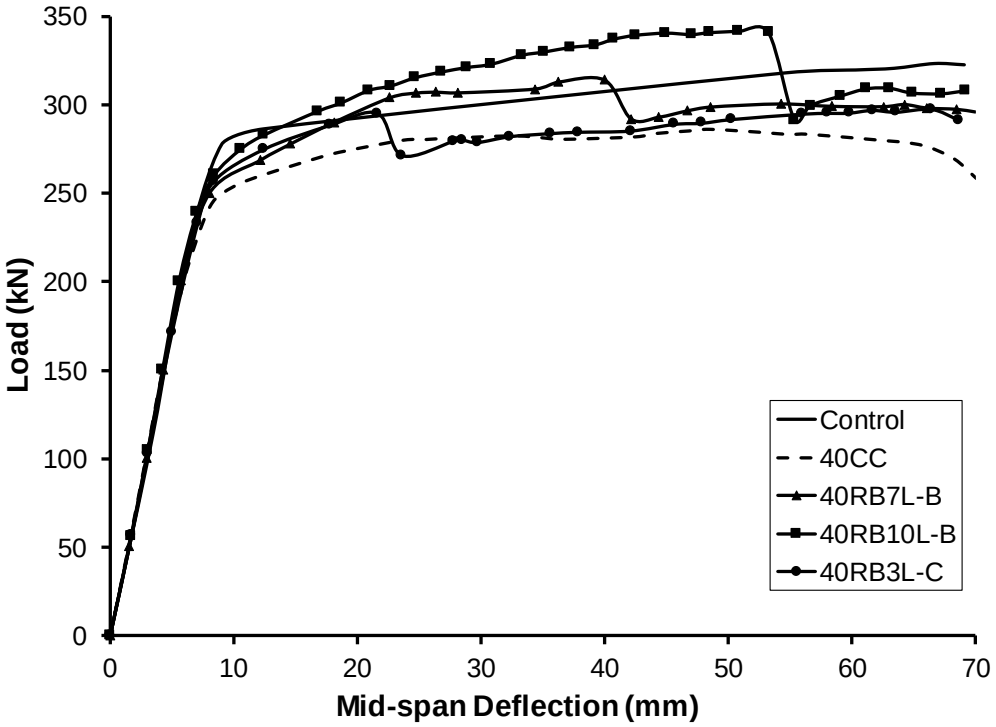

Figure 4.11: Load-deflection curve of 40% corrosion rehabilitated specimens (BFRP & CFRP)

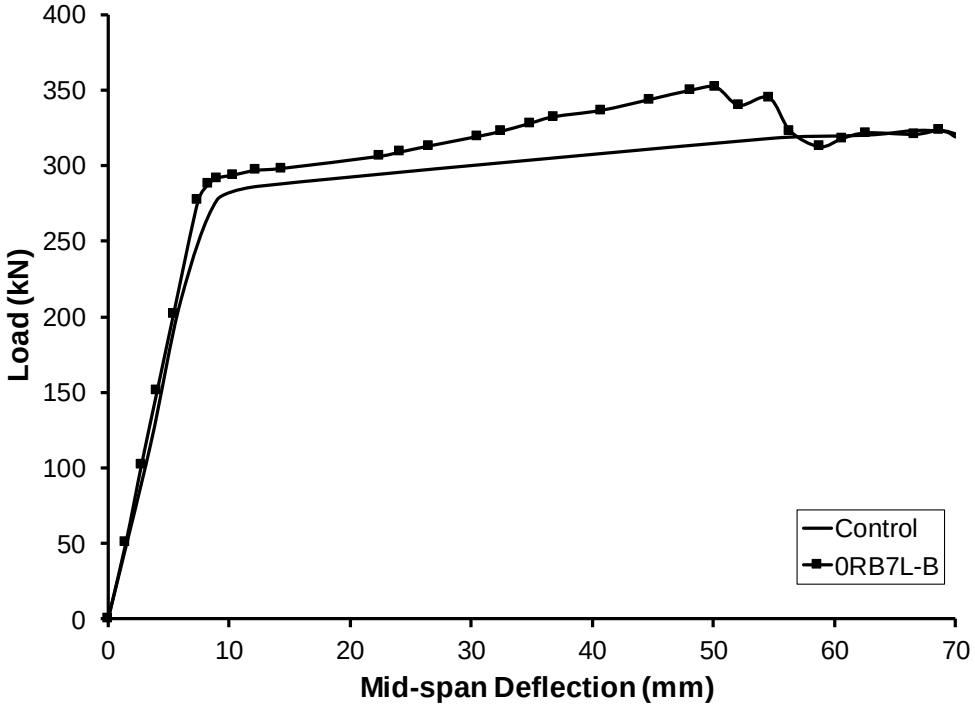

Figure 4.12: Load-deflection curve of strengthened and control specimen

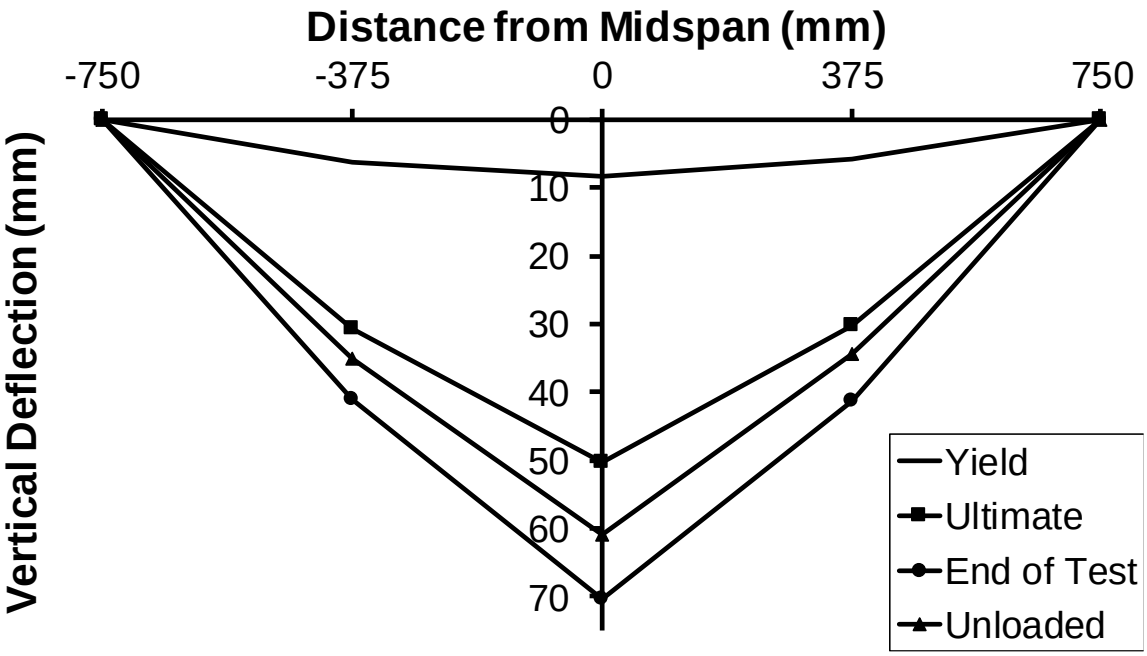

Figure 4.13: Deflection profile of 0RB7L-B specimen

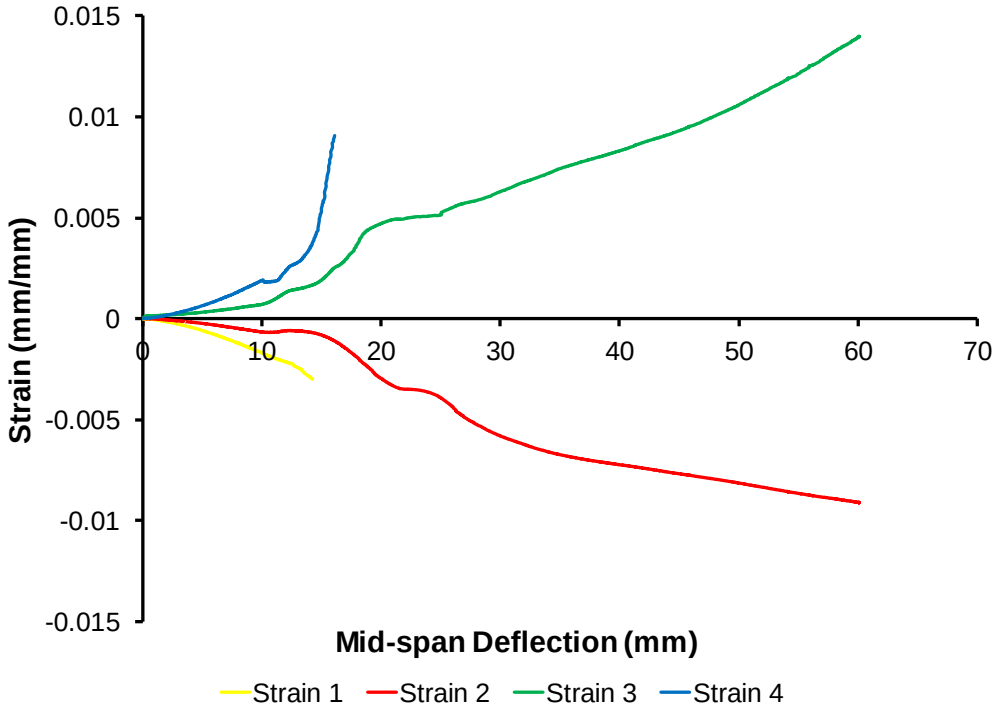

Figure 4.14: Strain-deflection curve of control specimen

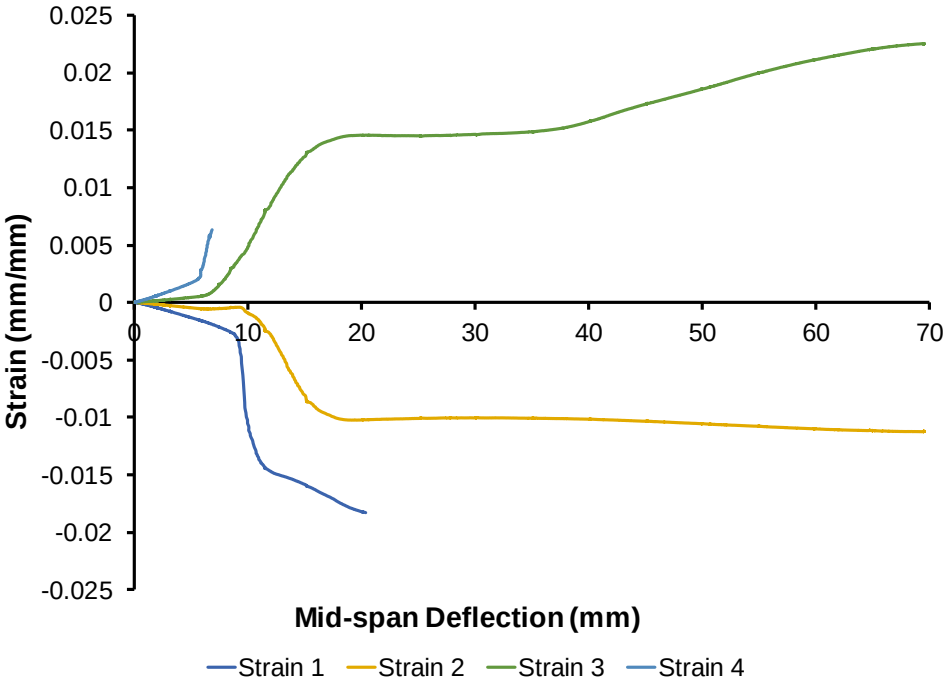

Figure 4.15: Strain-deflection curve of 20CC specimen

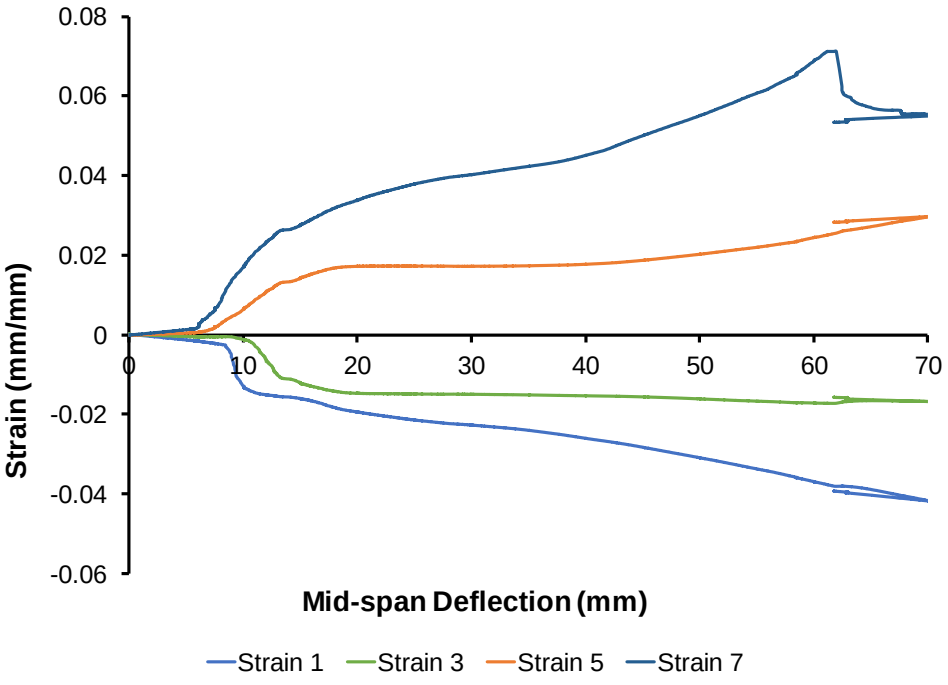

Figure 4.16: Strain-deflection curve of 20RB4L-B specimen

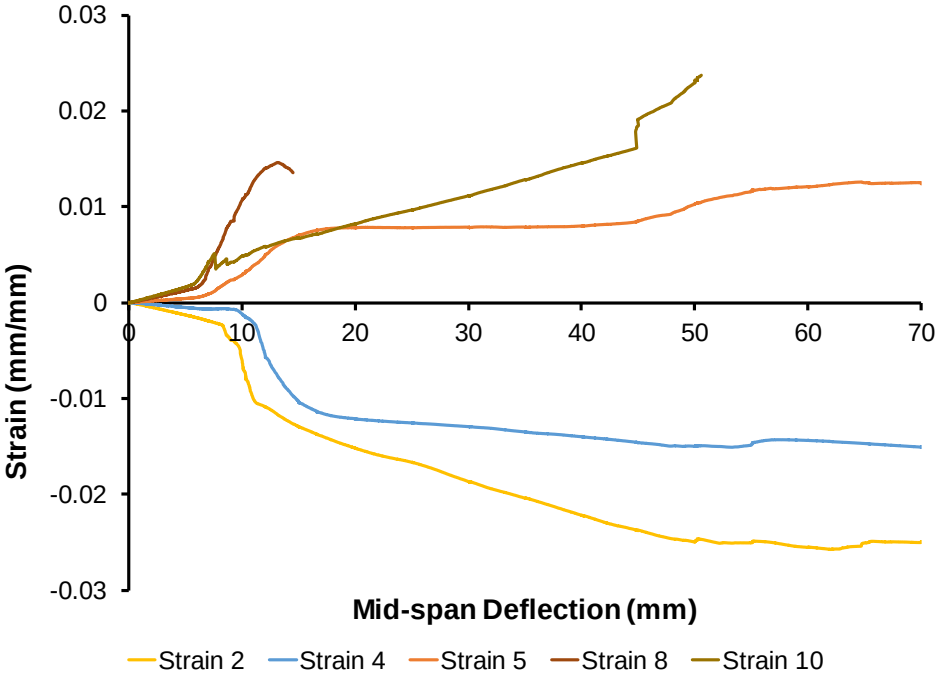

Figure 4.17: Strain-deflection curve of 20RB7L-B specimen

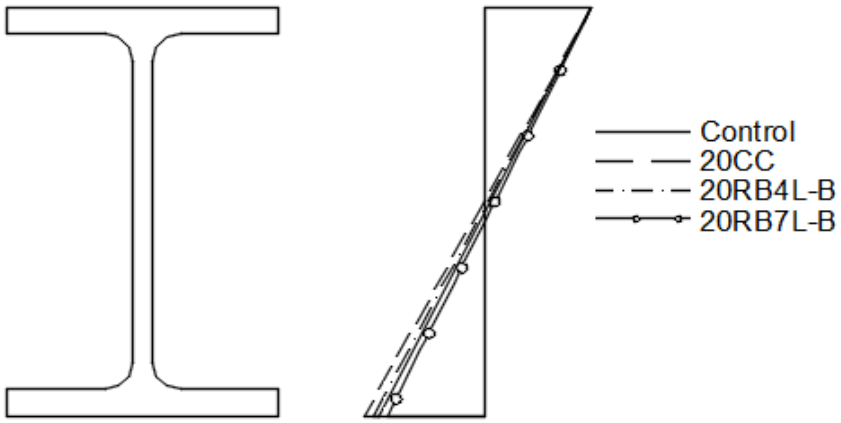

Figure 4.18: Neutral axis depth of 20% corrosion rehabilitated specimens

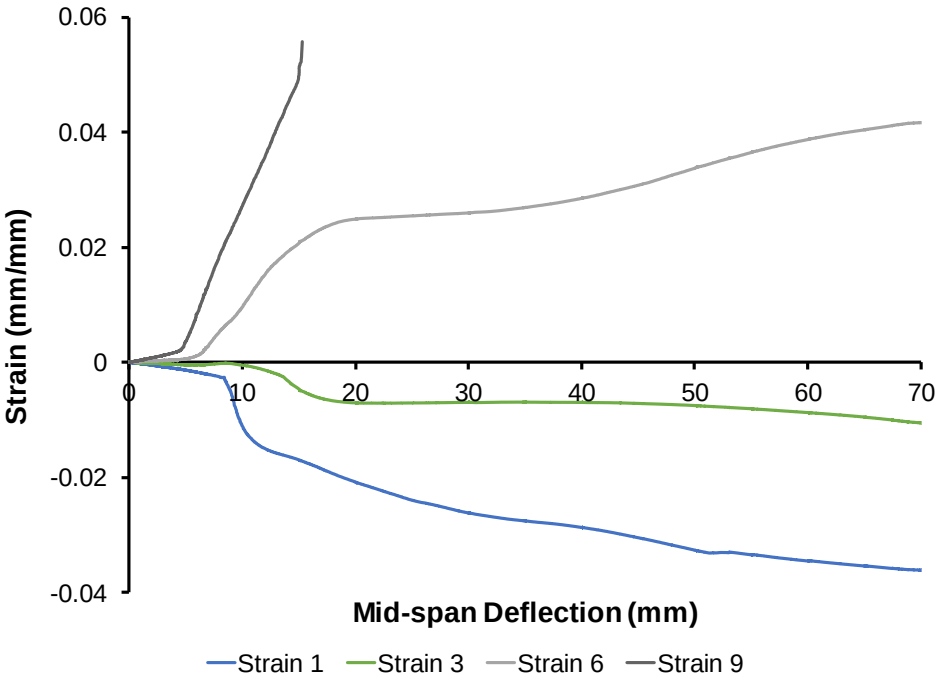

Figure 4.19: Strain-deflection curve of 40CC specimen

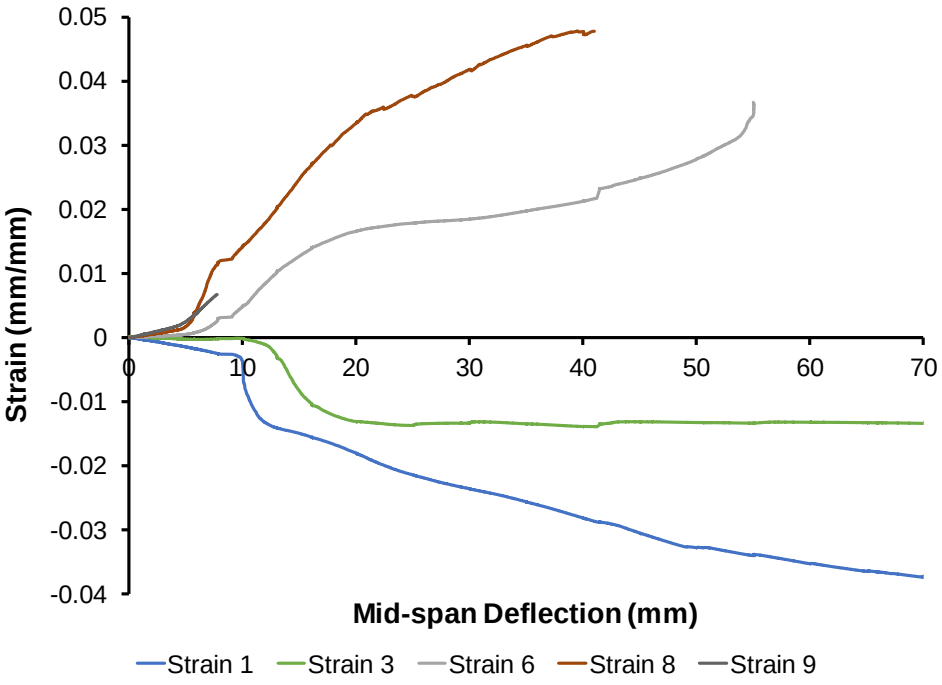

Figure 4.20: Strain-deflection curve of 40RB7L-B specimen

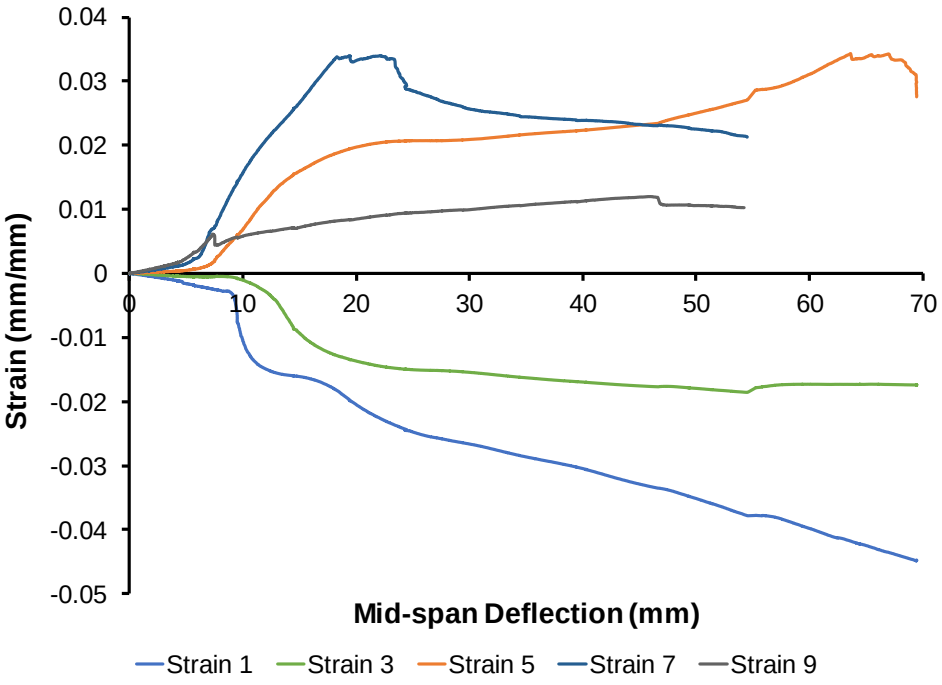

Figure 4.21: Strain-deflection curve of 40RB10L-B specimen

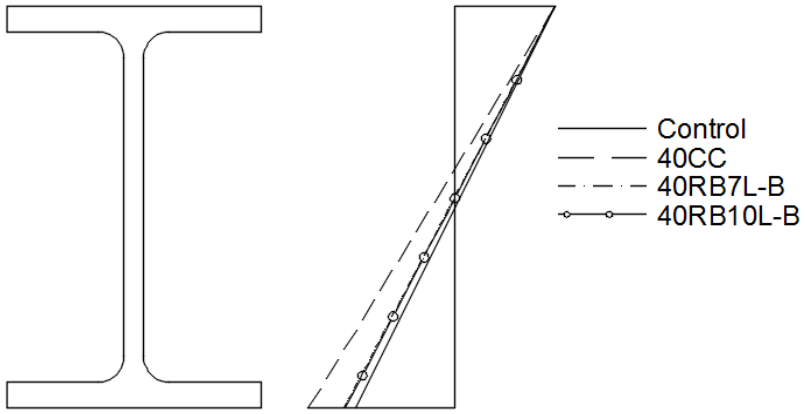

Figure 4.22: Neutral axis depth of 40% corrosion rehabilitated specimens with BFRP

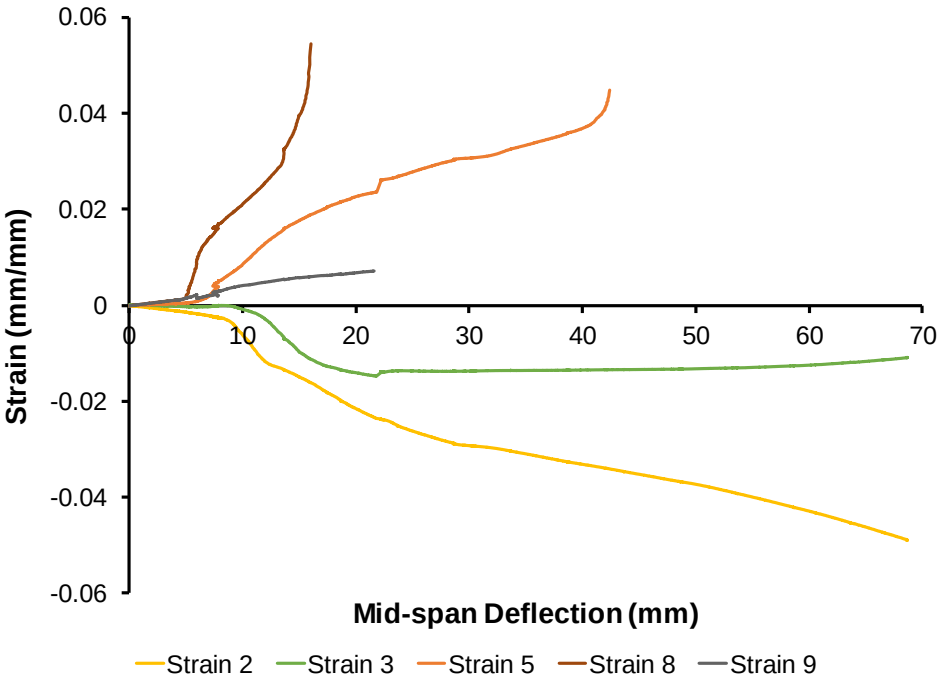

Figure 4.23: Strain-deflection curve of 40RB3L-C specimen

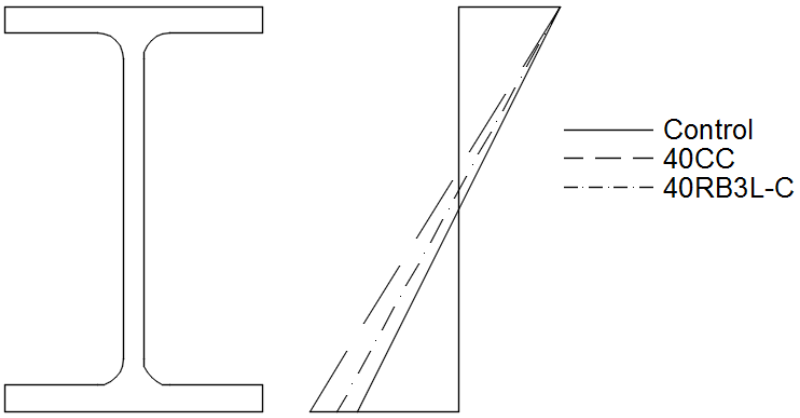

Figure 4.24: Strain compatibility of 40RB3L-C specimen

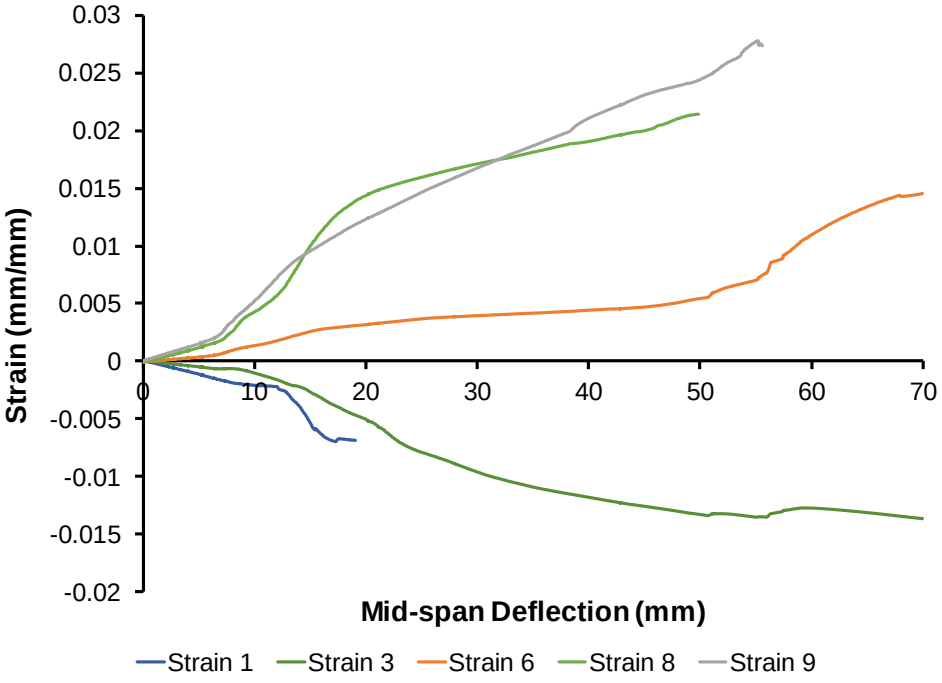

Figure 4.25: Strain-deflection curve of 0RB7L-B specimen

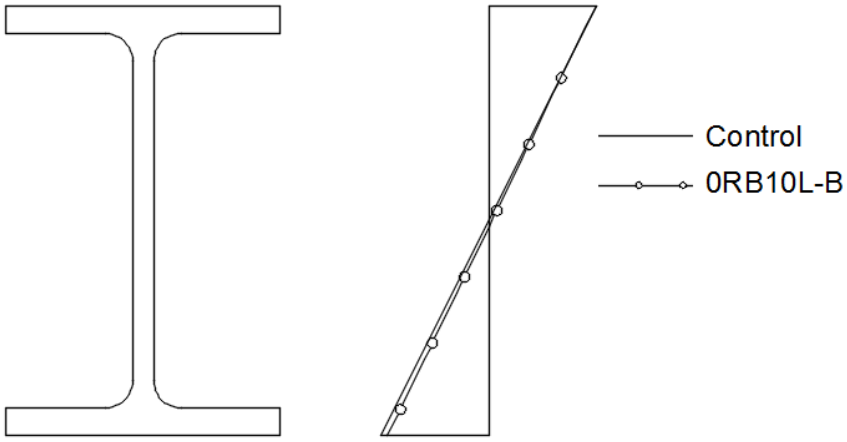

Figure 4.26: Strain compatibility of control and 0RB7L-B specimen

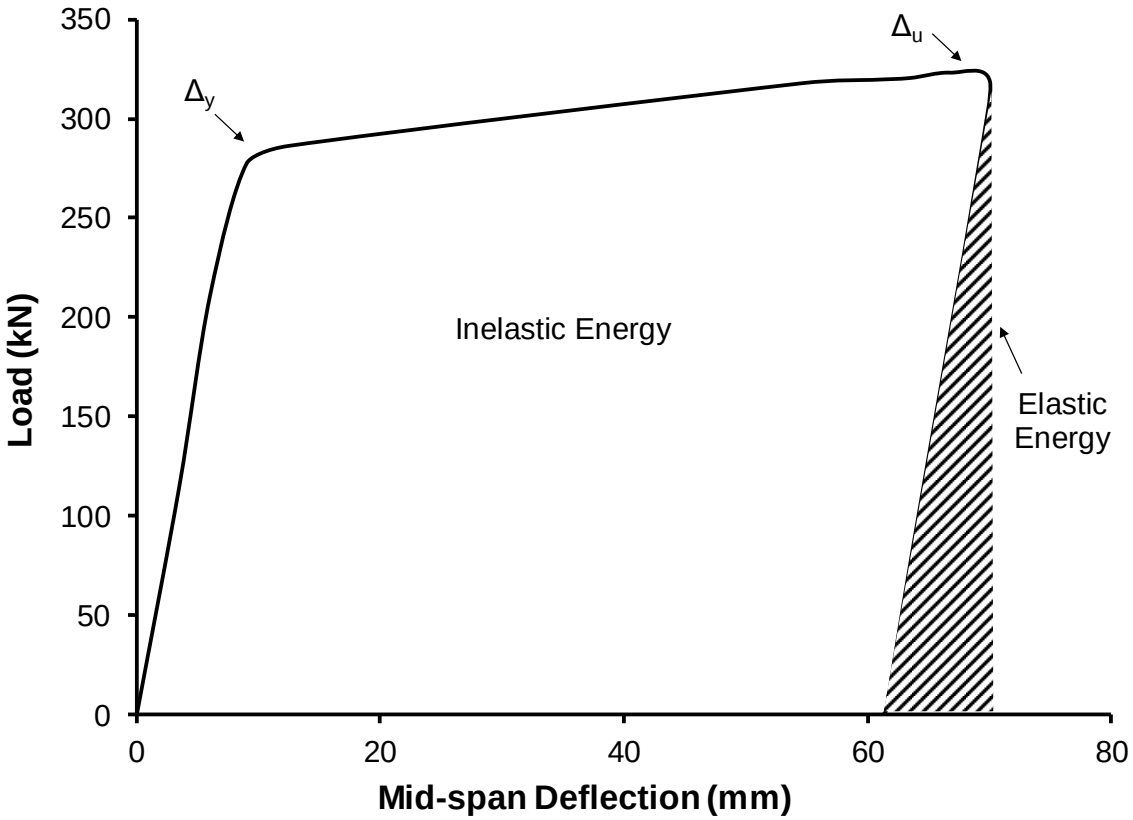

Figure 4.27: Ductility assessment based on energy dissipation

CHAPTER 5

Finite Element Analysis[5]

5.1 General

Experimental techniques are the most reliable method of understanding the behaviour of steel beams rehabilitated using BFRP fabrics. However, experimental techniques are expensive and time consuming. Hence, numerical technique using finite element method (FEM) was used to undertake a parametric study for determining the optimum thickness of BFRP fabrics needed for rehabilitation. The finite element (FE) model was developed using commercially available FE software, ABAQUS (SIMULIA 2016).

The specimens 0RB7L-B and 40RB3L-C were not modelled, as these two specimens were not directly related to the main objective of this study.

5.2 Geometry and Boundary Conditions

In order to simulate the pin and roller supports, only a line along the width of the beam was constrained to allow the supports to rotate realistically. The pin support was constrained in displacements *u1*, *u2*, and *u3*. The roller support was constrained in displacements *u1* and *u2*. The model configuration is shown in Figure 5.1.

The flange thickness of a stock W150x24 beam is 10.3 mm, however, after measuring the flange thickness of the specimen before testing, it was found the average flange thickness was 10.2 mm. Therefore, all models were created with a flange thickness of 10.2 mm.

[5] This chapter is the outcome of joint research

The corrosion of the steel beams was simulated by extruding a cut along the bottom flange of the beams. The two depths of corrosion were 2.04 mm (20% corrosion) and 4.08 mm (40% corrosion).

Epoxy resin was not simulated in the model because debonding did not occur in any of the rehabilitated beams as can be seen from the cross-sectional view of a rehabilitated beam shown in Figure 5.2. Hence, the BFRP was attached to the beam using a tie constraint. The filler material was also not simulated because it does not contribute to the structural behaviour, due to its' short bond length. The rehabilitation scheme of a modelled beam is shown in Figure 5.3.

5.3 Material Properties

The materials used in the models were steel and BFRP. The properties of the materials are discussed below.

5.3.1 Steel

A total of five steel coupons were tested with accordance to ASTM E8/E8M-15a as described in Section 3.4.1. The behaviour of the coupons was almost identical and the average values of yield stress and modulus of elasticity were used for the model. The true stress-strain curve of the steel was used for the model as shown in Figure 5.4.

Isotropic hardening was used in this model, and this is a very common strain hardening model found in finite element software. For isotropic hardening, the yield surface is assumed to maintain its' shape and the shape expands as hardening occurs, as shown in Figure 5.5. This hardening model ignores the Bauschinger effect, however, since there are no reversals in elastic-plastic strain, the isotropic hardening model can be used.

5.3.2 Basalt Fibre Reinforced Polymer

BFRP coupons were tested according to the ASTM standard D3039/D3039M–14, as discussed in Section 3.4.3. A linear elastic load-deflection behaviour was observed from the coupon tests, thus, the BFRP elasticity was modelled using the lamina criteria with a modulus of elasticity (E1) of 23.1 GPa and a Poisson's ratio of 0.35. For other values such as shear modulus and modulus of elasticity in the secondary direction (E2), very low values were used due to its' insignificance.

In order to simulate the damage to BFRP fabric, the criterion Hashin damage, fail stress and fail strain were utilized. The ultimate longitudinal tensile stress and strain used were 459 MPa and 0.022, respectively. Very low values were used for irrelevant properties such as; compressive strength, transverse tensile strength etc.

5.4 Mesh Selection

A 10 mm mesh was applied to the steel beams and the BFRP fabric. This mesh size was selected by conducting a mesh convergence study on specimen 40RB10L-B, with mesh sizes of 6 mm, 10 mm, 15 mm, and 20 mm. The load-deflection behaviour of models with these meshes is shown in Figure 5.6.

The load-deflection behaviour of all the models is identical until about a mid-span deflection of 30 mm. The load capacity of the model with the 20 mm mesh begins to decrease after this deflection. However, the load capacity of the model with the 15 mm mesh increases continuously and does not begin to decrease until about a deflection of 65 mm. Hence, the ideal load-deflection behaviour lies between these two curves and more desirable load-deflection curves were attained by using finer mesh sizes.

Models with mesh sizes 6 mm, and 10 mm exhibited very similar load-deflection behaviours as shown in Figure 5.6. The load capacities of these two models do not decrease prematurely or delay the decrease past the rupture point. Both models begin decreasing at

a mid-span deflection of about 50 mm, which is very close to the actual rupture point (53 mm) of 40RB10L-B. Hence, the load-deflection behaviours of these two models are much more desirable as the modelled results are very close to the experimental results.

The results of the models with 6 mm mesh and 10 mm mesh are very similar; however, a much larger amount of computational time is required to run the model with the 6 mm mesh. Hence, the 10 mm mesh was selected as the most optimum mesh size.

5.5 Model Validation

5.5.1 Control and Control Corrosion Specimen

Before modelling the rehabilitated specimen, the control and control corrosion specimen were first modelled in order to ensure the load-deflection behaviour of the bare steel beams can be modelled accurately. The load-deflection behaviour of the modelled and experimental control and control corrosion specimens are shown in Figures 5.7 – 5.9. The modelled load-deflection behaviour of these three specimen were extremely close to the experimental results, therefore, BFRP fabric was added to create models for the rehabilitated specimen.

5.5.2 Rehabilitated Specimen

The load-deflection curves of the modelled and experimental rehabilitated specimen are shown in Figures 5.10 - 5.13. The pre and post-yield load-deflection behaviour of the modelled specimen were very close to the experimental specimen. However, the rupture of BFRP could not be modelled, and was initiated manually.

The comparison of the yield loads and elastic stiffness between the experimental and modelled specimen are shown in Tables 5.1 and 5.2. The yield loads of all the modelled beams were within 5% of the experimental values, which indicates a very good correlation between the yield load of modelled and experimental specimens.

The modelled specimens had a greater stiffness than the experimental specimens, as shown in Table 5.2. Specimen 20RB4L-B showed the largest difference in stiffness as it showed an increase of 17.6% in elastic stiffness. The elastic stiffness increase of the three other rehabilitated specimens were less than 10%. Slightly increased elastic stiffness is typical for finite element models, due to the discretization involved in FE modelling.

Figure 5.14 shows the strain comparison of the 20RB4L-B specimen. All of the strain gages show a good correlation between the modelled and experimental data. The correlation between the experimental and model strains is extremely good until about 10 mm, which also explains the extremely close yield load capacities found for this specimen. After a deflection of 10 mm, the model strains increase at rate slightly lower than the experimental strains while following the same pattern as the experimental strains.

The strain comparison of the specimen 20RB7L-B is shown in Figure 5.15. Strain gage 1 failed at a deflection of 10 mm and the strain data for remainder of the rest was removed. A good correlation between all strain gages was observed.

Figure 5.16 shows the strain comparison for the 40RB7L-B specimen. Strain gages 1, 3, and 5 showed extremely good correlation with the experimental data, while the correlation of strain gage 7 was slightly lower. The rate of strain increase of the modelled strain gage 7 was slightly higher than the experimental. The strain data of strain gages 5 and 7 failed at a deflection of 40 mm, hence, the strain data after this deflection was removed.

The strain comparison of specimen 40RB10L-B is shown in Figure 5.17. The data of strain gages 5 and 7 were terminated at deflections of 40 and 20 mm, respectively, due to premature strain gage failure. All of the strain gages showed a very good correlation between the experimental and modelled data.

For all four models, the majority of the strain gages had a very good correlation between the experimental and modelled data. However, there was a large difference between the elastic stiffness of the modelled and experimental specimens, hence, this model cannot be used to conduct a parametric study for the rehabilitation of elastic stiffness.

5.6 Parametric Study

Restoration of the yield load was a primary objective of this parametric study, since under service load a structural member is not expected to be subjected to a load higher than its yield load. Hence, the validated FE model was used to determine the thickness of BFRP fabric required for restoring the yield load of corroded beams to the level of a control (virgin) specimen. The acquired numerical data was then curve-fit as shown in Figure 5.18, and the resulting equation (Equation 5.1) was obtained. In the experimental study, a maximum of 10 layers of BFRP was used for the 40RB10L-B specimen. This specimen could not restore the yield load to the level of a control (virgin) specimen. From the FE analysis, it can be found that 15 layers (6.75 mm) of BFRP fabric was needed to restore the yield load capacity.

The results of the experimental study showed that the earliest rupture of BFRP fabric occurred at a mid-span deflection of 40 mm (Figures 4.1 and 4.6). Hence, this deflection limit was used as a conservative estimate of the BFRP rupture-induced failure for the beams used in the numerical study. A parametric study was conducted to determine the thickness of BFRP fabric required for restoring the load capacity of corroded steel specimens to the level of a control (virgin) specimen at rupture (40 mm mid-span deflection). A linear relationship was found as shown in Figure 5.19, and Equation 5.2.

$$T = 0.0001c^3 - 0.0049c^2 + 0.1939c \qquad \text{Equation 5.1}$$

$$T = 0.0385c \qquad \text{Equation 5.2}$$

In the above equations, T is the thickness of BFRP fabric required to rehabilitate the yield load in Equation 5.1 and the rupture load in Equation 5.2, c is the percentage of corrosion of the beam. The maximum corrosion in the FE analyses was set to 60% of the flange thickness, as the rehabilitation of larger amounts of corrosion may not be practical.

5.7 Summary

The comparison of these results show that the load-deflection behaviour of the modelled specimens is very accurate and these models can be used to determine the optimum BFRP thickness required to restore the yield and BFRP rupture induced failure loads.

Table 5.1: Comparison of yield loads between experimental and modelled specimens

	Experimental Yield Load (kN)	Model Yield Load (kN)	Difference in Yield Load (%)
20RB4L-B	272	271	0.4
20RB7L-B	277	276	0.4
40RB7L-B	250	258	3.2
40RB10L-B	260	262	0.8

Table 5.2: Comparison of elastic stiffness between experimental and modelled specimens

	Experimental Elastic Stiffness (kN/mm)	Model Elastic Stiffness (kN/mm)	Difference in Elastic Stiffness (%)
20RB4L-B	30.1	35.4	17.6
20RB7L-B	32.6	34.3	5.2
40RB7L-B	31.1	33.4	7.4
40RB10L-B	30.8	33.8	9.7

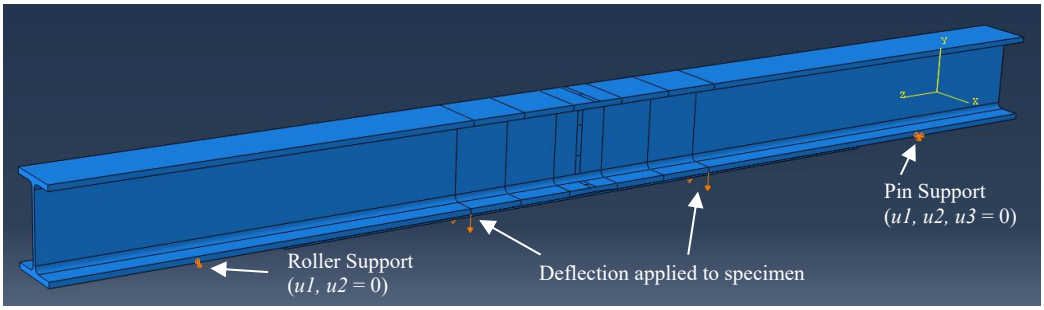

Figure 5.1: Model configuration

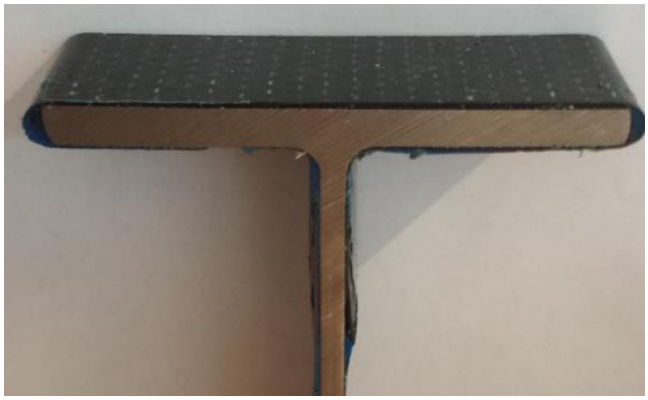

Figure 5.2: Cross-section of rehabilitated beam

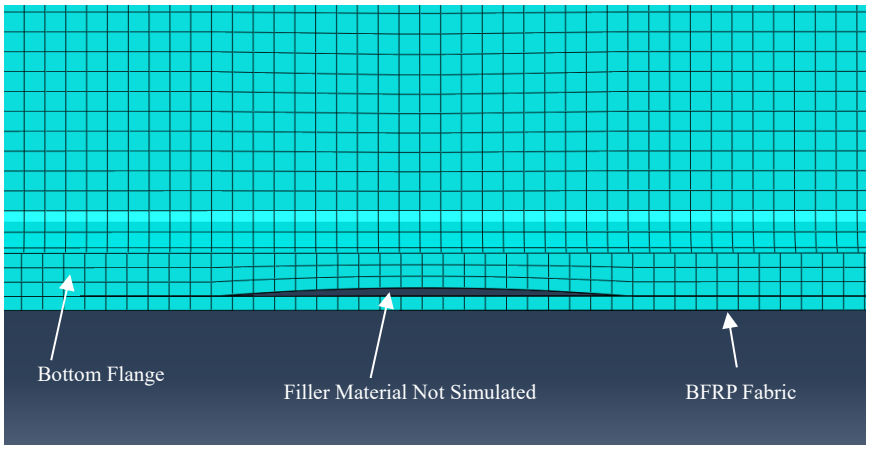

Figure 5.3: Rehabilitation scheme of a modelled specimen

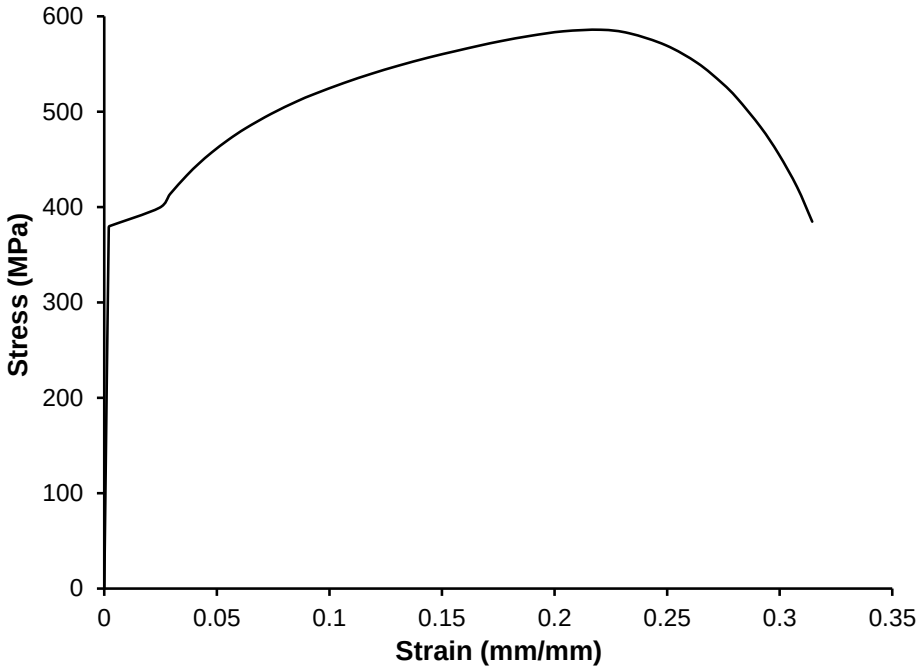

Figure 5.4: True stress-strain curve of steel

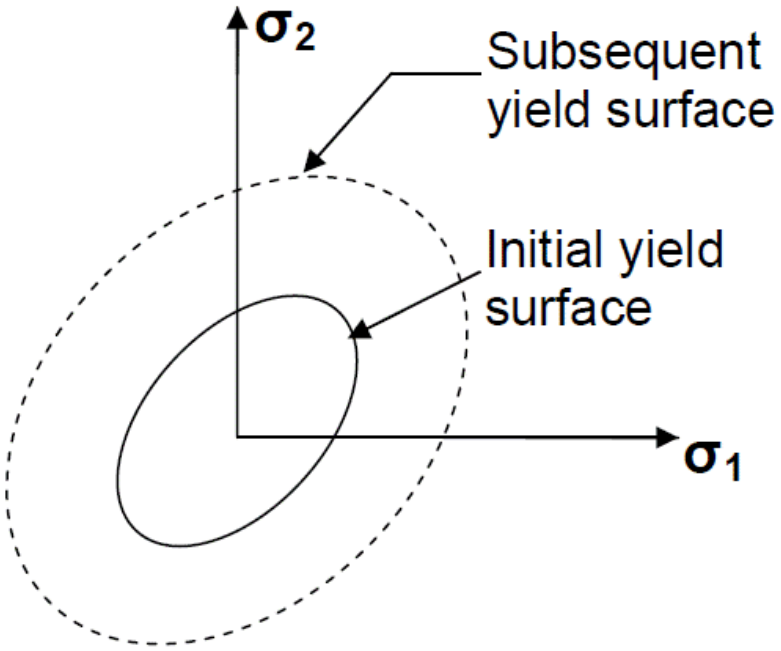

Figure 5.5: Isotropic hardening rule

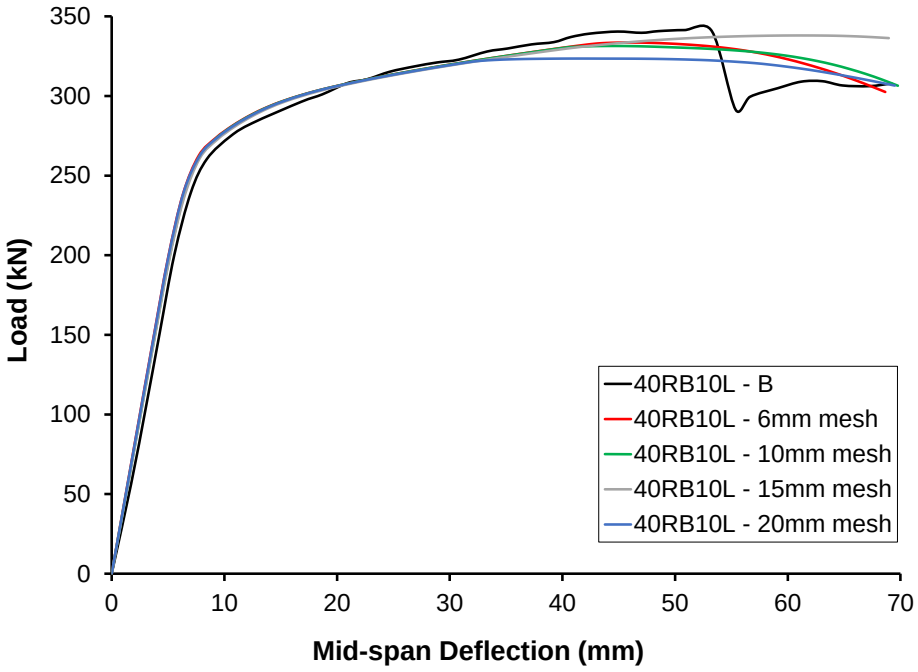

Figure 5.6: Load-deflection behaviour of meshed models

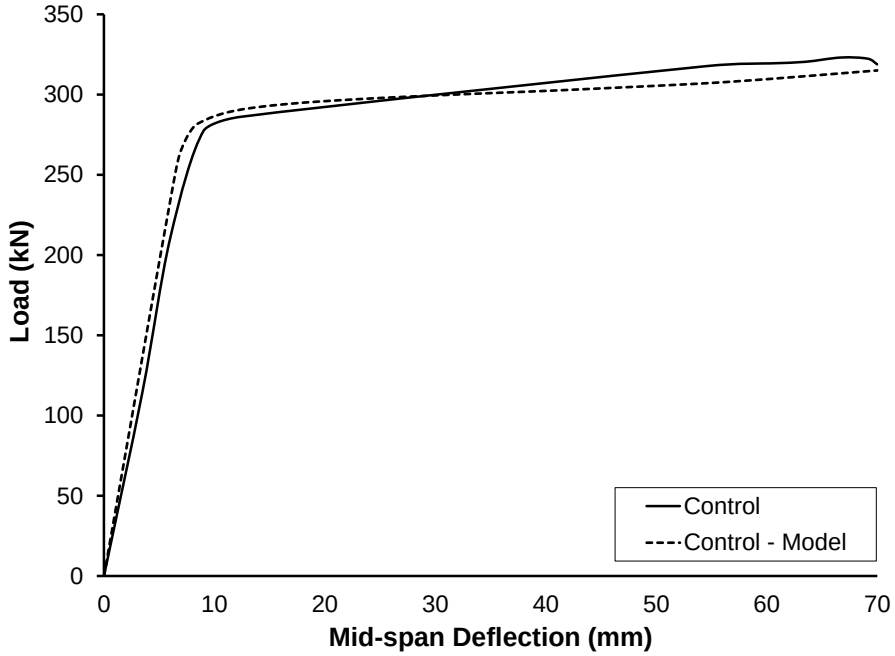

Figure 5.7: Finite element model of control specimen

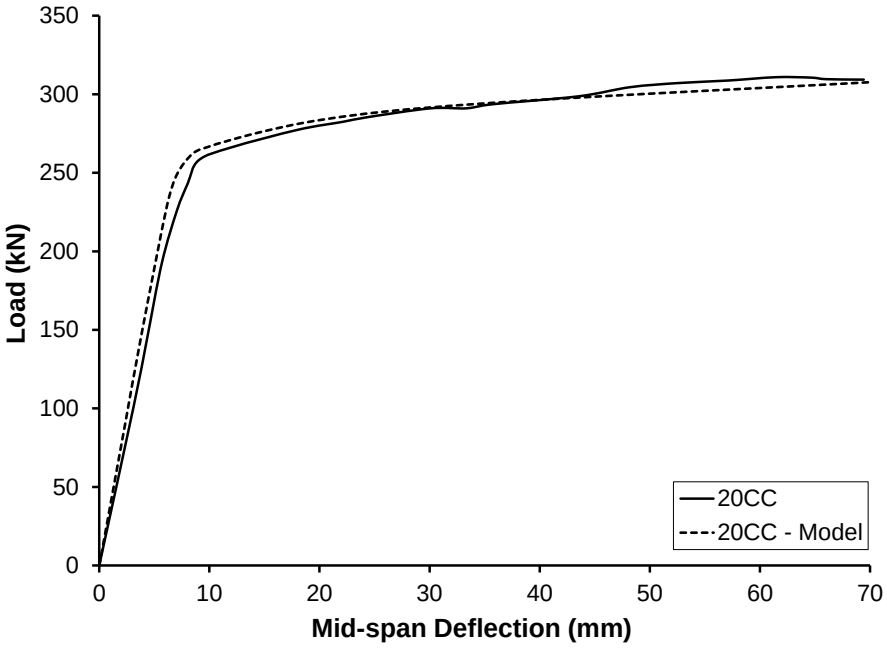

Figure 5.8: Finite element model of 20CC specimen

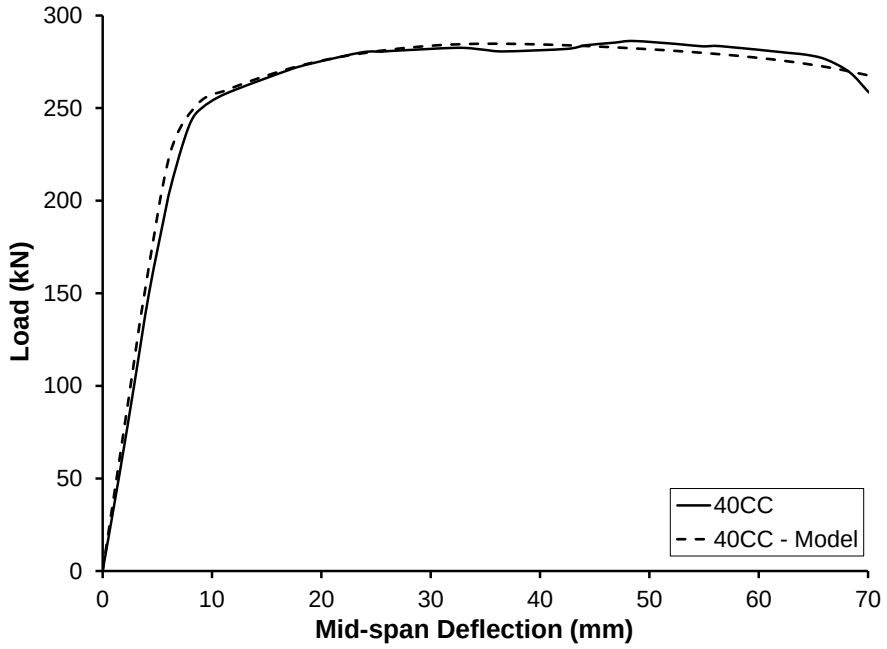

Figure 5.9: Finite element model of 40CC specimen

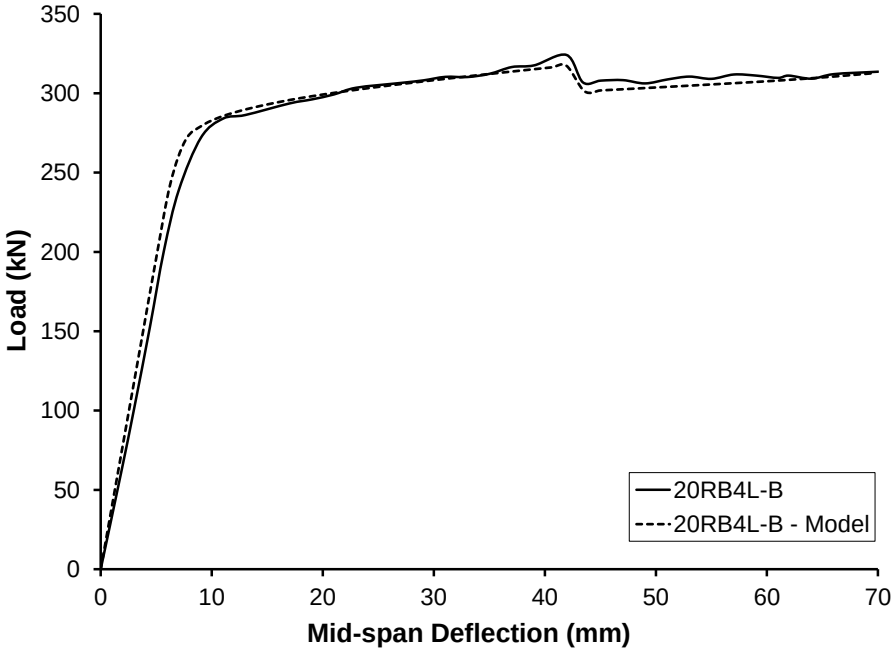

Figure 5.10: Finite element model of 20RB4L-B specimen

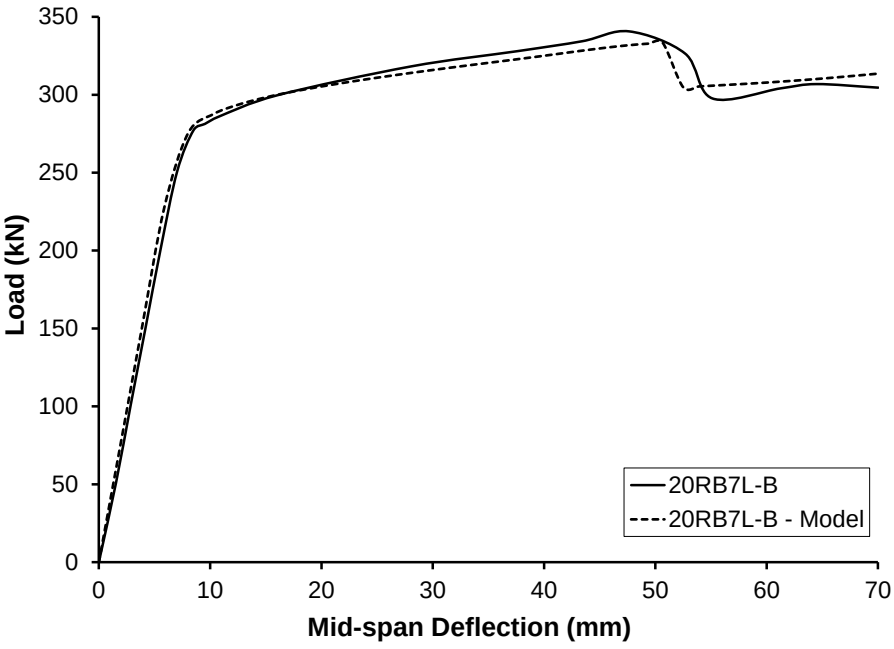

Figure 5.11: Finite element model of 20RB7L-B specimen

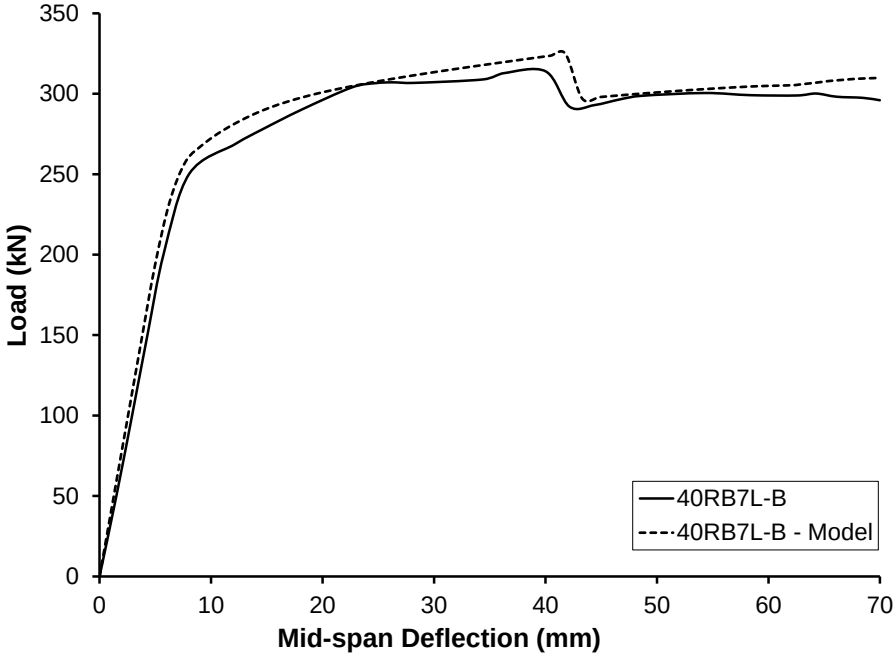

Figure 5.12: Finite element model of 40RB7L-B specimen

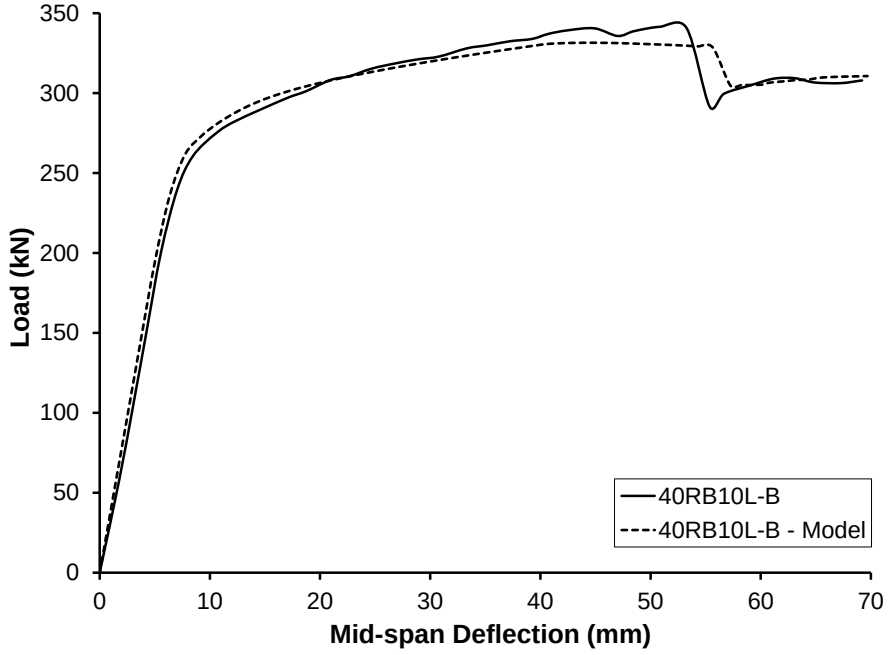

Figure 5.13: Finite element model of 40RB10L-B specimen

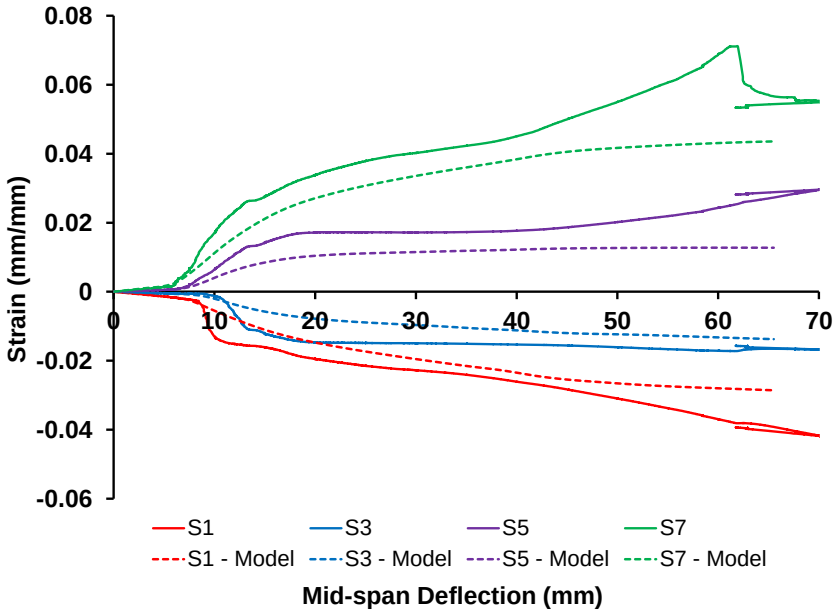

Figure 5.14: Strain comparison of 20RB4L-B specimen

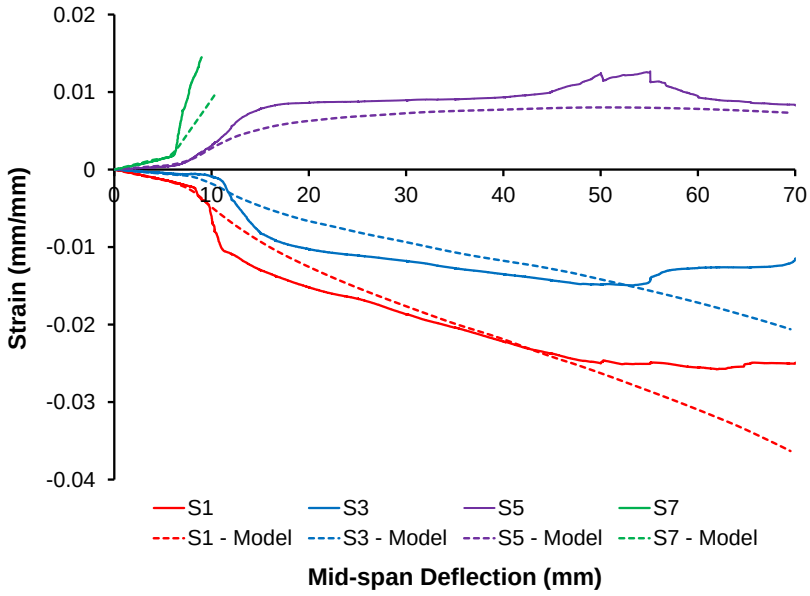

Figure 5.15: Strain comparison of 20RB7L-B specimen

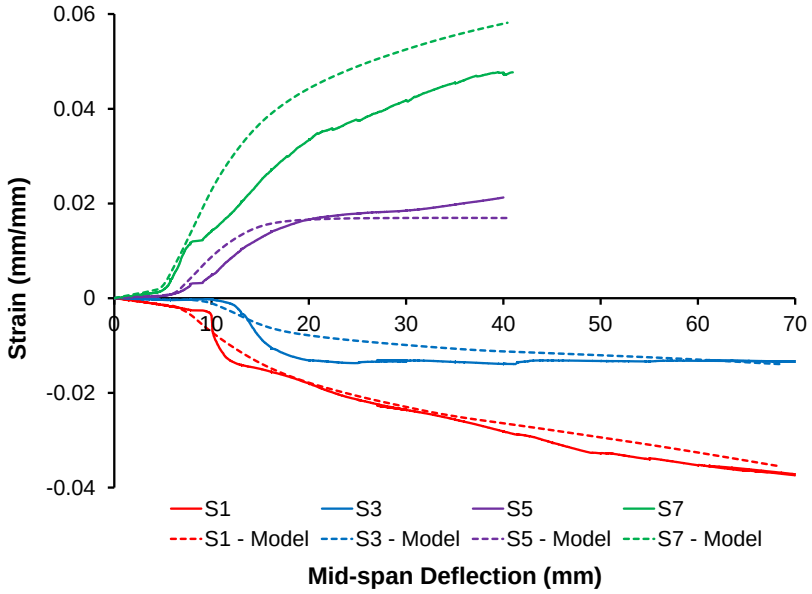

Figure 5.16: Strain comparison of 40RB7L-B specimen

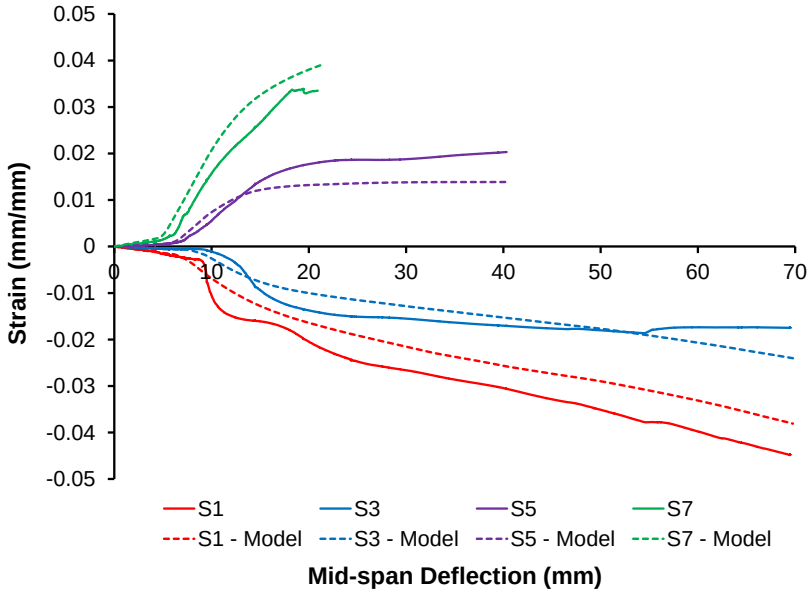

Figure 5.17: Strain comparison of 40RB10L-B specimen

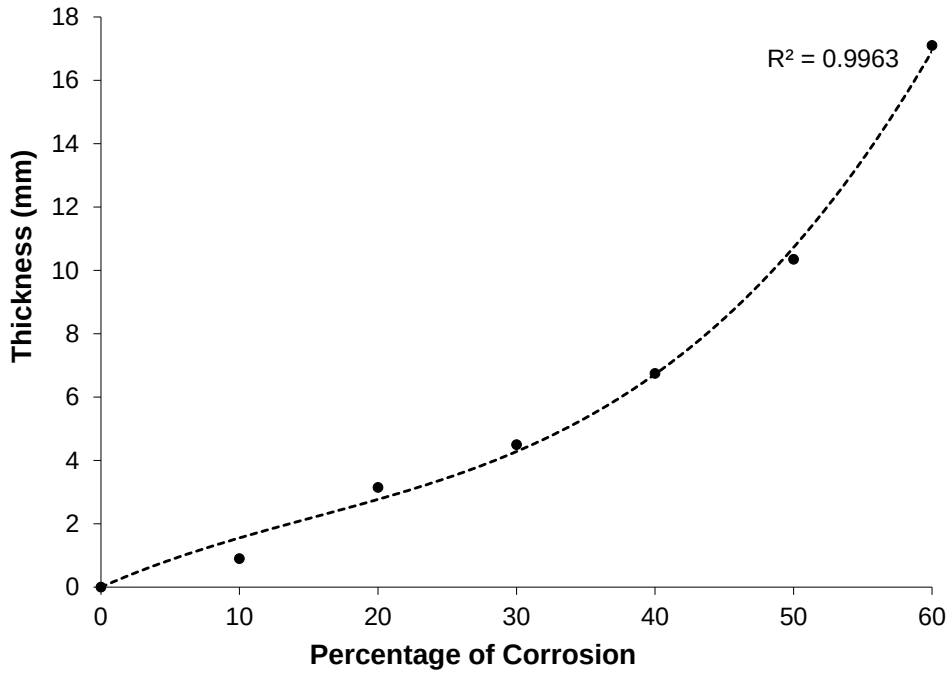

Figure 5.18: Thickness of BFRP fabric required for the rehabilitation of yield load

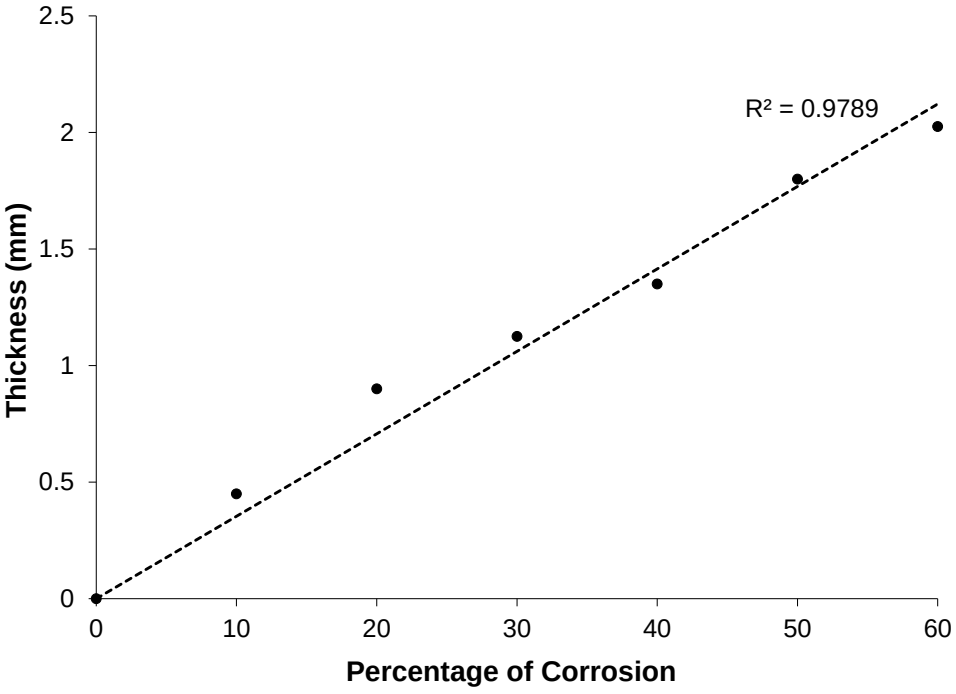

Figure 5.19: Thickness of BFRP fabric required for the rehabilitation of BFRP rupture-induced load

CHAPTER 6

Conclusions and Recommendations[6]

This thesis presents a technique for the flexural rehabilitation of corroded steel beams using BFRP fabric. Based on the results of the experimental study, and results of the finite element analysis, the following conclusions are made. However, these conclusions may be limited to the scope of the current study.

1. The yield load, ultimate load, and elastic stiffness of a steel beam with 20% corrosion in the bottom flange can be fully restored to the level of an uncorroded (virgin) beam, if a sufficient thickness of BFRP fabric is used and debonding is avoided.
2. The ultimate load and elastic stiffness of a steel beam with 40% corrosion in the bottom flange can also be fully restored to the level of an uncorroded (virgin) beam. However, restoration of the yield load of these rehabilitated specimen with 40% corrosion needs a larger number of BFRP layers. The numerical study found that for 40% corrosion, about 6.75 mm (15 layers of BFRP fabric) thick BFRP is needed.
3. The effectiveness of the rehabilitation scheme was observed by the significant improvement of the neutral axis depth of the rehabilitated specimens, as compared to the corroded specimens.
4. The ductility of a rehabilitated beam was found to be lower than the respective control (virgin) beam specimen. However, the ductility increases with the increasing number of BFRP fabric layers.
5. Empirical relationships using the FE analysis data are proposed and these relationships can be used for determining the optimum thickness of BFRP layers required to be able to restore the yield and BFRP rupture failure capacities.
6. Research studies using BFRP fabric for the shear rehabilitation/strengthening of steel beams should be conducted to realize the full potential of this fabric.

[6] This chapter is the outcome of joint research

REFERENCES

Adhikari R.S., Moselhi O., and Bagchi A. (2013), "A study of image-based element condition index for bridge inspection," *ISARC 2013 – 30th International Symposium on Automation and Robotics in the Construction, Mining and Petroleum Industries, Held in Conjunction with the World Mining Congress*, Montreal, August.

Al-Saidy A.H., Klaiber F.W., and Wipf T.J. (2004), "Repair of steel composite beams with carbon fiber-reinforced polymer plates," *Journal of Composites for Construction*, **8**(2), 163-172.

ASCE: Infrastructure Report Card (2013), 2013 Report Card for America's Infrastructure; American Society of Civil Engineers. www.infrastructurereportcard.org/a/#p/bridges/overview

ASTM (2014). Standard Test Method for Tensile Properties of Polymer Matrix Composite Materials. D3039/D3039M-14, ASTM International, PA.

ASTM (2015). Standard Test Methods for Tension Testing of Metallic Materials. E8/E8M-15a, ASTM International, PA.

Composites UK (2014), Methods of Composite Manufacture, Composites UK, Herts, United Kingdom. www.compositesuk.co.uk/composite-materials/processes

Chen M. and Das S. (2009), "Experimental study on repair of corroded steel beam using CFRP," *Steel and Composite Structures*, **9**(2), 103-118.

CSA S16-09 (2014), Handbook of Steel Construction, Canadian Institute of Steel Construction; Mississauga, Canada.

El Damatty A.A., Abushagur M., and Youssef M.A. (2003), "Experimental and analytical investigation of steel beams rehabilitated using GFRP sheets," *Steel and Composite Structures*, **3**(6), 421-438.

FHA: Federal Highway Administration (2017), Deficient Bridges by Highway System 2016; United States Department of Transportation, Washington, USA. www.fhwa.dot.gov/bridge/nbi/no-10/defbr16.cfm

Galal K., Seif H.M., and Tirca L. (2012), "Bond characteristics of various NSM FRP reinforcements in concrete," *Journal of Composites for Construction*, **16**(3), 265-276.

Garden H., Hollaway L., Thorne A. (1997), "A preliminary evaluation of carbon fibre reinforced polymer plates for strengthening reinforced concrete members", *Proceedings of the Institution of Civil Engineers – Structures and Buildings, N.A., May.*

Gillespie Jr. J. and Mertz D. (1996), "Rehabilitation of steel bridge girders through the application of advanced composite materials," IDEA Project Final Report – Contract NCHRP-93-ID011, Transportation Research Board – National Research Council.

Hammad A., Yan J., and Mostofi B. (2007), "Recent Development of Bridge Management Systems in Canada," *Annual Conference of the Transportation Association of Canada*, Saskatoon, October.

Harajli M.H. and Soudki K.A. (2003), "Shear strengthening of interior slab – column connections using carbon fiber-reinforced polymer sheets," *Journal of Composites for Construction*, **7**(2), 145-153.

Huang L., Li Y., Wang Y. (2013), "Strengthening effects of BFRP on reinforced concrete beams," *Journal of Southeast University*, **29**(2), 182-186.

Liu X., Silva P.F., and Nanni A. (2001), "Rehabilitation of steel bridge members with FRP members with FRP composite materials," *Proceedings of CCC 2001, Composites in Construction*, Porto, October.

Manalo A., Sirimanna C., Karunasena W., McGarva L., and Falzon P. (2016), "Pre-impregnated carbon fibre reinforced composite system for patch repair of steel I-beams," *Construction and Building Materials*, **105**(2016), 365-376.

McKnight S., Bourban P., Gillespie Jr. J., and Karbhari V. (1994), "Surface preparation of steel for adhesive bonding in rehabilitation applications", *Third Materials Engineering Conference, Infrastructure: New Materials and Methods of Repair*, San Diego, November.

NRC: National Research Council (2013), Critical Concrete Infrastructure: Extending the life of Canada's bridge network; National Research Council Canada. www.nrc-cnrc.gc.ca/ci-ic/article/v18n1-5

Photiou N.K., Hollaway L.C., and Chryssanthopoulos M.K. (2006). "Strengthening of an artificially degraded steel beam utilising a carbon/glass composite system," *Construction and Building Materials,* **20**(1-2), 11-21.

Sen R., Liby L., and Mullins G. (2001), "Strengthening steel bridge sections using CFRP laminates," *Composites: Part B*, **32**(2001), 309-322.

SIMULIA, 2016, Analysis User's Manuals, Dassault Systèmes Simulia Corp., Rising Sun Mills, Providence, RI, USA.

Sim J., Park C., and Moon D.Y. (2005), "Characteristics of basalt fiber as a strengthening material for concrete structures," *Composites: Part B*, **36**(2005), 504 – 512.

Soudki K. and Sherwood T. (2003), "Bond behaviour of corroded steel reinforcement in concrete wrapped with carbon fiber reinforced polymer sheets," *Journal of Materials in Civil Engineering,* **15**(4), 358-370.

Tavakkolizadeh M. and Saadatmanesh H. (2003), "Repair of damaged steel-concrete composite girders using carbon fiber-reinforced polymer sheets," *Journal of Composites for Construction*, **7**(4), 311-322.

Tomlinson D. and Fam A. (2014), "Performance of concrete beams reinforced with basalt FRP for flexure and shear," *Journal of Composites for Construction*, **19**(2), 1-10, 04014036.

Yuan F., Pan J., and Leung C.K.Y. (2013), "Flexural behaviours of ECC and concrete/ECC composite beams reinforced with basalt fiber-reinforced polymer," *Journal of Composites for Construction*, **17**(5), 591-602.

APPENDIX I – Initial Estimation of Optimum Fabric Thickness

The neutral axis (N.A.) depth for all specimens is measured from the top of the beam

Control Specimen

N.A. Depth = 80 mm

$$I_{CONTROL} = (2)\left(\left(\frac{(102)(10.2^3)}{12}\right) + (102)(10.2)(80 - 5.1)\right) + \left(\frac{(6.6)(160-2(10.2))^3}{12}\right) = 1.32\text{x}10^7\text{mm}^4$$

20CC

$$\text{N. A. Depth} = \frac{(10.2)(102)(5.1) + (6.6)(139.6)(80) + (8.16)(102)(153.88)}{(10.2)(102) + (6.6)(139.6) + (8.16)(102)}$$

$$= 74.12 \text{ mm}$$

$$I_{20CC} = \left(\left(\frac{(102)(10.2^3)}{12}\right) + (102)(10.2)(74.12 - 5.1)^2\right) + \left(\left(\frac{(6.6)(160 - 2(10.2))^3}{12}\right) + (6.6)(160 - 2(10.2))(80 - 74.12)^2\right) + \left(\left(\frac{(102)(8.16^3)}{12}\right) + (102)(8.16)(153.88 - 74.12)^2\right)$$

$$= 1.18\text{x}10^7\text{mm}^4$$

20RB7L

Modulus of Elasticity of Steel = 200 GPa

Modulus of Elasticity of Basalt ≈ 25 GPa

$$\text{Modular Ratio} = \frac{25 \text{ GPa}}{200 \text{ GPa}} = 0.125$$

Thickness of 1 Basalt Sheet = 0.45 mm

Thickness of Equivalent Steel Added to the Beam $= 7(0.45) * 0.125 = 0.4$ mm

N. A. Depth $= \frac{10.2(102)(5.1)+6.6(139.6)(80)+8.16(102)(153.88)+0.4(102)(157.96+0.2)}{(10.2)(102)+(6.6)(139.6)+(8.16)(102)+(0.4)(102)} =$

75.33 mm

$$I_{20RB7L} = \left(\left(\frac{(102)(10.2^3)}{12}\right) + (102)(10.2)(75.33 - 5.1)^2\right)$$
$$+ \left(\left(\frac{(6.6)(160 - 2(10.2))^3}{12}\right) + (6.6)(160 - 2(10.2))(80 - 75.33)^2\right)$$
$$+ \left(\left(\frac{(102)(8.16^3)}{12}\right) + (102)(8.16)(153.88 - 75.33)^2\right)$$
$$+ \left(\left(\frac{(102)(0.4^3)}{12}\right) + (102)(0.4)(160 - 2.04 + 0.4 - 75.33)^2\right)$$
$$= 1.21\text{x}10^7 \text{mm}^4$$

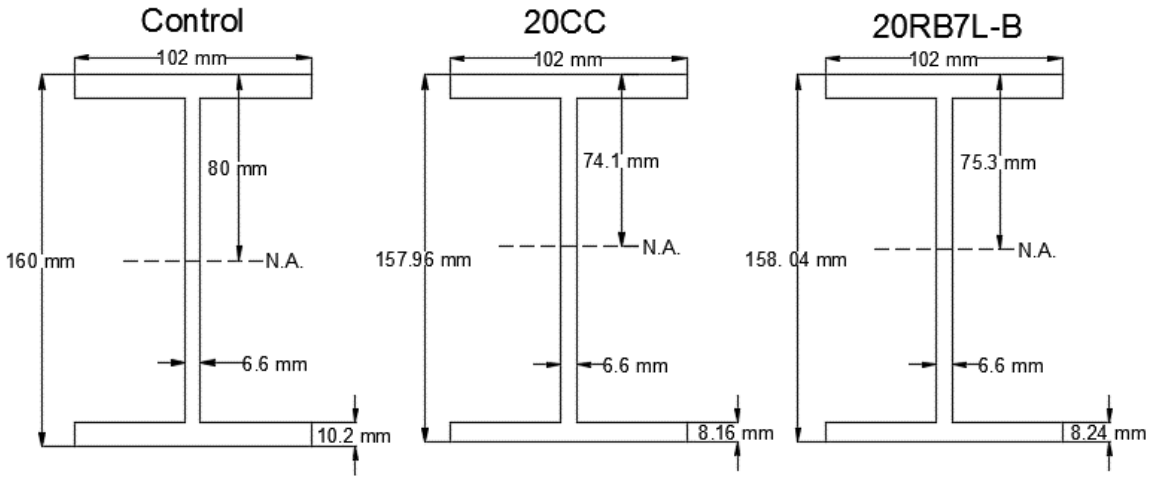

Estimation of Load Capacity

Yield Stress of Steel (f_y) = 379 MPa

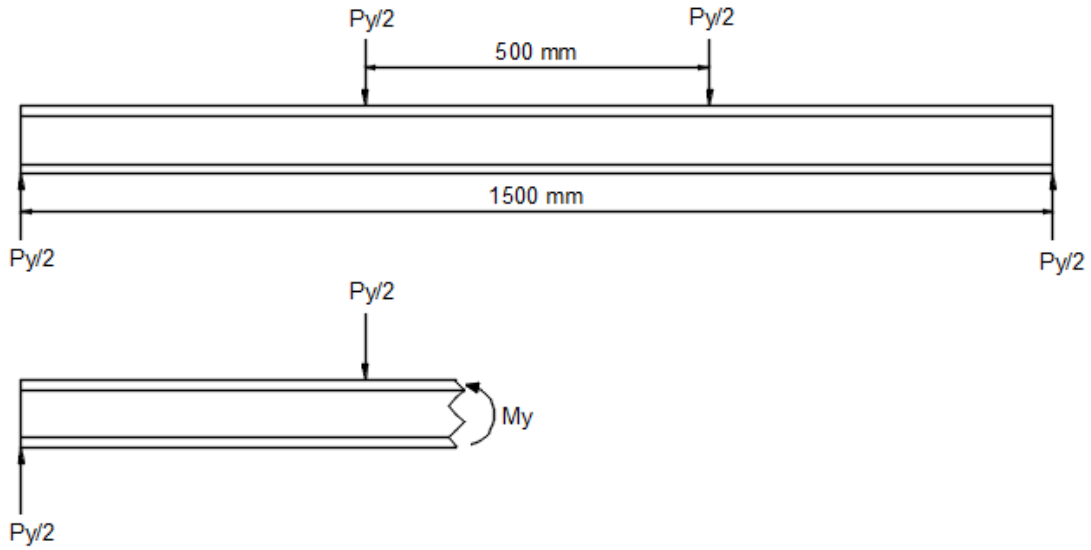

$$M_y = \frac{P_y}{2}(0.5)$$

Control Specimen:

$$f_{y=}\frac{M_y\bar{y}}{I}$$

$$M_y = \frac{(379)(1.32x10^7)}{80} = 62.5\ kN \cdot m$$

$$P_y = \frac{2M_y}{0.5} = 250\ kN$$

20RB7L:

$$f_{y=}\frac{M_y\bar{y}}{I}$$

$$M_y = \frac{(379)(1.21x10^7)}{75.33} = 60.9\ kN \cdot m$$

$$P_y = \frac{2M_y}{0.5} = 243.6\ kN$$

APPENDIX II – Materials Used in the Experimental Study

MasterBrace Epoxy Resin – SAT 4500 Part A

MasterBrace Epoxy Resin – SAT 4500 Part B

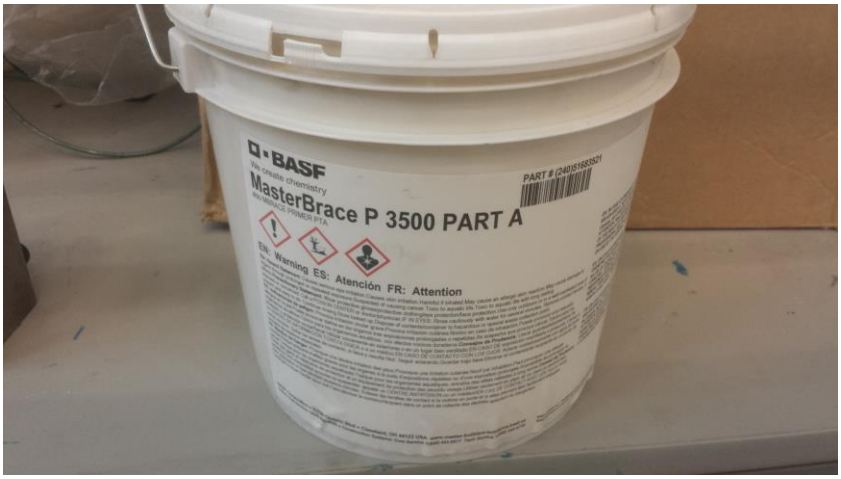

MasterBrace Primer - P3500, Part A

MasterBrace Primer – P3500, Part B

Loctite 401 strain gage glue

APPENDIX III – Preparation of Rehabilitated Beams

Application of primer to sandblasted beam

Application of small fabric pieces to corrosion gap

Saturation of base layer prior to applying longitudinal fabrics

Application of longitudinal fabrics

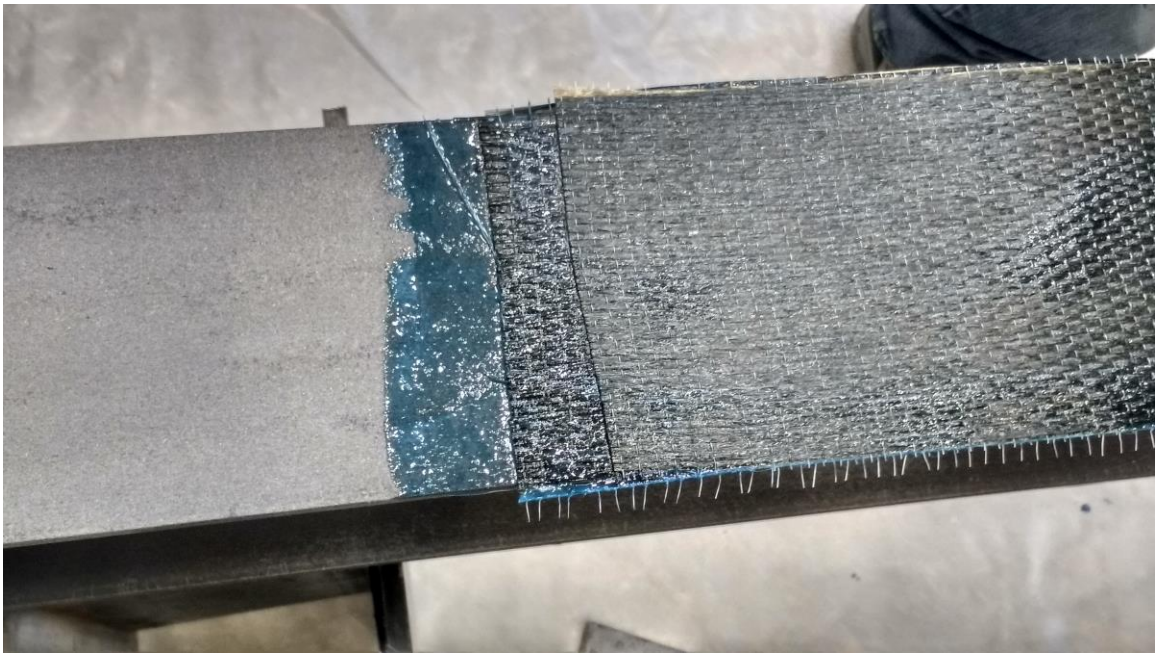

Tapering of longitudinal fabric endpoints between layers

Rehabilitated beam after the application of clamps

VITA AUCTORIS

NAME:	Sahan Jayasuriya
PLACE OF BIRTH:	Kandy, Sri Lanka
YEAR OF BIRTH:	1992
EDUCATION:	*BASc – Civil Engineering, 2014* *University of Windsor*